UNIVERSITY OF SÃO PAULO
SCHOOL OF ARTS, SCIENCES AND HUMANITIES
SUSTAINABILITY GRADUATE COLLEGE

MARÍLIA DE CARVALHO CAMPOS

Millennial-scale variability in eastern South American climate and western South Atlantic circulation during the last 70,000 years

São Paulo
2020

MARÍLIA DE CARVALHO CAMPOS

Millennial-scale variability in eastern South American climate and western South Atlantic circulation during the last 70,000 years

Corrected Version

Ph.D. Thesis presented to the Sustainability Graduate College at the School of Arts, Sciences and Humanities, University of São Paulo, Brazil to obtain the degree of Doctor of Science.

Concentration area:
Science and Technology

Supervisor:
Prof. Dr. Cristiano Mazur Chiessi

São Paulo
2020

CATALOGUING IN PUBLICATION
(University of São Paulo. School of Arts, Sciences and Humanities. Library)
CRB 8 -4936

Campos, Marília de Carvalho
Millennial-scale variability in eastern South American climate and western South Atlantic circulation during the last 70,000 years / Marília de Carvalho Campos ; supervisor, Cristiano Mazur Chiessi. – 2020.
108 p : il.

Thesis (Doctor of Science) - Graduate Program in Sustainability, School of Arts, Sciences and Humanities, University of São Paulo.
Corrected version.

1. Climate change - South America. 2. Quaternary. 3. São Francisco river. 4. Ocean circulation - Atlantic ocean. 5. Heirinch stadials. 6. Oceanic ventilation. 7. Sea surface salinity. 8. Geological oceanography. 9. Paleoceanography. 10. Paleoclimatology. 11. Sustainability. I. Chiessi, Cristiano Mazur, sup. II. Title.

CDD 22.ed.– 551.61098

Name: CAMPOS, Marília de Carvalho

Title: Millennial-scale variability in eastern South American climate and western South Atlantic circulation during the last 70,000 years

Ph.D. Thesis presented to the Sustainability Graduate College at the School of Arts, Sciences and Humanities, University of São Paulo, Brazil to obtain the degree of Doctor of Science.

Concentration area:
Science and Technology

Approved in: 26/05/2020

Academic jury

Prof. Dr.	Cristiano Mazur Chiessi	Institution:	EACH/USP
Judgment:	Approved	Signature:	_____
Prof. Dr.	Ana Luiza S. Albuquerque	Institution:	IQ/UFF
Judgment:	Approved	Signature:	_____
Prof. Dr.	Felipe A. L. Toledo	Institution:	IO/USP
Judgment:	Approved	Signature:	_____
Dr.	Thiago P. Santos	Institution:	IQ/UFF
Judgment:	Approved	Signature:	_____
Prof. Dr.	Francisco W. Cruz Junior	Institution:	IGc/USP
Judgment:	Approved	Signature:	_____

To my dear family and beloved ones.

Acknowledgments

Special thanks for my beloved fiancé, Adriano B. Garcia, for always being by my side no matter what. I am deeply grateful to him for his longstanding support and understanding for my PhD as well as my academic journey.

To my supervisor, Prof. Dr. Cristiano M. Chiessi, many thanks for the opportunities, support, patience and contributions to my academic growth.

To my supervisors abroad, Dr. Stefan Mulitza and Dr. Henning Kuhnert, for all scientific and technical support, as well as the patience. The time I spent at the MARUM – Center for Marine Environmental Science (University of Bremen, Germany) was really fruitful not only for my scientific trajectory but also because of the friends I made there.

I thank my laboratory friends and also my personal friends that directly or indirectly contributed to this study, specially Stefano Crivellari and Jaqueline Q. Ferreira for helping with some figures shown herein.

To FAPESP (grants 2012/17517-3, 2016/10242-0, 2018/06790-7 and 2018/15123-4), CAPES (grants 1976/2014 and 564/2015) and CNPq (grant 422255/2016-5) for the financial support. To the captain and crew of R/V Meteor for the logistic and technical assistance. To the School of Arts, Sciences and Humanities (University of São Paulo), my home institution, for offering the necessary infrastructure for the development of this study.

A scientist in his laboratory is not only a technician: he is also a child placed before natural phenomena which impress him like a fairy tale.

(CURIE, 1937, p. 341)

Abstract

CAMPOS, M. C. **Millennial-scale variability in eastern South American climate and western South Atlantic circulation during the last 70,000 years**. 2020. 108 p. Ph.D. Thesis - Sustainability Graduate College, School of Arts, Sciences and Humanities, University of São Paulo, São Paulo, 2020. Corrected version.

During the last glacial and deglacial periods, the Earth experienced several abrupt millennial-scale climate change events, named Heinrich Stadials (HS) and Dansgaard-Oeschger events. The HS in particular are commonly attributed to reductions in the strength of the Atlantic meridional overturning circulation (AMOC). Given the marked AMOC influence over global climate and the possibility of the AMOC to reduce its strength in the future due to ongoing climate change, the study of HS became a topic of key importance. Here we investigate the effects of last glacial and deglacial HS to eastern (E) South American hydroclimate as well as western South Atlantic oceanography. To do so, we studied marine sediment core M125-95-3 collected from the western tropical South Atlantic mid-depth (10.94°S, 36.20°W, 1897 m water depth), near the mouth of the São Francisco River (i.e., off E South America), spanning the last ca. 70,000 years. We produced radiocarbon ages from planktonic foraminifera, X-ray fluorescence analyses from bulk sediment samples, stable oxygen and carbon isotopic analyses from planktonic and benthic foraminifera, and Mg/Ca analyses from planktonic foraminifera. We conclude that the last glacial and deglacial HS were marked by positive precipitation anomalies over the São Francisco River drainage basin, and that this was the southernmost drainage basin from the South American Atlantic seaboard that experienced substantial increases in precipitation. We propose a new mechanism for explaining tropical South America HS positive precipitation anomalies. This mechanism involves austral summer precipitation increases only over E South America while the rest of tropical South America experienced precipitation increases during the winter, challenging the widely held assumption of a strengthened monsoon during HS. During the same abrupt events, the mid-depth western tropical South Atlantic experienced decreases in $\delta^{13}C$ and increases in sulfur (unprecedentedly used as a proxy for abrupt millennial-scale changes in bottom water ventilation) that we attributed to an increased Northern Component Water (NCW) residence time and to the accumulation of respired carbon at mid-depths. We also suggest that the negative $\delta^{13}C$ excursions progressively increase along the NCW southwards pathway, reaching its maximum in the western tropical South Atlantic from where the signal dissipates/dilutes by mixing with Southern Component Water. Regarding the upper water column, the western tropical South Atlantic surface waters were warmer and saltier during HS. Data from the Agulhas Leakage

region also recorded similar features, however, with larger positive excursions. We conclude that the heat and salt imported from the Indian Ocean during HS were only partially transferred to the western tropical South Atlantic. Thus, Indian Ocean salt that eventually reached the high latitudes of the North Atlantic helping on the recovering of the AMOC was most probably transported mainly within the thermocline. Finally, the data shown herein indicate that past events of weak AMOC profoundly affected South American hydroclimate and western South Atlantic oceanography.

Keywords: Late Quaternary. São Francisco River. South America. South Atlantic. Heinrich Stadials. Atlantic meridional overturning circulation. Precipitation. Oceanic ventilation. Sea surface temperature. Sea surface salinity.

Resumo

CAMPOS, M. C. **Variabilidade milenar no clima do leste da América do Sul e na circulação do oeste do Atlântico Sul durante os últimos 70.000 anos**. 2020. 108 f. Tese de Doutorado – Programa de Pós-graduação em Sustentabilidade, Escola de Artes, Ciências e Humanidades, Universidade de São Paulo, São Paulo, 2020. Versão corrigida.

Durante a última glaciação e a última deglaciação, a Terra passou por vários eventos de mudanças climáticas abruptas, chamados *Heinrich Stadial* (HS) e *Dansgaard-Oeschger*. Os HS são comumente atribuídos a reduções na intensidade da célula de revolvimento meridional do Atlântico (CRMA). Dada a marcante influência da CRMA no clima global e a possibilidade da redução da sua intensidade no futuro devido às mudanças climáticas em curso, o estudo dos HS se tornou um tópico de suma importância. Nesta tese, os efeitos dos HS da última glaciação e da última deglaciação no hidroclima do leste (E) da América do Sul bem como na circulação do oeste do Atlântico Sul foram investigados. Para tanto, o testemunho sedimentar marinho M125-95-3 coletado em profundidades médias do oeste do Atlântico Sul tropical (10,94°S, 36,20°W, 1897 m de profundidade), perto da desembocadura do Rio São Francisco (i.e., margem E da América do Sul), foi estudado para os últimos ca. 70.000 anos. Para esse testemunho foram produzidas idades radiocarbônicas a partir de foraminíferos planctônicos, análises de fluorescência de raios-X em amostras de sedimento total, análises de isótopos estáveis de oxigênio e carbono em foraminíferos planctônicos e bentônicos, e análises de Mg/Ca em foraminíferos planctônicos. Concluiu-se que os HS da última glaciação e da última deglaciação foram marcados por anomalias positivas de precipitação sobre a bacia de drenagem do Rio São Francisco, e que esta foi a bacia de drenagem mais austral da costa sul-americana banhada pelo Atlântico que apresentou aumento substancial na precipitação. Um novo mecanismo foi proposto para explicar as anomalias positivas de precipitação na América do Sul tropical durante os HS. Este mecanismo envolve aumentos na precipitação de verão apenas sobre o E da América do Sul, enquanto o resto da América do Sul tropical apresentou aumentos de precipitação no inverno, desafiando a hipótese amplamente difundida de fortalecimento da monção nos HS. Durante os mesmos eventos abruptos, as profundidades médias do oeste do Atlântico Sul tropical apresentaram reduções de $\delta^{13}C$ e aumentos de enxofre (seu uso como indicador de mudanças milenares na ventilação de fundo é inédito), que foram atribuídos a um aumento do tempo de residência da massa de água de origem norte (MAON) e a um acúmulo de carbono respirado nas profundidades médias. Também foi sugerido que as excursões negativas em $\delta^{13}C$ aumentaram progressivamente ao longo do caminho percorrido pela MAON

em direção ao sul, atingindo valores máximos no oeste do Atlântico Sul tropical, a partir de onde sofreu dissipação/diluição por mistura com a massa de água de origem sul. Com relação à porção superior da coluna de água, os dados apresentados aqui indicam que as águas superficiais do oeste do Atlântico Sul tropical estiveram mais quentes e salinas durante os HS. Dados advindos da região do vazamento das Agulhas também registraram feições similares, no entanto, com excursões positivas mais intensas. Concluiu-se que o calor e o sal importados do Oceano Índico durante os HS foram apenas parcialmente transferidos para o oeste do Atlântico Sul tropical. Assim, sugeriu-se que o sal do Oceano Índico que eventualmente alcançou as altas latitudes do Atlântico Norte e ajudou no restabelecimento da CRMA foi transportado, principalmente, pelas águas da termoclina. Finalmente, os dados apresentados nesta tese indicam que os eventos pretéritos de enfraquecimento da AMOC afetaram profundamente o hidroclima da América do Sul e a circulação do oeste do Atlântico Sul.

Palavras-chave: Quaternário tardio. Rio São Francisco. América do Sul. Atlântico Sul. *Heinrich Stadials*. Circulação meridional do Atlântico. Precipitação. Ventilação oceânica. Temperatura da superfície do mar. Salinidade da superfície do mar.

List of abbreviations

^{14}C	Radiocarbon
AABW	Antarctic Bottom Water
AAIW	Antarctic Intermediate Water
AC	Agulhas Current
ACC	Antarctic Circumpolar Current
AL	Agulhas Leakage
AMOC	Atlantic meridional overturning circulation
AMS	Accelerator mass spectrometry
BC	Brazil Current
BFAR	Benthic foraminifera accumulation rate
BP	Before present
CO_2	Carbon dioxide
CO_{2atm}	Atmospheric carbon dioxide
CPRM	Geological Brazilian Survey
CRMA	Célula de revolvimento meridional do Atlântico
$\delta^{13}C$	Carbon isotopic composition
$\delta^{13}C_{DIC}$	Carbon isotopic composition of the dissolved inorganic carbon
$\delta^{18}O$	Oxygen isotopic composition
$\delta^{18}O_{ivc\text{-}ssw}$	Ice volume corrected $\delta^{18}O_{ssw}$
$\delta^{18}O_{sw}$	Oxygen isotopic composition of the sea water
$\delta^{18}O_{ssw}$	$\delta^{18}O$ of surface sea water
D-O	Dansgaard-Oeschger
DWF	Deep water formation
E	Eastern
EDML	Epica Dronning Maud Land
EDP-XRF	Energy dispersive polarized X-ray fluorescence
ENSO	El Niño-Southern Oscillation
EOF	Orthogonal functions method
ESL	Estimated sea level
HP	High productivity
HS	Heinrich Stadials
ICP	Inductively coupled plasma
IRD	Ice-rafted debris
ITCZ	Intertropical Convergence Zone
ka	Thousand years
K	Kelvin
LGM	Last Glacial Maximum
MAON	Massa de água de origem norte
MC	Malvinas Current
MIS	Marine Isotope Stages
MOC	Meridional overturning circulation

MS	Mass spectrometer
N	North
NADW	North Atlantic Deep Water
NBC	North Brazil Current
NCEP	National Centers for Environmental Prediction
NCW	Northern Component Water
NE	Northeastern
NGRIP	North Greenland Ice Core Project
NW	Northwestern
OES	Optical emission spectrometer
PW	Petawatt
RAPID	Rapid Climate Change program
S	Sulfur
SAC	South Atlantic Current
SACW	South Atlantic Central Water
SACZ	South Atlantic Convergence Zone
SAMS	South American monsoon system
SCW	Southern Component Water
SE	Southeastern
SMOW	Vienna Standard Mean Ocean Water
SRTM	Shuttle Radar Topography Mission
SSEC	Southern branch of the South Equatorial Current
SSS	Sea surface salinity
SST	Sea surface temperature
Sv	Sverdrup
SW	Southern Hemisphere Westerlies
TW	Tropical Water
USGS	United States Geological Survey
VPDB	Vienna Pee Dee Belemnite
VSMOW	Vienna Standard Mean Ocean Water
XRF	X-ray fluorescence
YD	Younger Dryas

Table of contents

1 Introduction

1.1 Scientific background and motivation

The Earth's climate system is basically composed by air, water, ice, land, and vegetation (Fig. 1.1). The interactions among these components through time are described in terms of cause (usually named forcing or driver) and effect (usually named response). The forcing drives climate change and the response is the resultant climatic change (RUDDIMAN, 2001).

The external forcings of the climate system are plate tectonics, Earth's orbit and Sun's strength (left-hand panel, Fig. 1.1). In turn, the internal components change and interact in several ways (central panel, Fig. 1.1) producing internal responses (right-hand panel, Fig. 1.1). The internal responses are further complicated by the existence of feedbacks, non-linearities and tipping points of the climate system (LENTON et al., 2008). The response time can be very fast (e.g., atmospheric response) or slow (e.g., oceanic response), ranging from hours to thousands of years (RUDDIMAN, 2001).

Figure 1.1 - Earth's climate system and interactions of its components.

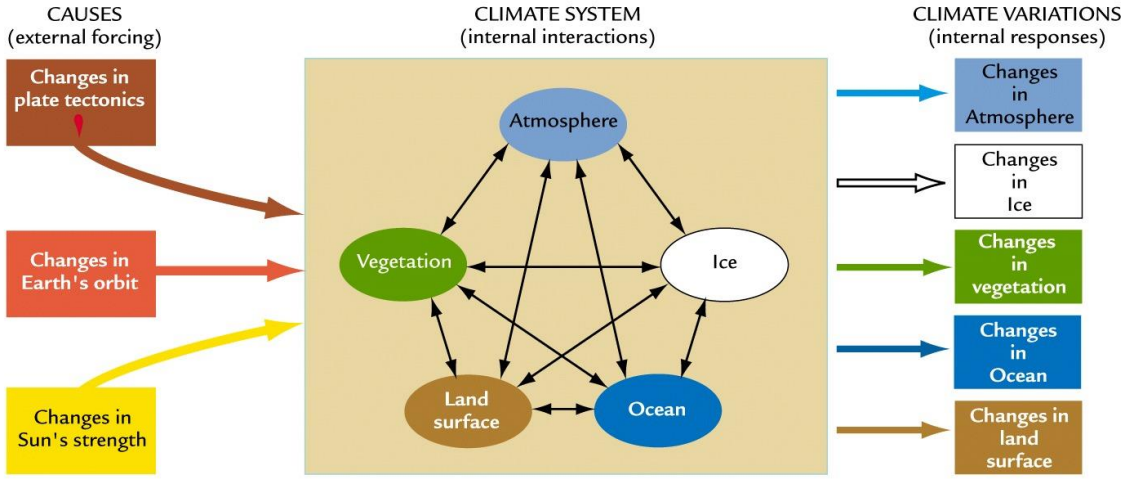

Font: Ruddiman (2001).

The climate system is highly influenced by the incoming energy from the Sun, as well as by its redistribution (in the form of heat) around the Earth by the atmosphere and the ocean. Because of (i) the angle of incidence of the Sun's rays and (ii) the albedo of different portions of the Earth's surface, the insolation is higher near the equator and decreases towards the poles. This difference drives the direction of heat distribution across the globe, i.e., from low to high latitudes. The atmosphere and the ocean promote the heat distribution through several cells. However, this distribution is not regular and the amount of energy changes at different latitudes and in different seasons (RUDDIMAN, 2001).

In the tropics, the Hadley cell comprehends the most important atmospheric cell which ascends near the equator and descends at ca. 30° in both hemispheres. The Hadley cell ascendant branch is formed by the Intertropical Convergence Zone (ITCZ), defined as the zonal mean band of maximum precipitation around the equator. It is formed where the southeast and northeast trade winds (i.e., the trade winds of the Southern Hemisphere and Northern Hemisphere, respectively) merge in the lower troposphere (GARREAUD et al., 2009). If the climate system was symmetric between both hemispheres, the mean annual position of the ITCZ should be along the equator. However, it is displaced to the north at around 5°N (Fig. 1.2) (MARSHALL et al., 2014).

Figure 1.2 - Mean annual global precipitation. The Intertropical Convergence Zone is seen slightly to the north of the equator. Blue lines indicate the meridional location of the maximum precipitation in the tropics at each longitude. The zonal mean precipitation is shown on the left-hand panel and is co-plotted with the zonal mean of the local maximum (blue lines) and centroid (dashed black lines).

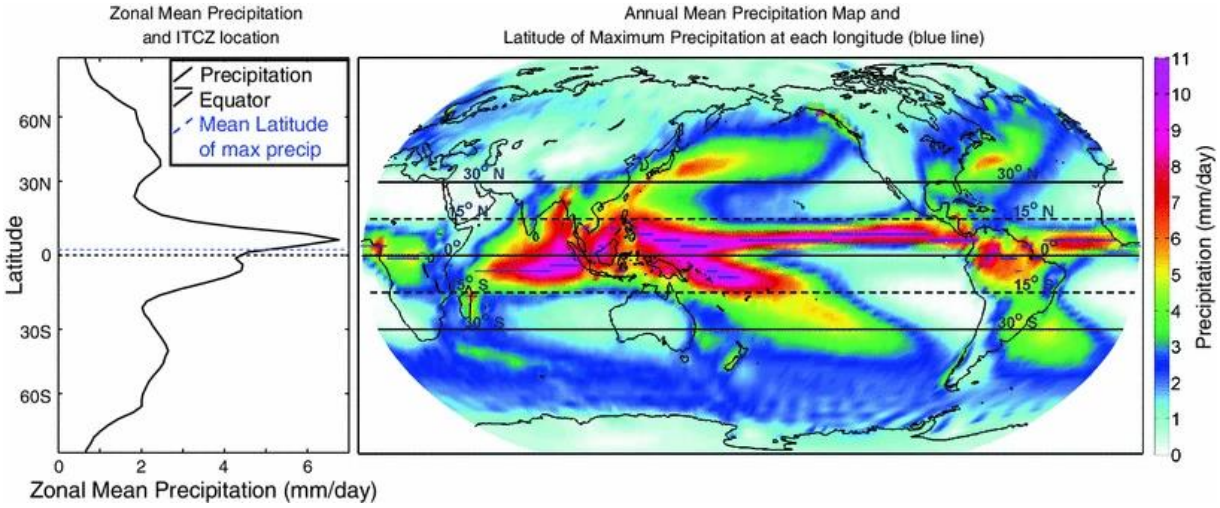

Font: Marshall et al. (2014).

Hemispheric differences in the insolation received at the surface (mainly because of differences in albedo) produce an imbalance of 0.2 Petawatt (PW; 1 PW = 10^{15} W) between both hemispheres (i.e., the Northern Hemisphere lacks 0.2 PW in relation to the Southern Hemisphere). The oceanic meridional circulation transports 0.4 PW northwards across the equator. This extra heat warms the Northern Hemisphere and brings the ITCZ to the North (Fig. 1.3). By doing so, the atmosphere is sending 0.2 PW back to the Southern Hemisphere and the interhemispheric imbalance is compensated (BROCCOLI et al., 2006; MARSHALL et al., 2014; ZHANG; DELWORTH, 2005).

Figure 1.3 - Observed hemispheric asymmetry of temperature in the atmosphere and ocean (in Kelvin, K) computed from the National Centers for Environmental Prediction (NCEP) reanalysis and the World Ocean Atlas.

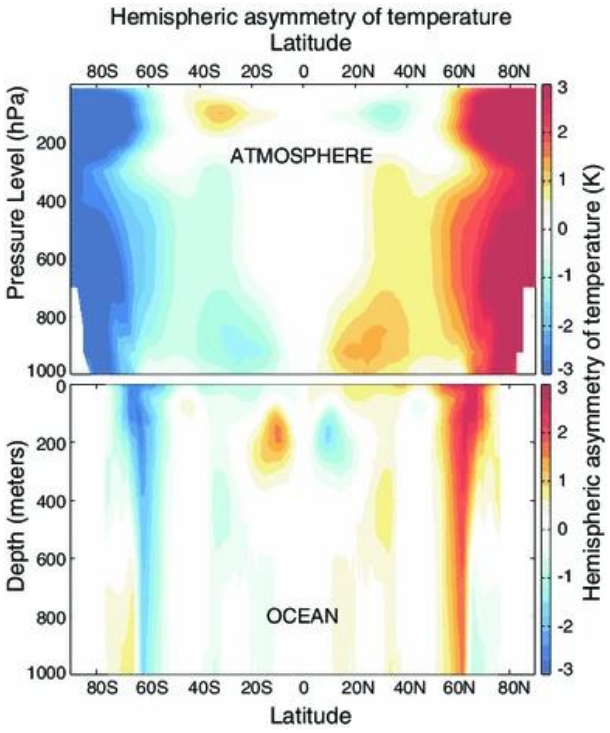

Font: Marshall et al. (2014).

The oceanic meridional overturning circulation (MOC) is a large-scale circulation of the global ocean which is a combination of currents driven by winds, differences in ocean heat and salinity, and tides (Fig. 1.4) (KUHLBRODT et al., 2007). The interactions of these drivers with the associated responses of the MOC are nonlinear and tipping points exist (RAHMSTORF, 2002).

The Atlantic sector of the MOC, i.e., Atlantic meridional overturning circulation (AMOC), transports surface warm and saline waters towards high latitudes of the North Atlantic, where they release heat to the atmosphere, reach critical density and sink, returning deep cold waters towards the South Atlantic (BRYDEN et al., 2005; RAHMSTORF, 2002).

Figure 1.4 - Simplified sketch of the global overturning circulation system. In the Atlantic, warm and saline waters flow northward from the Southern Ocean to the Labrador and Nordic Seas. There is no deep-water formation in the North Pacific, and its surface waters are relatively fresh. Deep-waters formed in the Southern Ocean become denser and thus spread in deeper levels than those from the North Atlantic. Wind-driven upwelling occurs along the Antarctic Circumpolar Current (ACC).

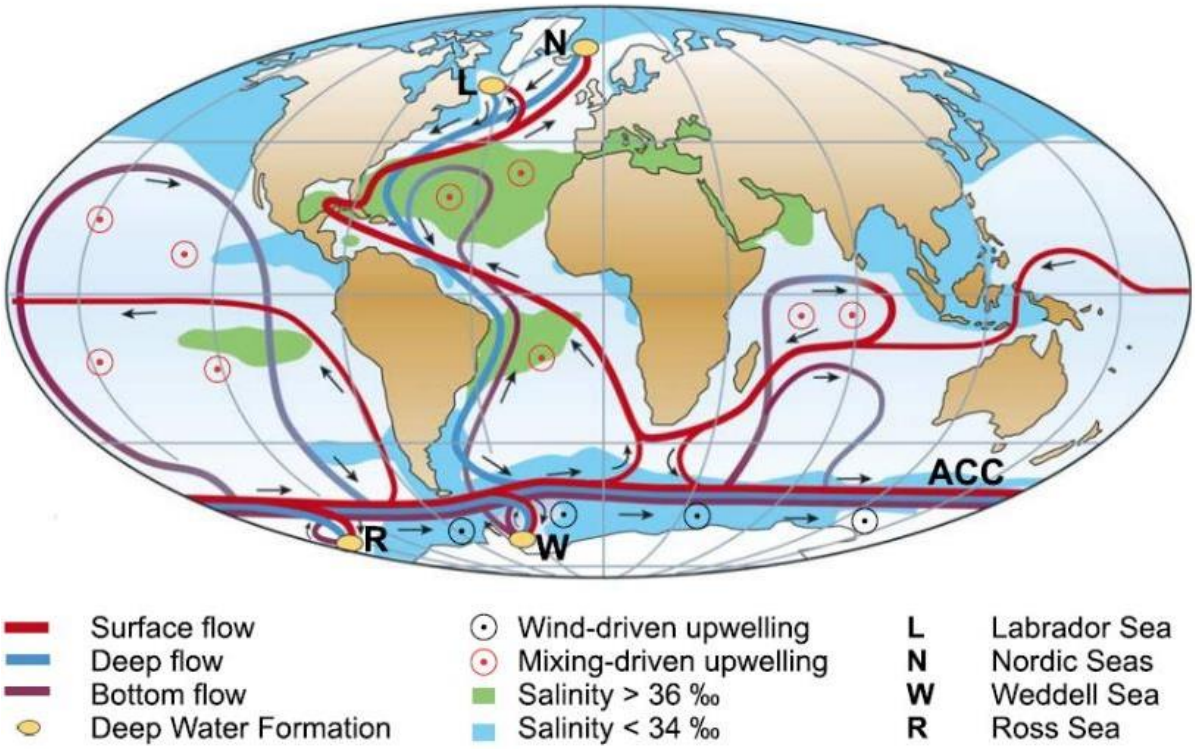

Font: Kuhlbrodt et al. (2007).

The AMOC branches extend throughout the Atlantic in both hemispheres, forming a circulation system with two main overturning cells. One deep cell, represented by the North Atlantic Deep Water (NADW) and one abyssal cell, represented by the Antarctic Bottom Water (AABW) (Fig. 1.5) (KUHLBRODT et al., 2007). The AMOC comprehends an extremely important and unique player of the Earth's climate system.

Figure 1.5 - Schematic meridional section of the Atlantic Ocean. The arrows indicate the several processes related to the Atlantic meridional overturning circulation. The blue-to-yellow filling represents zonally averaged density values (low-to-high) derived from observational data. The thermocline is the region where the temperature gradient is large, separates the light and warm upper waters from the denser and cooler deep waters. The two main upwelling mechanisms, wind-driven and mixing-driven, are shown. Deep water formation (DWF) occurs in the high northern and southern latitudes, creating North Atlantic Deep Water (NADW) and Antarctic Bottom Water (AABW), respectively. The newly formed NADW has to flow over the shallow sill between Greenland, Iceland and Scotland, before flowing towards the South Atlantic.

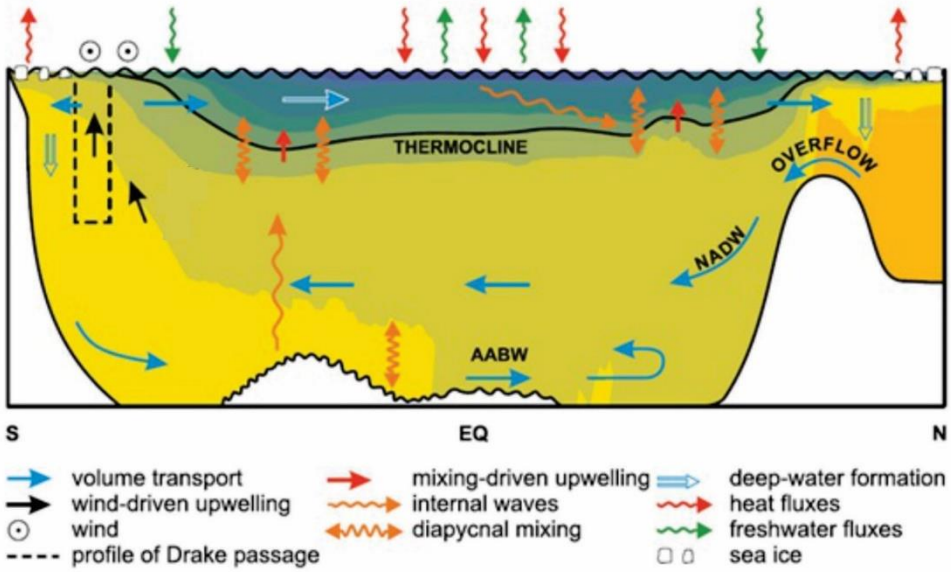

Font: Adapted from Kuhlbrodt et al. (2007).

Linear surface temperature trends for the last century are positive almost everywhere in the world, exception made for the NADW formation region, where a cooling occurred. This conspicuous cooling was attributed to a slowdown in the AMOC that delivers less heat to the region as it weakens (Fig. 1.6) (RAHMSTORF et al., 2015).

Figure 1.6 - Linear trends of annual surface temperature from 1901 to 2013.

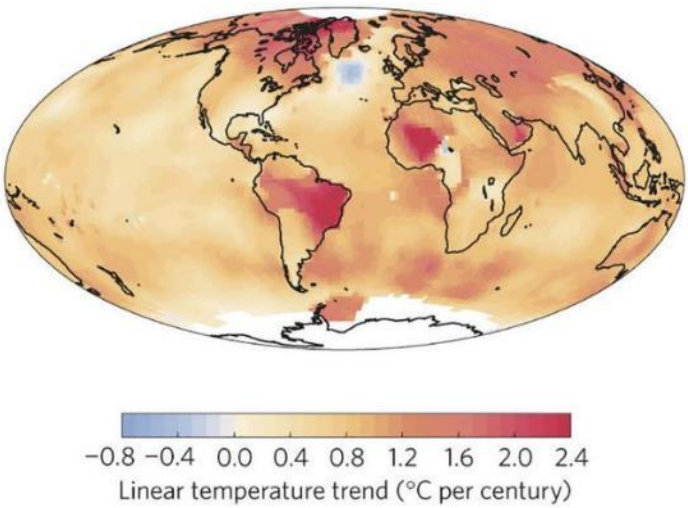

Font: Rahmstorf et al. (2015).

Just recently (since 2004), the AMOC strength started to be continuously measured by the Rapid Climate Change program (RAPID) at 26.5°N in the North Atlantic. The 10-year time series shows an overall weakening trend (Fig. 1.7) (SROKOSZ; BRYDEN, 2015).

Figure 1.7 - Ten-year time series of the strength of the Atlantic meridional overturning circulation measured at 26.5°N. The grey line represents the 10-day filtered measurements, and the red line is the 180-day filtered time series.

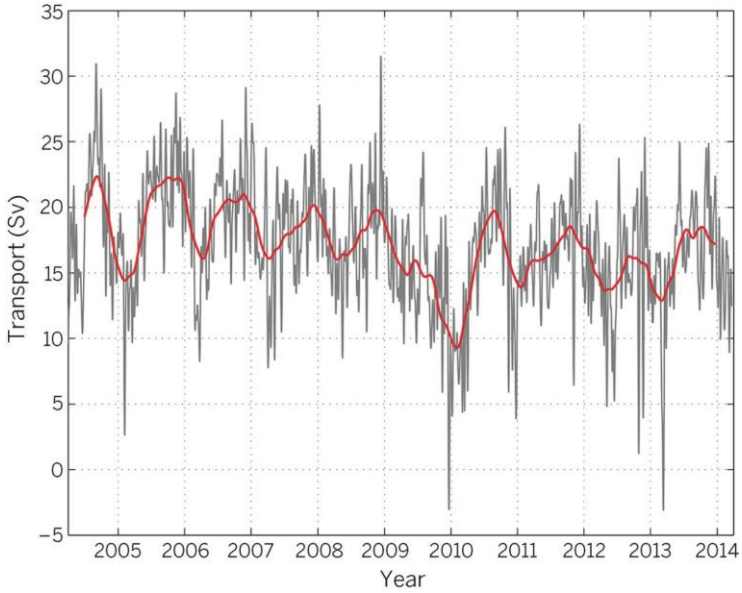

Font: Srokosz and Bryden (2015).

This is the longest time series of AMOC direct measurements and, thus, indirect measurements have been used to deduce how the AMOC behavior was before 2004. DIMA and LOHMANN (2010), based on orthogonal functions method (EOF) applied on two global sea surface temperature (SST) datasets, looked at SST evolution since 1870 in order to identify dominant modes of climate variability. After removing a global warming trend, they identified two particular modes, a global mode and an Atlantic mode. The global mode is related to a slow (multidecadal) adjustment of the global MOC and shows a SST interhemispheric symmetry. Instead, the Atlantic mode is related to a fast (interannual) adjustment of the North Atlantic overturning circulation and shows a pronounced SST interhemispheric asymmetry. Both modes implicate in the weakening of the AMOC and a combination of them seems to modulate the modern AMOC.

Climate modelling studies predict that the weakening of the AMOC could reach ca. 44% until the end of the century, under the more extreme greenhouse gases emission scenario (e.g., WEAVER et al., 2012). However, recent studies suggest that the used models have systematically overestimated the AMOC stability and largely neglected Greenland ice sheet

mass loss (e.g., BAKKER et al., 2016; LIU et al., 2017). This scenario is dramatic since a marked weakening of the AMOC poses major threats to global flora, fauna (THOMAS et al., 2004) and society (PATZ et al., 2005).

To better constrain present and future climate change, a detailed knowledge about past periods (i.e., longer than the instrumental record) during which the rate and/or magnitude of changes related to AMOC are, to some extent, comparable to present and future changes is of fundamental importance. Indeed, the geological record provides a fantastic opportunity to explore the different flavors of the climate system that are otherwise not registered in the instrumental record and for which uncertainties in climate models are prohibitive.

During the last glacial and deglacial period, the Earth experienced several abrupt millennial-scale climate change events which are commonly attributed to changes in the AMOC strength (RAHMSTORF, 2002). These abrupt events are clearly recorded in glacial ice from Greenland (ANDERSEN et al., 2004) and are called Dansgaard-Oeschger (D-O) events (Fig. 1.8).

Fig 1.8 – Stable oxygen isotopic composition ($\delta^{18}O$) of Greenland ice, which serves as a proxy for temperature. The Younger Dryas (YD) and Heinrich Stadials (HS) Dansgaard-Oeschger cold events in the high latitudes of the Northern Hemisphere are indicated by the blue bars. Marine Isotope Stages (MIS) boundaries are depicted in the upper x-axis.

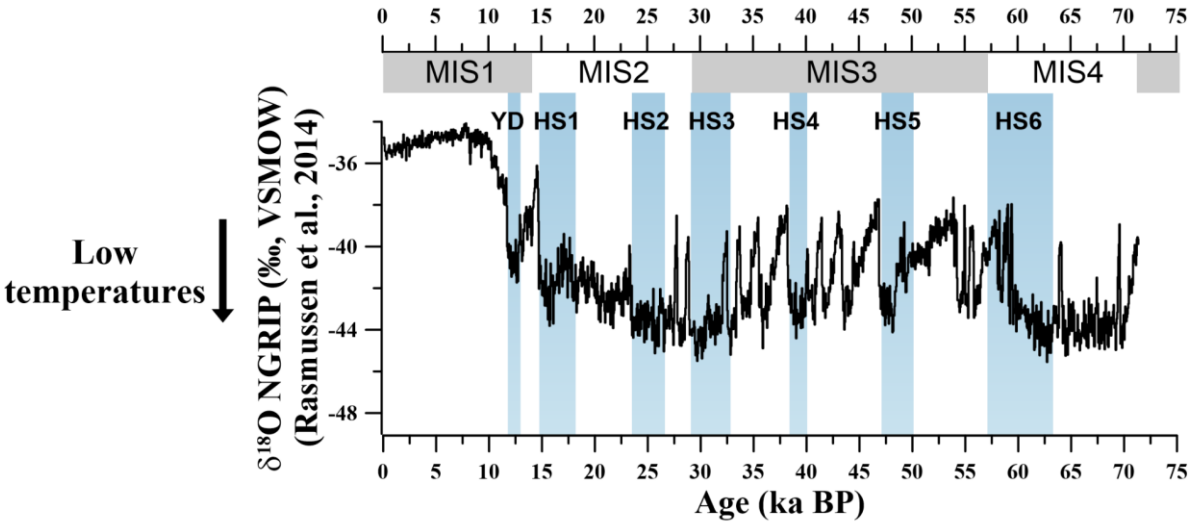

Font: Rasmussen et al. (2014).

They are composed by cold (named stadials) and warm (named interstadials) intervals (at Greenland) marked by weaker and stronger AMOC, respectively. However, there is not yet a consensus regarding what might cause AMOC changes during these events. During stadials, freshwater input into the high latitudes of the North Atlantic is usually invoked as the main driver. Since a higher amount of low salinity waters at the NADW formation region should

reduce or even interrupt deep-water formation, a slowdown or collapse of the whole AMOC would occur (CROWLEY, 1992; MIX et al., 1986). Indeed, layers of ice-rafted debris (IRD) identified at North Atlantic sediments coinciding with some stadial intervals support the input of freshwater throughout massive iceberg discharges (BOND et al., 1992; HEINRICH, 1988; HEMMING, 2004). The stadials related to the IRD layers were named Heinrich Stadials (HS) (Fig. 1.8).

Given the marked AMOC influence over global climate and the possibility of the AMOC to reduce its strength in the future due to ongoing climate change, the study of HS became a topic of key importance. This thesis shows new data recording the effects of changes in the AMOC strength associated with HS of the last glacial and deglacial periods. We investigated marine sediment core M125-95-3 collected at the western tropical South Atlantic mid-depth (10.94°S, 36.20°W, 1897 m water depth, 10.4 m cm core length) (BAHR et al., 2016), near the mouth of the São Francisco River, spanning ca. 70 thousand years before present (ka BP). We produced (i) radiocarbon (^{14}C) ages from planktonic foraminifera, (ii) X-ray fluorescence (XRF) analyses from bulk sediment samples, (iii) stable oxygen and carbon isotopic ($\delta^{18}O$ and $\delta^{13}C$) analyses from planktonic and benthic foraminifera, and (iv) Mg/Ca analyses from planktonic foraminifera. The high temporal resolution of this marine sediment core together with its position allowed us to constrain changes in the hydroclimate of eastern (E) South America, as well as in bottom and upper water conditions in the western tropical South Atlantic during HS.

1.2 Objectives

This thesis investigates the effects of last glacial and deglacial abrupt millennial-scale climate change events (i.e., HS) to eastern South American climate and western South Atlantic circulation. To reach this objective, the following scientific questions were addressed:

1. How did the São Francisco River drainage basin (i.e., E South America) precipitation respond to the HS of the last glacial and deglacial?
2. How did the western tropical South Atlantic bottom water ventilation respond to the HS of the last glacial and deglacial?
3. How did the mixed-layer of the western tropical South Atlantic respond to the HS of the last glacial and deglacial?

2 Environmental setting

2.1 Modern oceanic and atmospheric circulation

Our marine sediment core was collected from the bifurcation of the southern branch of the South Equatorial Current (SSEC) (Fig. 2.1). The SSEC bifurcation occurs between 8°S and 13°S originating the Brazil Current (BC) and the North Brazil Current (NBC) (SILVA et al., 2009). These western boundary currents carry (sub)tropical water masses southward and northwestward, respectively. The BC mean flux is ca. 4 Sv, while the NBC is ca. 26 Sv (Fig. 2.1a, c) (JOHNS et al., 1998; PETERSON; STRAMMA, 1991; RODRIGUES et al., 2007; STRAMMA et al., 1990).

Close to the bifurcation of the SSEC, both currents carry warm, saline and nutrient-depleted waters markedly influenced by the Tropical Water (TW) (upper ca. 150 m of the water column) (GARCIA et al., 2013; LOCARNINI et al., 2013; ZWENG et al., 2013).

Between 15-20°S, the BC gains vertical expression with the contribution of South Atlantic Central Water (SACW) (from ca. 150 down to 500 m water depth). Around 33-38°S this current encounters the Malvinas Current (MC), and both turn southeastwards in a region known as the Brazil-Malvinas Confluence that flows offshore as the South Atlantic Current (SAC) and the northern branch of the Antarctic Circumpolar Current (ACC), respectively (Fig. 2.1a, c) (OLSON et al., 1988; PETERSON; STRAMMA, 1991).

The NBC enters the Northern Hemisphere accounting for the upper-level northward transport of the AMOC. Its transport is dominated by the upper 150 m flow. At the surface, the NBC continues up to ca. 6-7°N where it suffers seasonal retroflection into North Equatorial Countercurrent and the remaining flux joins the North Equatorial Current. At thermocline depth, it is believed that a portion of the NBC flux feeds Equatorial Undercurrent while another portion continues up to 3-4°N and feeds the North Equatorial Undercurrent (JOHNS et al., 1998; PETERSON; STRAMMA, 1991).

Changes in the upper oceanic properties and circulation patterns are closely linked to changes in atmospheric circulation. Positive SST anomalies in the western South Atlantic, likely related to the weakening of the AMOC (KNIGHT et al., 2005), have been correlated to the increase in precipitation over the tropical South America (CHAVES; NOBRE, 2004; STOUFFER et al., 2006). Austral summer convective rains are responsible for more than 50% of the total annual precipitation over tropical South America to the east of the Andes (CARVALHO et al., 2002; 2004; FIGUEROA et al., 1995; GARREAUD et al., 2009).

Figure 2.1 - Location of marine sediment core M125-95-3 (yellow dot), surface ocean currents in the western South Atlantic (black arrows) (PETERSON; STRAMMA, 1991), sea surface temperatures (LOCARNINI et al., 2013) and precipitation (XIE; ARKIN, 1997) (Image provided by Physical Sciences Division, Earth System Research Laboratory, NOAA, Boulder, Colorado, from their Web site at http://www.esrl.noaa.gov/psd/) during austral summer (January-March) (**a** and **b**) and austral winter (July-September) (**c** and **d**). White dashed lines indicate the Intertropical Convergence Zone (ITCZ) and South Atlantic Converge Zone (SACZ) which are important phenomena in South American hydroclimate, both being related to the South America monsoon system (SAMS). The black area depicts the São Francisco River drainage basin. ACC: Antarctic Circumpolar Current; BC: Brazil Current; MC: Malvinas Current; NBC: North Brazil Current; SAC: South Atlantic Current; SSEC: Southern branch of the South Equatorial Current.

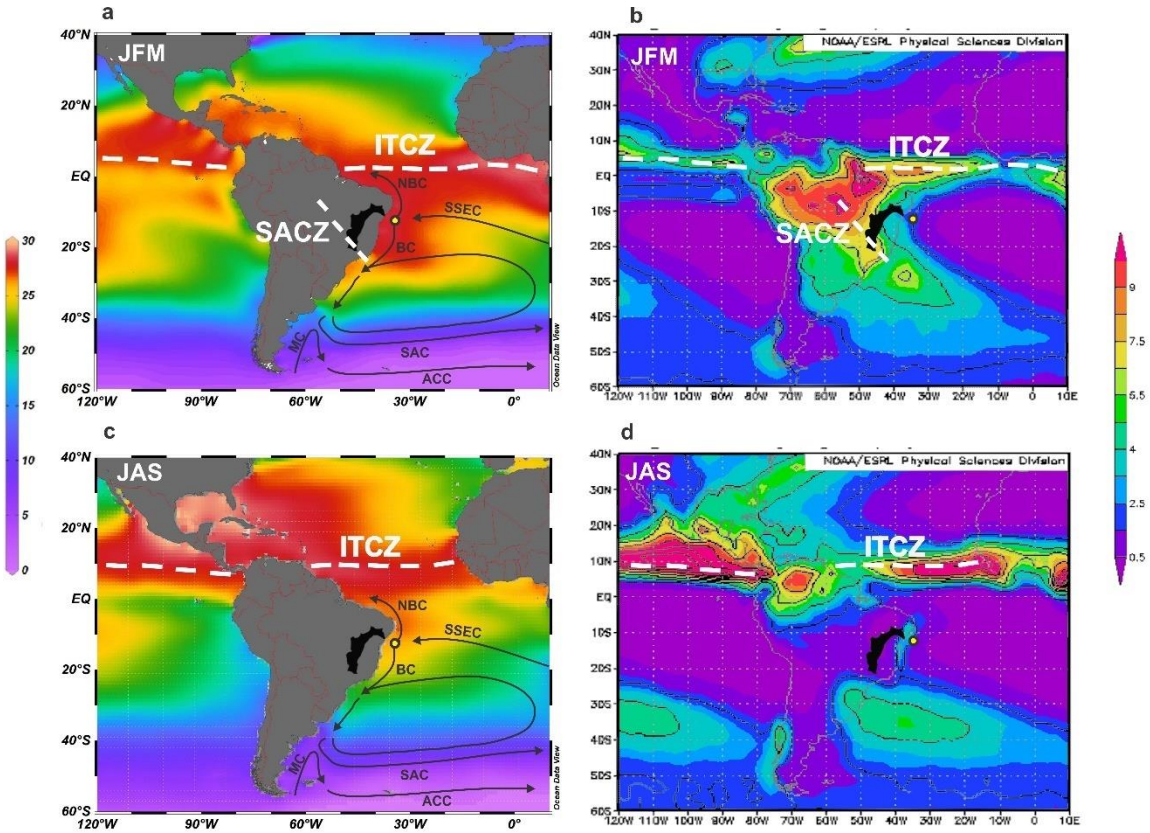

The main atmospheric feature responsible for these convective rains is the South America monsoon system (SAMS) and its related components, namely the ITCZ, and the South Atlantic Convergence Zone (SACZ) (CARVALHO et al., 2004; ZHOU; LAU, 1998).

The ITCZ can be understood as a global oceanic convective belt located in the equatorial region. It is collocated with the ascendant branch of the Hadley cell dividing the southeast and northeast trade winds (MARSHALL et al., 2014). The ITCZ mean latitudinal position is ca. 5°N, however, it shifts seasonally towards the summer hemisphere (WALISER; GAUTIER, 1993) affecting the position of the SSEC bifurcation. During austral spring/summer (autumn/winter), the ITCZ is southernmost (northernmost) and the SSEC bifurcation shifts to lower (higher) latitudes (RODRIGUES et al., 2007; SILVA et al., 2009).

The SACZ can be understood as a northwest–southeast elongated convective belt that typically originates in the western Amazon basin in early August and extends southeastwards above the northern portion of southeastern South America, frequently reaching the adjacent western South Atlantic (CARVALHO et al., 2002; 2004). This zone is marked by strong convection at low-tropospheric levels that is accompanied by upper-tropospheric divergence (VAN DER WIEL et al., 2015). It is noteworthy that not only the Andes topography but also the Amazonian latent heat source are fundamental elements to the generation and location of the SACZ (FIGUEROA et al., 1995). The SACZ is a crucial source of precipitation to the São Francisco River drainage basin, which is a source of continental-borne sediments to herein study site.

Northern Hemisphere SST anomalies also play an important role in control the strength and position of the SAMS, where negative (positive) SST anomalies are responsible for a strong (weak) SAMS (JUNQUAS et al., 2012; TALENTO; BARREIRO, 2018).

2.3 São Francisco River drainage basin (eastern South America)

The São Francisco River drainage basin is the largest drainage basin in the E South America, covering ca. 7.5% (638,466 km²) of Brazil (i.e., Alagoas, Bahia, Distrito Federal, Goias, Minas Gerais, Pernambuco, and Sergipe) with geographical limits extending from ca. 7°S to 22°S and from ca. 48°W to 36°W (Fig. 2.2) (ANA, 2015).

Figure 2.2 - **(a)** Simplified geological map of the São Francisco River drainage basin (Data: Geological Brazilian Survey - CPRM). **(b)** Digital terrain elevation model of the São Francisco River drainage basin obtained through Shuttle Radar Topography Mission (SRTM) from United States Geological Survey (USGS). The shadow scale represents the hypsometry. Yellow dot depicts the location of marine sediment core M125-95-3.

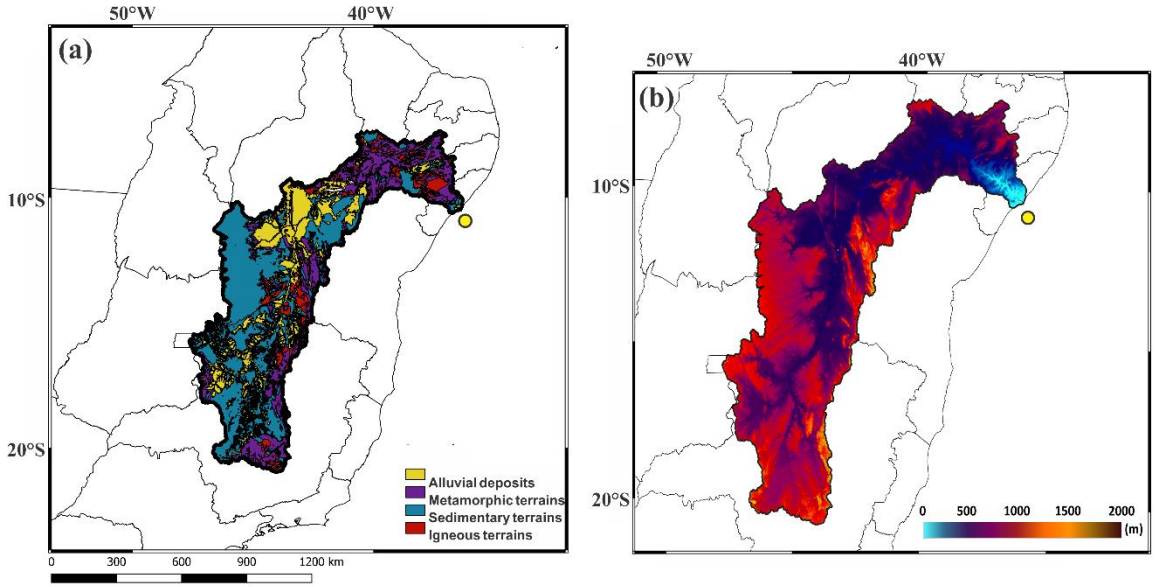

Font: personal communication, Ferreira (2016).

The São Francisco River is born at the Serra da Canastra (Minas Gerais), flows in a south-north direction through Bahia and Pernambuco, then turns to the southeast reaching the western South Atlantic around 10.5°S on the border between Alagoas and Sergipe (Fig. 2.2).

The São Francisco River is 2,800 km long and its mean annual flow is ca. 2,980 m^3/s^1 (DOMINGUEZ, 1996). The region presents low pluviosity and high evapotranspiration and, thus, most of the basin show semiarid climate with prolonged drought season. The mean annual precipitation is ca. 1,003 mm (very low compared to the national annual mean, i.e., 1,761 mm) concentrated during the austral summer. Both dry and wet extreme events are commonly described for the basin. Agriculture is the main economic activity and the drainage basin is used to produce power electricity (10,473 megawatt – 12% of the national production) (ANA, 2017).

3 General methodological aspects

3.1 Sampling and preparation of the samples

For the analyses performed on foraminiferal tests of marine sediment core M125-95-3, i.e., ^{14}C ages, $\delta^{18}O$ and $\delta^{13}C$ analyses, and Mg/Ca analyses, the following steps were executed:

- Sampling of marine sediment core M125-95-3 with syringes of 10 cm^3;
- Measurement of the samples weight (humid weight), oven-drying at 50 °C for 24 hours, and new weight measurement (dry weight);
- Addition of sodium tetraborate solution and resting for a few minutes;
- Wet-sieving with sieves of 63 and 125 μm;
- Oven-drying at 50 °C of the material retained in the sieves for 24 hours;
- Hand-picking under a binocular microscope of the planktonic and benthic foraminifera species.

For the XRF core scanner analyses performed on marine sediment core M125-95-3, u-channels of 105 cm length (2 cm width, 2 cm depth) were sampled.

For the conventional XRF analyses performed on marine sediment core M125-95-3, the following steps were executed:

- Sampling of marine sediment core M125-95-3 with syringes of 10 cm^3;
- Measurement of the samples weight (humid weight), oven-drying at 50 °C for at least 24 and maximally 48 hours, and new weight measurement (dry weight);
- Hand-grinding of the samples with an agate mortar;
- Compression of the homogenized material in specific capsules.

3.2 Age model

Radiocarbon dating (^{14}C) is the most used method for establishing chronological models in paleoceanography and paleoclimatology studies of the last ca. 40 ka. The age of a fossil sample can be identified by the measurement of its ^{14}C content, considering that the initial ^{14}C concentration as well as the half-life of the ^{14}C are known. After correction for reservoir effect (BARD, 1988) and calibration for past changes in the atmospheric ^{14}C concentration (REIMER et al., 2013), the resulting ^{14}C of a marine fossil sample can be used to establish accurate age models for sedimentary sequences as well as to identify sedimentation rates.

Here, the radiocarbon ages were based on the ^{14}C content of planktonic foraminiferal tests. Foraminifera are marine unicellular microorganisms (protozoan) which are one of the main components of marine carbonates. Since they are an important tool to reconstruct past marine environmental changes, their use in paleoceanography and paleoclimatology studies is

extensive. The advantages of the use of foraminifera are related to the marked abundance in marine sediments, the excellent preservation of their tests in the sedimentary record and their known habitat (ROHLING; COOKE, 1999).

To extend the age model beyond the radiocarbon method limit (i.e., ca. 40 ka), we used benthic foraminifera $\delta^{18}O$ as a stratigraphic tool (section 3.4) (LISIECKI; RAYMO, 2005).

3.3 X-ray fluorescence analyses

Events of marked precipitation over the continent are frequently related to increased fluvial discharge and consequent erosion and transport of terrigenous sediments from their source areas (e.g., São Francisco River drainage basin) to their final depositional sites (e.g., western tropical South Atlantic). Additionally, changes in sea level also influence the delivery of terrigenous sediments to the final depositional sites, i.e., lower (higher) sea level is related to increased (decreased) delivery of terrigenous sediments to the continental slope.

Therefore, the presence of layers enriched in terrigenous elements in marine sediments may indicate major events of erosion and transport of terrigenous sediments from the continent to the ocean suggesting increased humidity over the continent and/or low sea level (the opposite rationale occurs when layers are enriched in biogenic carbonate) (ARZ et al., 1998; CHIESSI et al., 2009; VOIGT et al., 2013; ZHANG et al., 2015). Furthermore, terrigenous elements that reflect chemical weathering can also be used as a proxy for precipitation changes in tropical regions since the more intense is the precipitation the more intense is the chemical weathering (CHIESSI et al., 2010; GOVIN et al., 2012; MULITZA et al., 2008).

Precipitation reconstructions based on marine archives are particularly useful since they are able to capture hydroclimate signals that are integrated over whole drainage basins avoiding local signals that could bias paleoclimate reconstructions.

3.4 Stable oxygen and carbon isotopic analyses in foraminiferal tests

Since most foraminiferal species calcify its carbonate test near to equilibrium with the ambient seawater, the isotopic ratios of foraminiferal tests record the isotopic ratios of the ambient seawater during the carbonate precipitation (ROHLING; COOKE, 1999). Thus, foraminiferal tests are used as carriers of the $\delta^{18}O$ and $\delta^{13}C$ signals of the water masses where they calcify (CHIESSI et al., 2007; ROHLING; COOKE, 1999).

We worked with three foraminifera species (CLÉROUX et al., 2013; LUTZE, 1986; STEPH et al., 2009): (i) *Globigerinoides ruber* pink, mixed layer planktonic species that calcifies at ca. 30 m; (ii) *Cibicidoides pachyderma*, epifaunal species that calcifies on the sediment in the

bottom of the water column; and (iii) *Uvigerina* spp., shallow infaunal species that calcifies at the water-sediment interface in the bottom of the water column (CLÉROUX et al., 2013; STEPH et al., 2009).

The $\delta^{18}O$ of foraminiferal tests reflects the temperature and the $\delta^{18}O$ of the sea water ($\delta^{18}O_{sw}$) where the tests calcified (the last is directly related to salinity) (DUPLESSY et al., 1988; EMILIANI, 1955). While temperature and $\delta^{18}O$ of foraminifera are negatively correlated, $\delta^{18}O_{sw}$ and $\delta^{18}O$ of foraminifera are positively correlated, so that higher temperatures decrease $\delta^{18}O$ of foraminifera, whereas higher salinities increase $\delta^{18}O$ of foraminifera (ROHLING; COOKE, 1999). Planktonic foraminifera $\delta^{18}O$ was used to constrain past changes in SST and sea surface salinity (SSS) (coupled with Mg/Ca analyses, see section 3.5) (DUPLESSY et al., 1991; EMILIANI, 1955), while benthic foraminifera $\delta^{18}O$ was used as a stratigraphic tool (LISIECKI; RAYMO, 2005) allowing the construction of an age model for marine sediment core M125-95-3 (coupled with ^{14}C dating, section 3.2).

The $\delta^{13}C$ of foraminiferal tests reflects the $\delta^{13}C$ of dissolved inorganic carbon ($\delta^{13}C_{DIC}$) which is related to the nutrient content and largely follows water mass structure and circulation (HOWE et al., 2016; KROOPNICK, 1985). Benthic foraminifera $\delta^{13}C$ were used to track past changes in bottom waters structure and circulation.

3.5 Mg/Ca analyses in planktonic foraminifera

Mg/Ca values from tests of foraminifera are a well-established paleotemperature indicator (ANAND et al., 2003; CRIVELLARI et al., 2019; LEA et al., 1999; NÜRNBERG et al., 1996), particularly useful in the reconstruction of SST through the analyses of foraminifera that dwell in the uppermost water column.

The main advantage of foraminiferal Mg/Ca paleothermometry is that both the temperature estimation through Mg/Ca and the analysis of $\delta^{18}O$ are obtained from tests of the same fossil organism (GROENEVELD; CHIESSI, 2011). Thus, since (i) planktonic foraminiferal $\delta^{18}O$ is controlled by SST and $\delta^{18}O_{sw}$ (a proxy for SSS) and (ii) *G. ruber* pink (the species used here) Mg/Ca has small sensitivity to changes in salinity (i.e., 3.3 +/- 1.7% per salinity unit) (HÖNISCH et al., 2013), Mg/Ca values represent a powerful tool to decouple the temperature and salinity effect on $\delta^{18}O$ records, allowing the identification of individual estimates for each parameter (GROENEVELD; CHIESSI, 2011).

Several cleaning steps are required in the preparation of the tests of foraminifera to Mg/Ca analyses in order to remove possible contamination, which, if not done, can significantly alter

the reconstructed temperature (BARKER et al., 2003). To convert Mg/Ca ratios into SST we used the calibration equation for *G. ruber* pink from REGENBERG et al. (2009) [Mg/Ca = 0.23 exp (0.111 * SST)].

4 A new mechanism for millennial scale positive precipitation anomalies over tropical South America

Marília C. Campos[a*], Cristiano M. Chiessi[a], Matthias Prange[b], Stefan Mulitza[b], Henning Kuhnert[b], André Paul[b], Igor M. Venancio[c], Ana Luiza S. Albuquerque[d], Francisco W. Cruz[e], André Bahr[f]

[a] School of Arts, Sciences and Humanities, University of São Paulo, São Paulo, Brazil

[b] MARUM – Center for Marine Environmental Sciences, University of Bremen, Bremen, Germany

[c] Center for Weather Forecasting and Climate Studies (CPTEC), National Institute for Space Research (INPE), Cachoeira Paulista, Brazil

[d] Graduate Program in Geochemistry, Fluminense Federal University, Niterói, Brazil

[e] Institute of Geosciences, University of São Paulo, São Paulo, Brazil

[f] Institute of Earth Sciences, Heidelberg University, Heidelberg, Germany

* Corresponding author: marilia.carvalho.campos@usp.br

Published in *Quaternary Science Reviews* (2019) 225, 105990

(https://doi.org/10.1016/j.quascirev.2019.105990)

4.1 Abstract

Continental and marine paleoclimate archives from northwestern and northeastern South America recorded positive precipitation anomalies during Heinrich Stadials (HS). These anomalies have been classically attributed to enhanced austral summer (monsoon) precipitation. However, the lack of marine paleoclimate records off eastern South America as well as inconsistencies between southeastern South American continental and marine records hamper a comprehensive understanding of the mechanism responsible for (sub-) tropical South American hydroclimate response to HS. Here we investigate piston core M125-95-3 collected off eastern South America (10.94°S) and simulate South American HS conditions with a high-resolution version of an atmosphere-ocean general circulation model. Further, meridional changes in precipitation over (sub-) tropical South America were assessed with a thorough compilation of previously available marine paleorecords. Our ln(Ti/Ca) and ln(Fe/K) data show increases during HS6-Younger Dryas. It is the first core off eastern South America and the southernmost from the Atlantic continental margin of South America that unequivocally records HS-related positive precipitation anomalies. Based on our new data, model results and

the compilation of available marine records, we propose a new mechanism for the positive precipitation anomalies over tropical South America during HS. The new mechanism involves austral summer precipitation increases only over eastern South America while the rest of tropical South America experienced precipitation increases during the winter, challenging the widely held assumption of a strengthened monsoon. South American precipitation changes were triggered by dynamic and thermodynamic processes including a stronger moisture supply from the equatorial North Atlantic (tropical South Atlantic) in austral winter (summer).

4.2 Introduction

Reductions in the Atlantic meridional overturning circulation (AMOC) cross-equatorial heat transport associated with Heinrich Stadials (HS) affected South American hydroclimate (ARZ et al., 1998; KAGEYAMA et al., 2013). The mechanism usually invoked to explain HS precipitation anomalies over South America includes an enhanced South American monsoon system (SAMS), a southward migration of the Intertropical Convergence Zone (ITCZ) and an intensification of the South Atlantic Convergence Zone (SACZ) (KANNER et al., 2012; PETERSON et al., 2000; STRÍKIS et al., 2015).

Continental paleoclimate records from northern (N) South America (e.g., ZULAR et al., 2019) show negative precipitation anomalies during HS that are supported by model simulations (KAGEYAMA et al., 2013; MOHTADI et al., 2016). Positive precipitation anomalies over northwestern (NW) (e.g., BAKER et al., 2001; KANNER et al., 2012), northeastern (NE) (e.g., CRUZ et al., 2009; LEDRU et al., 2006), and eastern (E) (e.g., STRÍKIS et al., 2018; WANG et al., 2004) South America during HS are equally supported by model results (KAGEYAMA et al., 2013; MOHTADI et al., 2016). On the other hand, some continental paleoclimate records from southeastern (SE) South America (CRUZ et al., 2007; WANG et al., 2006) suggest positive precipitation anomalies during HS, but are not supported by model simulations, which suggest no or even negative changes in precipitation (KAGEYAMA et al., 2013; MOHTADI et al., 2016).

Marine paleoclimate records from the Atlantic continental margin of South America agree with model simulations and suggest negative precipitation anomalies over N South America (e.g., BAHR et al., 2018; DEPLAZES et al., 2013), positive precipitation anomalies over NW (e.g., CRIVELLARI et al., 2018; ZHANG et al., 2017) and NE (e.g., ARZ et al., 1998; MULITZA et al., 2017) South America and no major changes in precipitation over SE South America (e.g., BEHLING et al., 2002; GU et al., 2017) during HS. So far, no marine paleoclimate record covering the late Quaternary is available between ca. 7°S and 20°S off E South America.

The inconsistency between continental and marine paleoclimate records from SE South America together with the lack of marine records off E South America hamper the validation of the proposed mechanism behind (sub-) tropical South American hydroclimate response to HS.

Here we reduce the gap of marine paleoclimate records between 7°S and 20°S by investigating piston core M125-95-3 collected at 10.94°S (Fig. 4.1a). Our core site is influenced by the terrigenous discharge of the São Francisco River and recorded the hydroclimate history of E South America for the last ca. 70 ka. To reconstruct changes in precipitation over the São Francisco River drainage basin we determined the major elemental intensity along the piston core. In order to investigate meridional changes in precipitation over (sub-) tropical South America we performed a thorough compilation of available marine paleoclimate records. To scrutinize the mechanism responsible for hydroclimate changes, we performed a HS simulation with a high-resolution version of the atmosphere-ocean general circulation model CCSM3 (COLLINS et al., 2006).

Based on the combination of data from our core, the compilation of marine paleoclimate records and the model results we propose a new mechanism responsible for the last glacial HS positive precipitation anomalies over tropical South America to the south of the equator. The new mechanism involves dynamic and thermodynamic processes and shows an austral winter (summer) equatorial North Atlantic (tropical South Atlantic) moisture flux contributing to wetter conditions over NW South America (E South America) during HS.

4.3 Regional setting

During austral summer (winter), the main source of moisture for tropical South America is the North Atlantic (South Atlantic) via prevailing NE trade winds (SE trade winds). The austral summer NE trade winds moisture transport allows the development of the SAMS, whose convective rains are responsible for more than 50% of the total annual precipitation over tropical South America to the east of the Andes (ZHOU; LAU, 1998). The onset of the SAMS occurs during austral spring (October), reaching its mature phase during the austral summer (December-February) with intense convection over the southern Amazon basin, and demising during austral fall (April) (MARENGO et al., 2001).

The ITCZ and the SACZ are important phenomena in South American hydroclimate, both related to the SAMS. The ITCZ can be understood as a global convective belt over the oceans associated to the ascending branch of the Hadley cell and to the convergence of the NE and SE trade winds. In order to compensate the AMOC's northward cross-equatorial heat transport, the

ITCZ mean latitudinal position is around 5°N (MARSHALL et al., 2014). The ITCZ shifts seasonally towards the summer hemisphere, following the highest sea surface temperatures (SST) (SCHNEIDER et al., 2014). It is believed that the southward migration of the ITCZ can induce periods of enhanced SAMS (VUILLE et al., 2012). The SACZ can be understood as a NW-SE elongated convective belt that typically originates in the western Amazon basin in early August and extends southeastwards above SE South America, frequently reaching the adjacent western South Atlantic (CARVALHO et al., 2004). During intense (weak) phases and, thus, enhanced (reduced) SAMS, the SACZ is displaced northwards (southwards) promoting a decrease in precipitation over SE South America south (north) of ca. 25°S (ROBERTSON; MECHOSO, 2000).

Despite the SAMS/SACZ influence, SE South America shows no marked seasonality, and year-round precipitation has two distinct sources: while the SAMS is the source for austral summer/early autumn precipitation, the extratropical South Atlantic is the precipitation source for the winter/early spring (ZHOU; LAU, 1998).

Northern Hemisphere SST anomalies also play a fundamental role in South American hydroclimate by influencing the strength of the SAMS, where negative (positive) SST anomalies are related to a strong (weak) SAMS (TALENTO; BARREIRO, 2018). In addition, positive SST anomalies in the western South Atlantic have been correlated to increased SACZ precipitation (CHAVES; NOBRE, 2004).

The São Francisco River drainage basin is the source of terrigenous sediments to our core site. It is the largest drainage basin in E South America (Fig. 4.1a). Most of the drainage basin shows a semi-arid climate but its headlands show humid conditions due to the influence of the SACZ, where most of the precipitation occurs during the austral summer. Its annual-mean water discharge is around 2980 m^3/s (DOMINGUEZ, 1996). Additionally, other five South American drainage basins are depicted in Fig. 4.1a and will be discussed herein. They are the Amazon (ca. 200000 m^3/s; LENTZ (1995)), Parnaíba (ca. 640 m^3/s; KNOPPERS et al. (1999)), Doce (ca. 624.4 m^3/s; OLIVEIRA and DA SILVA QUARESMA (2017)), Itajaí (ca. 230 m^3/s; SCHETTINI (2002)) and La Plata (ca. 21000 m^3/s; BERBERY and BARROS (2002)) River drainage basins.

The marine records compiled herein were collected from the Atlantic continental margin off South America. At this portion of the western Atlantic, the upper water column (down to ca. 500 m water depth) is influenced by the northward flowing North Brazil Current and southward flowing Brazil Current, both originating at 10-14°S (PETERSON; STRAMMA, 1991; STRAMMA; ENGLAND, 1999). Between ca. 500 and 1200 m water depth, the western

Atlantic is dominated by a northward and a southward flowing branch of the Intermediate Western Boundary Current originating at ca. 25°S (STRAMMA; ENGLAND, 1999). The Deep Western Boundary Current flows southwards between ca. 1200 and 4000 m water depth (STRAMMA; ENGLAND, 1999). It is noteworthy that the southwestern South Atlantic presents regions of strong bottom current activity (e.g., FAUGÈRES; STOW, 1993) that could bias the climatic signal of the SE South American cores compiled here (BEHLING et al., 2002; CAMPOS et al., 2019a; GU et al., 2017). However, contouritic deposits in this region (DUARTE; VIANA, 2007) are only present at deeper water depths and hence do not affect the compiled marine cores.

4.4 Material and methods

4.4.1 Marine sediment core

We investigated piston core M125-95-3 (10.94°S, 36.20°W, 1897 m water depth, 10.4 m core length) collected from the continental slope off E South America near the São Francisco River mouth during RV Meteor cruise M125 (BAHR et al., 2016) (Table 4.1; Fig. 4.1a). Since our focus relies on the abrupt millennial scale events (i.e., HS) of the last glacial (i.e., Marine Isotope Stages (MIS) 4-2), we analyzed the uppermost ca. 7.4 m of the piston core that covers the last ca. 70 ka.

We further compiled paleoclimate data from other 13 marine sediment cores collected from the Atlantic continental margin of South America spanning from 11.62°N to 32.69°S (Table 4.1; Fig. 4.1a).

Figure 4.1 - **(a)** Location of piston core M125-95-3 (this study, brown diamond) and previously published marine paleoclimate records (circles) discussed herein (see Table 4.1 for more information). Green, blue and red rectangles show the selected regions for the computation of spatially averaged precipitation anomalies representing different (simplified) South American drainage basins (outlined and labeled in black). Panels **(b)-(g)** show simulated Heinrich Stadial 1 (HS1) minus Last Glacial Maximum (LGM) monthly-mean precipitation (red and blue filling) and HS1 minus LGM annual-mean precipitation (grey dashed line) with 2σ standard error (grey envelope) (mm/day) for the **(b)** Amazon River drainage basin (northwestern (NW) South America), **(c)** Parnaíba River drainage basin (northeastern (NE) South America), **(d)** São Francisco River drainage basin (eastern (E) South America), **(e)** Doce River drainage basin (southeastern (SE) South America), **(f)** Itajaí River drainage basin (SE South America), and **(g)** La Plata River drainage basin (SE South America). In the annual-mean, anomalies of rivers **(e)-(g)** are not significant at the 0.05 significance level. Model experiments were performed with CCSM3 (COLLINS et al., 2006; PRANGE et al., 2015). This figure was partially produced with Ocean Data View (SCHLITZER, 2017).

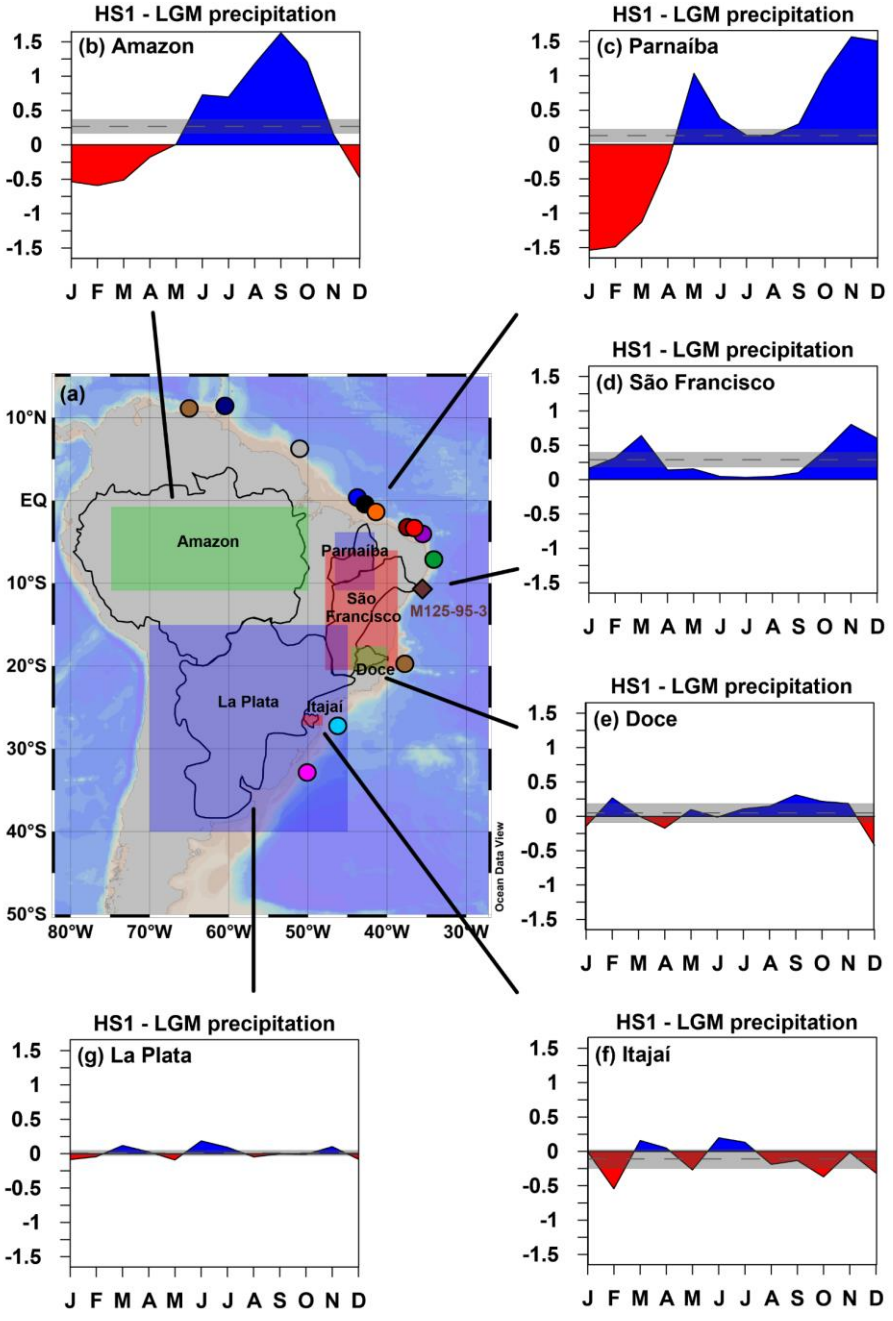

Table 4.1. Marine sediment cores from northern (N), northwestern (NW), northeastern (NE), eastern (E) and southeastern (SE) South America investigated in this study.

Core ID	Region	Latitude	Longitude	Water depth (m)	Reference
M78/1-235-1	N South America	11.62˚N	60.97˚W	852	Bahr et al. (2018) and Poggemann (2018)
MD03-2621	N South America	10.68˚N	64.97˚W	847	Deplazes et al. (2013)
GeoB16224-1	NW South America	6.66˚N	52.08˚W	2510	Zhang et al. (2017)
CDH86	NE South America	0.33˚N	44.20˚W	3107	Nace et al. (2014)
GL1248	NE South America	0.92˚S	43.40˚W	2264	Venancio et al. (2018)
GeoB16202-2	NE South America	1.91˚S	41.59˚W	2248	Mulitza et al. (2017)
GeoB3104-1	NE South America	3.67˚S	37.72˚W	767	Arz et al. (1998)
GeoB3912-1	NE South America	3.67˚S	37.72˚W	772	Arz et al. (1998)
GeoB3910-2	NE South America	4.25˚S	36.35˚W	2362	Jaeschke et al. (2007)
GeoB3176-1	NE South America	7.01˚S	34.44˚W	1385	Arz et al. (1999)
M125-95-3	E South America	10.94˚S	36.20˚W	1897	this study
GeoB3229-2	SE South America	19.64˚S	38.72˚W	780	Behling et al. (2002)
GeoB2107-3	SE South America	27.18˚S	46.45˚W	1048	Gu et al. (2017)
GeoB6212-1	SE South America	32.69˚S	50.11˚W	1010	Campos et al. (2019)

4.4.2 Age model

The chronology of piston core M125-95-3 is based on nine planktonic foraminifera accelerator mass spectrometry (AMS) radiocarbon ages and three benthic foraminifera oxygen isotopic composition ($\delta^{18}O$) tie-points aligned to a benthic $\delta^{18}O$ reference curve from GOVIN et al. (2014) (Table 4.2; Fig. 4.2).

For every radiocarbon sample we hand-picked under a binocular microscope ca. 10 mg of fossil tests of planktonic foraminifera *Globigerinoides ruber* from the sediment fraction larger than 150 μm. In the absence of enough *G. ruber* tests, radiocarbon samples were completed with other planktonic foraminifera species. Samples were analyzed at the Beta Analytic Radiocarbon Dating Laboratory, USA (Table 4.2). Radiocarbon ages were calibrated with the IntCal13 curve (REIMER et al., 2013) with a variable simulated reservoir age from the transient modelling experiments in BUTZIN et al. (2017). Reservoir age and 1σ uncertainty of the simulated radiocarbon was assigned from the nearest gridbox to our core location and corresponding to

our measured radiocarbon age range. Three age reversals at 100, 144, and 154 cm were not included in the age model and may be due to bioturbation bringing younger material to greater depths. Radiocarbon ages cover the uppermost 452 cm (ca. 40 ka before present (BP)) of our core.

Table 4.2. Accelerator mass spectrometer radiocarbon ages and tie-points aligned to reference curve MD95-2042 (GOVIN et al., 2014) used to construct the age model of piston core M125-95-3.

Depth (cm)	Lab ID	Radiocarbon age ± 1σ error (a BP)	Calibrated age (cal a BP)	Tie-point age ± estimated error (a BP)
6	462829	1940 ± 30	1472	
54	479391	8390 ± 30	8892	
84	490135	12270 ± 30	13638	
100	462830	8310 ± 40	*	
144	490136	10700 ± 30	*	
154	479392	7360 ± 30	*	
200	462831	17820 ± 60	20701	
254	479393	21440 ± 60	24816	
308	490137	25160 ± 90	28443	
340	462832	27620 ± 150	30898	
400	462833	32170 ± 220	35372	
452	479395	35180 ± 230	39087	
498				47000 ± 2141
582				59300 ± 2049
738				71100 ± 2137

* Radiocarbon age reversals that were not included in the age model.

We performed $\delta^{18}O$ analyses on 142 samples of benthic foraminifera *Uvigerina* spp. Around 10 *Uvigerina* spp. specimens per sample were handpicked under a binocular microscope from the sediment fraction larger than 125 μm. Analyses were conducted with a gas isotope ratio mass spectrometer (Finnigan MAT252) coupled to an automated carbonate preparation device (Kiel III) at the MARUM – Center for Marine Environmental Sciences, University of Bremen,

Germany. Output data were calibrated against an in-house standard (Solnhofen limestone) that is itself calibrated against the NBS19 standard. Results are reported in per mil (parts per thousand, i.e., ‰) versus Vienna Pee Dee Belemnite (VPDB). Standard deviation of in-house standard replicate measurements was 0.06‰ for the measured period. The three tie-points are based on the alignment of M125-95-3 *Uvigerina* spp. $\delta^{18}O$ to a reference curve from GOVIN et al. (2014) (details regarding the tie-points can be found in supplementary material Table 4.S1 and Fig. 4.S1).

The age model was performed with the software PaleoDataView v. 0.8.3.4 (LANGNER; MULITZA, 2019) using the age modelling tool BACON v. 2.2 (BLAAUW; CHRISTEN, 2011). Default parameter settings were used, except for mem.mean (set to 0.4) and mean.strength (set to 4). 10,000 realizations and a t-distribution with 9 degrees of freedom (t.a=9, t.b=10) were applied. All ages are reported as years (a) BP (present is 1950 AD).

Figure 4.2 - Age model (black dashed line and enveloping curves) and sedimentation rates (grey line) for piston core M125-95-3 produced with software PaleoDataView v. 0.8.3.4 (LANGNER; MULITZA, 2019) using the age modelling tool BACON v. 2.2 (BLAAUW; CHRISTEN, 2011). For the age model, the black (orange) squares depict calibrated radiocarbon ages (tie-points), the dashed line depicts median ages, and the upper (lower) black line depicts maximum (minimum) ages. Open crossed squares are age reversals.

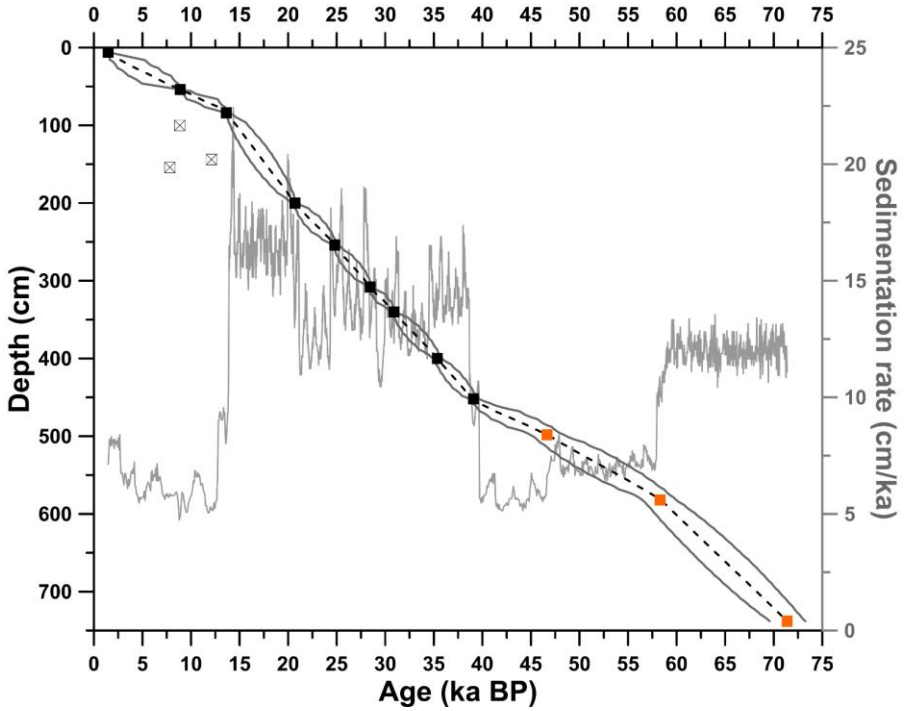

4.4.3 Major element composition

X-ray fluorescence (XRF) core scanner data were collected every 5 mm down-core over a 0.6 cm^2 area with down-core slit size of 5 mm using generator settings of 10 kV, a current of 0.065

mA and a sampling time of 8 seconds. Analyses were performed at the surface of u-channels sampled from the archive half of piston core M125-95-3. We used the XRF Core Scanner III (AVAATECH Serial No. 12) at the MARUM – Center for Marine Environmental Sciences, University of Bremen, Germany. The surface of the u-channels was covered with a 4 μm thin SPEXCerti Prep Ultralene1 foil to avoid contamination of the XRF measurement unit and desiccation of the sediment. The herein reported data have been acquired by a SGX Sensortech Silicon Drift Detector (Model SiriusSD® D65133Be-INF with 133eV X-ray resolution), a Topaz-X High- Resolution Digital MCA and an Oxford Instruments 100W Neptune X-Ray tube with rhodium (Rh) target material. Raw data were processed by the analysis of X-ray spectra by iterative least square software (WIN AXIL) package from Canberra Eurisys.

Dried and homogenized powder samples analyzed via energy dispersive polarized XRF (EDP-XRF) has been proven useful to verify XRF core scanner elemental intensities in an efficient way (TJALLINGII et al., 2007). Thus, we also analyzed elemental concentrations by EDP-XRF on bulk sediment samples from the working half every 20 cm. Around 10 cm^3 of sample were freeze-dried and homogenized with a hand agate mortar. We replicated 10% of the samples in order to check the efficiency of the sample preparation and the equipment reproducibility (sd: 2.7% Ca; 2.6% Ti; 3.2% Fe; 1.8% K). Analyses were performed at the Fluminense Federal University, Brazil.

In order to capture changes in the input of terrigenous inorganic sediments to our core site (and, thus, precipitation over São Francisco River drainage basin) as well as changes in chemical weathering over the São Francisco River drainage basin we use ln(Ti/Ca) and ln(Fe/K), respectively (GOVIN et al., 2012; MULITZA et al., 2008). The less commonly used ln(Fe/K) ratio is based on the different mobility of both elements during chemical weathering. Since potassium is much more mobile than iron, high ln(Fe/K) values indicate intense chemical weathering.

4.4.4 Climate model experiment

We analyzed the results from a freshwater hosing experiment (0.2 Sv injected into the northern North Atlantic for 400 years resulting in a ~50% weakening of the AMOC from about 12 Sv to 6 Sv) conducted under full Last Glacial Maximum (LGM) background climatic conditions (following the protocol of the Paleoclimate Modelling Intercomparison Project Phase 2, for details see EROKHINA et al. (2017)) mimicking HS1 (PRANGE et al., 2015). The atmosphere-ocean general circulation model CCSM3 (COLLINS et al., 2006) in the high-resolution version T85 (1.4° atmosphere transform grid; ocean grid resolution nominal 1°) was used. Therefore,

the model resolution used in this study is much higher than in previous LGM hosing studies; e.g., in the multi-model study by KAGEYAMA et al. (2013) atmospheric grid resolutions ranged from T21 (5.6° transform grid) to T42 (2.8° transform grid). Analysis is based on annual-mean and seasonal-mean (extended austral summer, November-March; extended austral winter, May-September) climatologies calculated from 50-year averages. Additionally, we calculated the monthly-mean precipitation differences (HS1 minus LGM) for the Amazon, Parnaíba, São Francisco, Doce, Itajaí and La Plata River drainage basins (simplified catchment areas depicted in Fig. 4.1a).

4.5 Results

4.5.1 Age model

The uppermost 7.4 m of core M125-95-3 covers the last ca. 70 ka, i.e., since MIS4, with a mean sedimentation rate of 11.9 cm/ka (Fig. 4.2). The lowest sedimentation rate (4.7 cm/ka) occurs within the early MIS1 (ca. 8.8 ka BP) while the highest value (22.4 cm/ka) was recorded within MIS2 (ca. 14.4 ka BP) (Fig. 4.2).

4.5.2 Oxygen isotopic composition of benthic foraminifera

Uvigerina spp. $\delta^{18}O$ ranges from 2.63 to 5.02‰ (Fig. 4.3c). The lowest value occurs during the late Holocene around 3.4 ka BP (MIS1) while the highest value occurs during the LGM around 19.3 ka BP (MIS2). The final stage of the glacial inception, i.e., the transition from MIS5a to MIS4, is located at the base of our record around 70 ka BP. MIS4 is marked by a gradual decrease in $\delta^{18}O$ values that peaks around 59 ka BP. During MIS3, relative low values around 47 ka BP are coeval with HS5. MIS2 shows a gradual trend towards higher $\delta^{18}O$ values. The last deglaciation is marked by two major sharp decreases in $\delta^{18}O$ around 18.4 and 11.5 ka BP, synchronous (within age model uncertainties) to HS1 and the Younger Dryas (YD).

4.5.3 Major element composition

XRF core scanner ln(Ti/Ca) values (expressed as count ratios) vary between -3.88 and 1.46 (Fig. 4.3b). Positive peaks during MIS4-2 are coeval with HS of the last glacial (i.e., HS6-YD), while the lowest values occur during the early Holocene. XRF core scanner ln(Fe/K) values range from 1.23 to 2.47 and the highest values occur during MIS1 (around the YD) (Fig. 4.3a). ln(Fe/K) values also increase during HS, but increases show lower relative magnitude compared to increases in ln(Ti/Ca). EDP-XRF ln(Ti/Ca) values vary between -3.83 and 0.51 (Fig. 4.3b)

and EDP-XRF ln(Fe/K) between 1 and 1.36 (Fig. 4.3a). XRF core scanner and EDP-XRF values show similar trends.

Figure 4.3 - Isotopic and geochemical records from piston core M125-95-3 for the last ca. 70 ka. **(a)** X-ray fluorescence (XRF) core scanner ln(Fe/K) (purple line; the axis was broken from 2.2 to 2.4) and energy dispersed polarized (EDP) XRF ln(Fe/K) (grey circles); **(b)** XRF core scanner ln(Ti/Ca) (brown line) and EDP-XRF ln(Ti/Ca) (grey circles); and **(c)** *Uvigerina* spp. stable oxygen isotopic composition ($\delta^{18}O$). Black (orange) squares at the bottom of the panel depict calibrated radiocarbon ages (tie-points) with 2σ standard error. Pink vertical bars represent abrupt millennial scale events Younger Dryas (YD) and Heinrich Stadial (HS) 1 to 6. Marine Isotope Stages (MIS) are depicted below the upper axis.

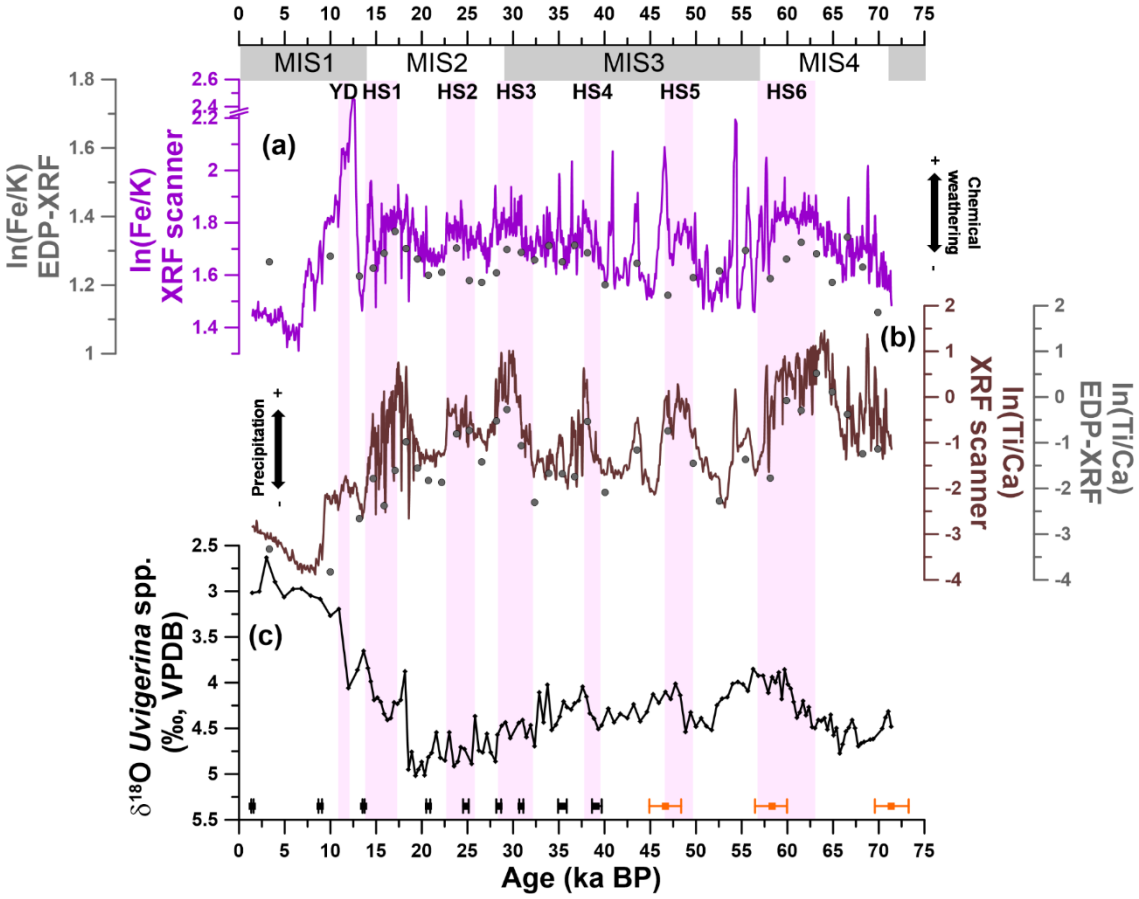

4.5.4 Climate model experiment

Annual-mean HS1 minus LGM precipitation (Fig. 4.4a) shows positive anomalies over most of tropical South America except for N South America, which exhibits negative anomalies. SE South America shows no major change in precipitation. Seasonal-mean HS1 minus LGM precipitation (Fig. 4.4b-c) shows a southward shifted ITCZ and a meridional rainfall anomaly dipole over tropical South America, during both austral summer and winter. The dipole pattern is restricted to E South America between ca. 0° and 20°S during austral summer, and shifts further north, about the equator between ca. 10°N and 10°S, during austral winter. SE South

America, in turn, shows no major change in precipitation in either season except for an austral summer negative anomaly over its western portion.

Figure 4.4 - Heinrich Stadial (HS) 1 minus Last Glacial Maximum (LGM) precipitation simulated with CCSM3. **(a)** Annual-mean, **(b)** extended austral summer (i.e., November-March (NDJFM)), and **(c)** extended austral winter (i.e., May-September (MJJAS)) rainfall.

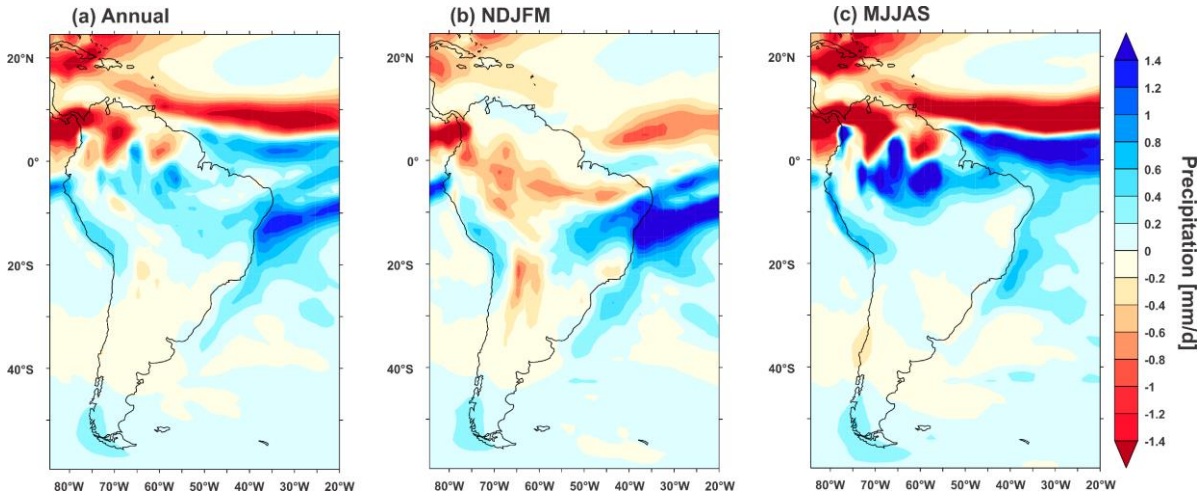

Seasonal-mean HS1 minus LGM surface temperature (Fig. 4.5a-b) shows, in general, negative (positive) anomalies in the Northern Hemisphere (Southern Hemisphere) during both seasons. Seasonal-mean HS1 minus LGM total precipitable water (Fig. 4.5c-d) shows strong negative (positive) anomalies over the North Atlantic (South Atlantic) also during both seasons, thermodynamically linked to temperature anomalies. In addition, during austral summer (Fig. 4.5c), there are negative (positive) anomalies in precipitable water over N, NW and SE (NE and E) South America. During austral winter (Fig. 4.5d), on the other hand, a widespread positive anomaly in precipitable water dominates tropical South America to the south of the equator. The HS1 minus LGM low level circulation (i.e., 900 hPa) (Fig. 4.5a-b) shows wind anomalies with a northerly component over tropical South America during both seasons. Austral summer HS1 minus LGM moisture transport (Fig. 4.5c) shows an anomalous cyclonic pattern over E South America resulting in enhanced ocean-continent moisture transport south of ca. 15°S. During austral winter (Fig. 4.5d), more moisture from the equatorial Atlantic enters tropical South America. Absolute moisture transport for the LGM is shown in the supplementary material (Fig. 4.S2).

Monthly-mean HS1 minus LGM precipitation over the drainage basins depicted in Fig. 4.1a indicates that the Amazon (i.e., 0.27 +/- 0.10 mm/day), Parnaíba (i.e., 0.13 +/- 0.10 mm/day) and São Francisco (i.e., 0.29 +/- 0.11 mm/day) River drainage basins experience marked positive precipitation anomalies, while the Doce (i.e., 0.05 +/- 0.14 mm/day), Itajaí (i.e., -0.11

+/- 0.14 mm/day) and La Plata (i.e., 0.01 +/- 0.04 mm/day) River drainage basins show no significant differences (Fig. 4.1b-g). We note that the magnitude of the modeled precipitation anomalies may depend on the strength of the AMOC perturbation.

Figure 4.5 - Heinrich Stadial (HS) 1 minus Last Glacial Maximum (LGM) seasonal-mean surface temperature and total precipitable water along with 900 hPa winds (m/s) and vertically integrated moisture transport (kg/(m·s)) simulated with CCSM3. **(a)** Extended austral summer (i.e., November-March (NDJFM)) surface temperature and 900 hPa wind; **(b)** extended austral winter (i.e., May-September (MJJAS)) surface temperature and 900 hPa wind; **(c)** extended austral summer (i.e., NDJFM) precipitable water and moisture transport; and **(d)** extended austral winter (i.e., MJJAS) precipitable water and moisture transport. Only every 2nd vector in each direction is plotted.

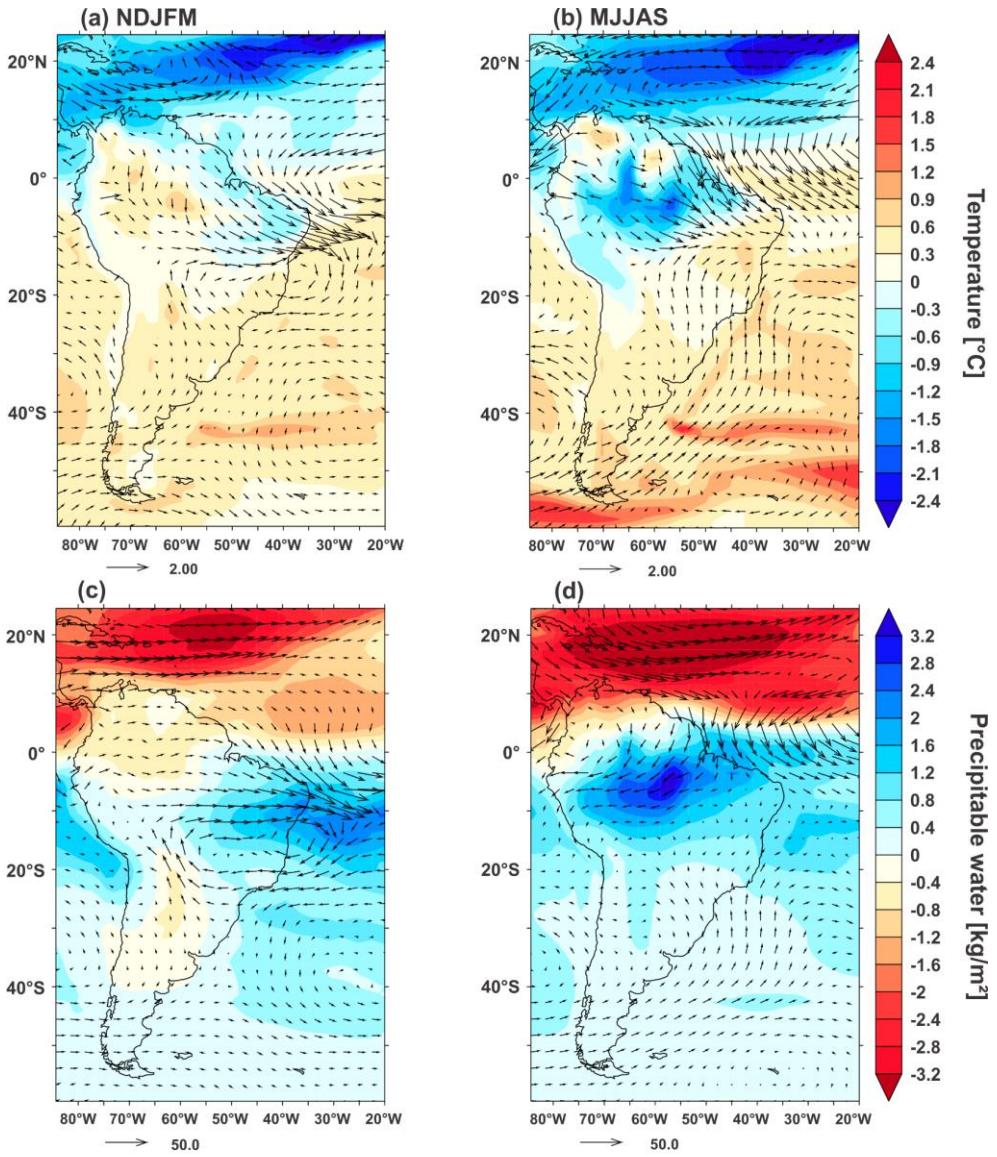

4.6 Discussion

4.6.1 The marine paleoclimate record of changes in precipitation over (sub-) tropical South America during HS

Marine paleoclimate archives consistently recorded tropical precipitation changes during last glacial HS over N (BAHR et al., 2018; DEPLAZES et al., 2013), NW (ZHANG et al., 2017) and NE (ARZ et al., 1998; 1999; JAESCHKE et al., 2007; MULITZA et al., 2017; NACE et al., 2014; VENANCIO et al., 2018) South America (Fig. 4.6a-j). These archives recorded the response of fluvial discharge to changes in precipitation over specific drainage basins. During HS, they suggest dry conditions over N South America (BAHR et al., 2018; DEPLAZES et al., 2013) and wet conditions over NW (ZHANG et al., 2017) and NE (ARZ et al., 1998; 1999; JAESCHKE et al., 2007; MULITZA et al., 2017; NACE et al., 2014; VENANCIO et al., 2018) South America. This pattern agrees with a previously suggested southward migration of the ITCZ and tropical rain belt (e.g., BROCCOLI et al., 2006; SCHNEIDER et al., 2014) that is corroborated by our simulated HS1 minus LGM annual-mean precipitation pattern (Fig. 4.4a). Additionally, our monthly-mean HS1 minus LGM precipitation results (Fig. 4.1b-c) further support the positive precipitation anomalies suggested for the Amazon and Parnaíba River drainage basin cores (Fig. 4.6c-f).

On the other hand, marine paleoclimate archives collected to the south of 20°S off SE South America (BEHLING et al., 2002; CAMPOS et al., 2019a; GU et al., 2017) (Fig. 4.6l-n) show no changes in terrigenous input during last glacial HS, suggesting that precipitation anomalies over those drainage basins were not intense enough to produce increased fluvial discharge to the SE South American continental margin. Indeed, our annual and monthly mean HS1 minus LGM precipitation results show no major anomalies over the drainage basins of the Doce, Itajaí and La Plata Rivers (Figs. 4.1e-g; 4.4a).

Figure 4.6 - Marine paleoclimate records from the Atlantic continental margin of South America (color coded according to Fig. 4.1a). **(a)** Lightness (L*) from northern (N) South American core MD03-2621 (DEPLAZES et al., 2013) (brown line represents a 399-point running average); **(b)** L* from N South American core M78/1-235-1 (BAHR et al., 2018; POGGEMANN et al., 2018); **(c)** ln(Ti/Ca) from core GeoB16224-1 that represents northwestern (NW) South American (ZHANG et al., 2017); **(d)** ln(Ti/Ca) from northeastern (NE) South American core CDH86 (NACE et al., 2014); **(e)** ln(Ti/Ca) from NE South American core GL1248 (VENANCIO et al., 2018); **(f)** ln(Fe/Ca) from NE South American core GeoB16202-2 (MULITZA et al., 2017); **(g)** ln(Ti/Ca) from NE South American core GeoB3104-1 (ARZ et al., 1998); **(h)** ln(Ti/Ca) from NE South American core GeoB3912-1 (ARZ et al., 1998); **(i)** ln(Ti/Ca) from NE South American core GeoB3910-2 (JAESCHKE et al., 2007); **(j)** ln(Ti/Ca) from NE South American core GeoB3176-1 (ARZ et al., 1999); **(k)** ln(Ti/Ca) from eastern (E) South American core

M125-95-3 (this study); **(l)** ln(Ti/Ca) from southeastern (SE) South American core GeoB3229-2 (BEHLING et al., 2002); **(m)** ln(Fe/Ca) from SE South American core GeoB2107-3 (GU et al., 2017); and **(n)** ln(Ti/Ca) from SE South American core GeoB6212-1 (CAMPOS et al., 2019a). Black (orange) squares at the bottom of the panel depict calibrated radiocarbon ages (tie-points) with 2σ standard error. Pink vertical bars represent abrupt millennial scale climate change events Younger Dryas (YD) and Heinrich Stadial (HS) 1 to 6. Marine Isotope Stages (MIS) are depicted below the upper axis.

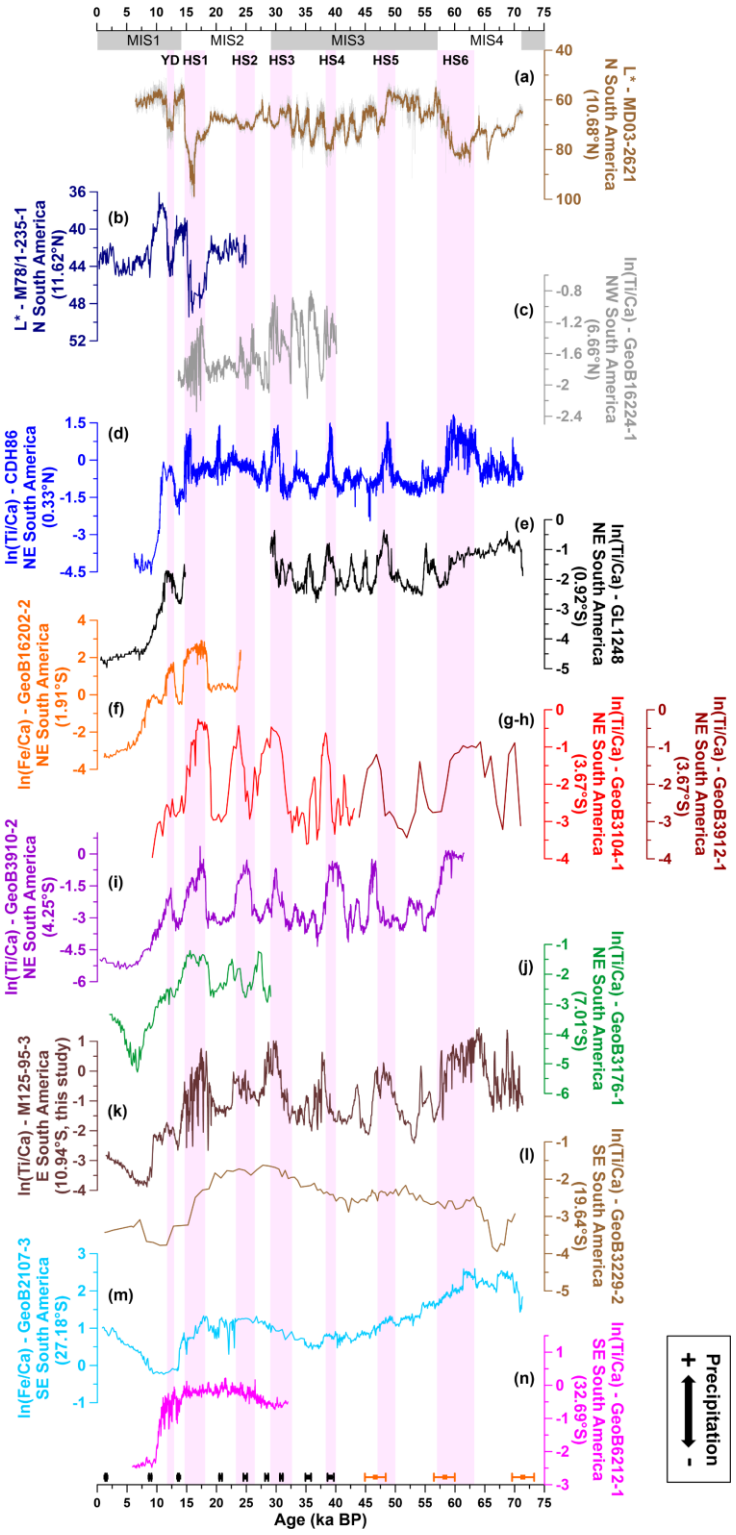

Our marine paleoclimate archive (i.e., 10.94°S, off E South America, Fig. 4.6k) fills the gap between the presence of HS signals recorded in marine records to the north of 7°S and the absence of HS signals recorded by marine records to the south of 20°S. It shows recurrent peaks in ln(Ti/Ca) during the last glacial period suggesting systematic increases in the discharge of terrigenous sediments by the São Francisco River to the adjacent continental margin during HS6-YD. In addition, our model results show positive precipitation anomalies over the São Francisco River drainage basin (Figs. 4.1d; 4.4a).

We suggest that E South America experienced positive precipitation anomalies during all HS of the last glacial. Our new archive is the first marine record off E South America and the southernmost from the Atlantic continental margin of South America to consistently record increased precipitation over E South America during HS. Additionally, our ln(Fe/K) data varies coevally with our ln(Ti/Ca) record, supporting our suggestion that the increases in ln(Ti/Ca) were indeed associated to increased continental precipitation (Fig. 4.3a). Higher ln(Fe/K) values indicate enhanced chemical weathering (GOVIN et al., 2012; MULITZA et al., 2008), likely caused by increased precipitation over the São Francisco River drainage basin.

The meridional impact of HS-induced precipitation anomalies over South America seems to decrease from north to south (Fig. 4.6). The N (Fig. 4.6a-b), NW (Fig. 4.6c) and NE (Fig. 4.6d-j) South American cores recorded HS with signals of large amplitude. Our record (i.e., E South American; Fig. 4.6k) still shows marked HS-signals but of lower amplitude. Conversely, the SE South American cores (Fig. 4.6l-n) have not responded to HS. A decreasing amplitude in HS-related signal is also evident in our model results (Figs. 4.1b-g; 4.4a). Our record also shows a long-term trend that seems to be driven by the combination of sea level and orbital changes. A similar long-term trend can also be identified in SE South American cores (Fig. 4.6l-n). Indeed, GU et al. (2017) related the long-term trend present in their ln(Fe/Ca) record (Fig. 4.6m) to changes in sea level and orbital obliquity. The high magnitude of the HS signal captured by the N, NW and NE South American archives may have dampened the long-term trend. Since our focus here relies on the abrupt millennial scale events of the last glacial, a detailed discussion regarding orbital scale signals is out of our scope.

4.6.2 The continental paleoclimate record of changes in precipitation over (sub-) tropical South America during HS

Tropical South American archives consistently recorded last glacial HS induced precipitation anomalies related to the southward migration of the ITCZ (e.g., BAKER et al., 2001; KANNER et al., 2012; ZULAR et al., 2019). These anomalies are negative over N South America

(ZULAR et al., 2019) and positive over NW (BAKER et al., 2001; KANNER et al., 2012) and NE (CRUZ et al., 2009; LEDRU et al., 2006) South America. The anomalies recorded by N, NW and NE hydroclimate reconstructions are largely supported by previous modeling studies (e.g., BROCCOLI et al., 2006; KAGEYAMA et al., 2013) as well as by our model results for annual-mean HS1 minus LGM precipitation (Fig. 4.4a). Also, our monthly-mean HS1 minus LGM precipitation results (Fig. 4.1b-c) further corroborate the positive precipitation anomalies recorded by NW and NE South American records (e.g., BAKER et al., 2001; CRUZ et al., 2009; KANNER et al., 2012). Hydroclimate records from E South America (e.g., STRÍKIS et al., 2018; WANG et al., 2004) also show positive precipitation anomalies during HS of the last glacial and are equally supported by previous modeling studies (e.g., BROCCOLI et al., 2006; KAGEYAMA et al., 2013) as well as by our modeled HS1 minus LGM precipitation (Figs. 4.1c; 4.4a).

The scenario over SE South America is not as clear as the one over N, NW, NE and E South America. SE South American records with appropriate resolution to capture HS of the last glacial mainly stem from stalagmites (CRUZ et al., 2005; HESSLER et al., 2010; WANG et al., 2006). Stalagmite $\delta^{18}O$ (and local precipitation $\delta^{18}O$) are mainly affected by moisture source, amount of rainfall and temperature. Based on modern conditions, millennial scale negative anomalies in the $\delta^{18}O$ of stalagmites from SE South America (e.g., Botuverá cave (27.22°S) and Santana cave (24.53°S)) were first related to an increase in the intensity of the SAMS, which is one of the moisture sources to SE South America (i.e., source effect) (CRUZ et al., 2005).

Later, trace elements (i.e., Mg/Ca and Sr/Ca) from a Botuverá cave stalagmite were used as a proxy for the local amount of rainfall (CRUZ et al., 2007). Since the authors identified a positive correlation between stalagmite trace element ratios and $\delta^{18}O$ for the whole record on orbital scale, they reassessed previous (CRUZ et al., 2005) interpretations suggesting that periods of negative $\delta^{18}O$ anomalies (lower trace element ratios) in the stalagmites were not only related to moisture source (^{18}O-depleted moisture transported from the Amazon basin towards SE South America), but also to higher amount of local precipitation in response to a stronger SAMS (i.e., a mixture of source and local amount effects). However, despite the stalagmite $\delta^{18}O$ negative anomalies, the positive correlation with trace elements is not clear on millennial scale, hindering a conclusive statement about the mechanism (source effect, local amount effect, or both) controlling the $\delta^{18}O$ negative anomalies on SE South American stalagmites during HS. Recently, MILLO et al. (2017) analyzed the isotopic composition of fossil dripwater from a

Botuverá cave stalagmite and suggested that the $\delta^{18}O$ of SE South American stalagmites is not appropriate for quantitative (local amount effect) interpretations.

By using a water isotope-enabled general circulation model, LEWIS et al. (2010) simulated precipitation $\delta^{18}O$ for HS-like conditions and classified the caves from SE South America as dominated by local amount effect. However, the authors indicated that the transport of ^{18}O-depleted moisture from the Amazon basin towards SE South America during periods of strong SAMS also contributed to the low $\delta^{18}O$ of local precipitation (moisture source effect).

Non-speleothem paleoclimate archives from SE South America (BEHLING et al., 2002; CAMPOS et al., 2019a; GU et al., 2017) do not record the hydroclimate signal of HS of the last glacial, indicating that if local precipitation increased during HS, these anomalies were not intense enough to produce increased fluvial discharge to the continental margin (Fig. 4.6l-n). The records from BEHLING et al. (2002), CAMPOS et al. (2019a) and GU et al. (2017) are supported by previous numerical simulations (KAGEYAMA et al., 2013; MOHTADI et al., 2016). Also, our annual and monthly mean HS1 minus LGM precipitation results (Figs. 4.1e-g; 4.4a) show a reduction in the intensity of precipitation anomalies from tropical to subtropical South America, reinforcing our suggestion of a north-south decrease in the meridional impact of HS-induced precipitation anomalies over South America.

Importantly, El Niño–Southern Oscillation (ENSO) is known to influence variability of the La Plata River discharge (PIOLA et al., 2005). However, since (i) marine sediment cores from the continental slope usually have no appropriate temporal resolution to address interannual variability (e.g., ZHANG et al., 2015) and (ii) reconstructions of ENSO variability are not well established during HS for both paleorecords (FELIS et al., 2012; KOUTAVAS et al., 2002; LEDUC et al., 2009) and numerical simulations (LIU et al., 2014; MERKEL et al., 2010), we refrain addressing any ENSO impacts on South American precipitation during HS.

4.6.3 A new mechanism for precipitation changes over tropical South America

The annual-mean HS1 minus LGM precipitation anomaly (Fig. 4.4a) apparently corroborates the mechanism usually invoked to explain the increase in precipitation over tropical South America to the south of the equator during HS of the last glacial (KANNER et al., 2012; PETERSON et al., 2000; STRÍKIS et al., 2015). According to this mechanism, an austral summer enhanced SAMS was accompanied by the southward migration of the ITCZ and a strong SACZ (CRUZ et al., 2005; KANNER et al., 2012; PETERSON et al., 2000; STRÍKIS et al., 2015). However, the detailed analyses of the seasonal-mean HS1 minus LGM anomalies

from our model experiment (Figs. 4.4b-c; 4.5) suggests a different mechanism. The annual-mean pattern results from a complex combination of the individual seasonal response patterns, which involves dynamic and thermodynamic processes.

In modern climate, a strong AMOC promotes an oceanic northward net cross-equatorial energy transport. To compensate this inter-hemispheric asymmetry, the net cross-equatorial energy transport performed by the atmosphere is directed southward (MARSHALL et al., 2014; MOHTADI et al., 2016). To accomplish that, the location of the ascendant branch of the Hadley cell and, thus, the ITCZ are placed to the north of the equator. However, during HS of the last glacial, a substantially weaker or disrupted AMOC would decrease the northward ocean heat transport and induce a weakening or reversal of the atmospheric cross-equatorial energy transport. In response, a cooling (warming) of the North Atlantic (South Atlantic) and a reorganization of the global Hadley cell would occur, promoting a southward ITCZ shift (BROCCOLI et al., 2006; MOHTADI et al., 2016; MULITZA et al., 2017; SCHNEIDER et al., 2014). In association with the migration of the ITCZ, a meridional rainfall anomaly dipole emerges over tropical South America (Fig. 4.4) and can be considered the continental counterpart of the marine ITCZ shift. During austral summer (winter), the dipole is located between ca. 0° and 20°S (10°N and 10°S) (Fig. 4.4b-c). This precipitation dipole is primarily a dynamic response to cooling (warming) of the Northern Hemisphere (Southern Hemisphere) and associated with northerly low-level wind anomalies that are generally directed along surface temperature gradients (Fig. 4.5a-b) (cf. LINDZEN; NIGAM, 1987).

In addition to this dynamic response, thermodynamic processes also play an important role in setting up tropical South American precipitation during HS of the last glacial. During austral summer (winter), the North Atlantic (South Atlantic) is the main source of moisture for tropical South America via prevailing NE trade winds (SE trade winds) (Fig. 4.S2). Due to the HS cooling of the North Atlantic the atmospheric moisture content over the Northern Hemisphere is reduced (Fig. 4.5c-d). Consequently, in austral summer cooler and drier air is transported by the prevailing NE trade winds (Figs. 4.S2; 4.5c) from the tropical North Atlantic into the continent, resulting in reduced transport of moisture to feed rainfall over tropical South America. Moreover, cooler and drier low-level NE trade winds transport less moist static energy into the continent. A resulting decrease in low-level moist static energy stabilizes the atmospheric vertical column and inhibits convection (COOK; VIZY, 2006; NEELIN; HELD, 1987).

Thus, differently from previous suggestions (e.g. KANNER et al., 2012; PETERSON et al., 2000; STRÍKIS et al., 2015), last glacial HS austral summers were characterized by drier

conditions over vast tropical South American regions, including the Amazon and the northern portion of the Parnaíba River drainage basins (Figs. 4.1b-c; 4.4b). Increased austral summer rainfall over E South America between ca. 15°S and 25°S is associated with an anomalous cyclonic circulation and moisture transport from the anomalously warm South Atlantic into the continent (Figs. 4.4b; 4.5c).

Last glacial HS austral winters show wetter conditions prevailing over most tropical South America to the south of the equator (Fig. 4.4c). During austral winters, enhanced precipitation over the western Amazon (ca. 0°-10°S) is fed by moisture from the eastern Amazon region and the equatorial North Atlantic (Fig. 4.5d). Positive SST anomalies in the eastern equatorial Pacific, likely a response to the weakened AMOC during HS, have been reported to enhance western Amazon precipitation by promoting a regional easterly low-level wind anomaly and moisture recycling from the central Amazon towards the Andes (TIMMERMANN et al., 2007; ZHANG et al., 2016). The São Francisco, Doce, Itajaí and La Plata River drainage basins are not affected by these anomalous moisture transports (Figs. 4.1d-g; 4.4c). It is worth noting that our model simulates enhanced precipitation over the central Andes (Fig. 4.4) in line with multiple HS proxy records (e.g. ZHANG et al., 2016).

Therefore, our new mechanism explains that the positive precipitation anomalies that occurred over the São Francisco River drainage basin during HS of the last glacial were related to an austral summer tropical South Atlantic moisture flux instead of an austral summer intensified SACZ. Also, our model experiments give no support to a mechanism that invokes an austral summer enhanced SAMS as responsible for wetter conditions over the Amazon basin and further south during HS. Instead, we propose an austral winter equatorial Atlantic moisture flux as a source of additional rainfall (Fig. 4.5d). Furthermore, this new mechanism contradicts the suggested relationship between stronger SAMS convective activity over the Amazon basin, transference of the low $\delta^{18}O$ signal towards SE South America and increased local amount of rain.

4.7 Conclusions

Our core collected at 10.94°S contributes to reduce the gap of marine paleoclimate records between 7°S and 20°S off E South America. It is the first marine archive off E South America and the southernmost from the Atlantic continental margin of South America that consistently records the hydroclimate signal of HS of the last glacial. Our core suggests positive precipitation anomalies over the São Francisco River drainage basin during HS6-YD. Based on new data from our core, a thorough compilation of previously available marine paleoclimate

records and results from a high-resolution atmosphere-ocean general circulation model, we show that the HS-induced positive precipitation anomalies over (sub-) tropical South America to the south of the equator is latitude-dependent, decreasing from north to south. Also, we propose a new mechanism responsible for the HS positive precipitation anomalies over tropical South America to the south of the equator. During HS austral summers, cooler and drier air was transported from the tropical North Atlantic into tropical South America via prevailing NE trade winds. Consequently, drier conditions prevailed over tropical South America. An exception is made for E South America, that was affected by anomalous tropical South Atlantic cyclonic circulation. During HS austral winters, enhanced moisture was transported from the equatorial Atlantic into tropical South America. Wetter conditions occurred over most of tropical South America to the south of equator. The new mechanism proposed herein highlights the need of a broad approach to explain South American HS hydroclimate conditions that goes beyond changes in SAMS. Dynamic and thermodynamic processes, seasonal changes as well as the tropical Atlantic moisture source played crucial roles in setting up millennial scale precipitation anomalies over tropical South America.

Acknowledgements

We thank two anonymous reviewers for their comments and suggestions that improved the manuscript. Logistic and technical assistance was provided by the captain and crew of the R/V Meteor. New data shown herein are archived in Pangaea (doi:10.1594/PANGAEA.905181). M.C. Campos acknowledges the financial support from FAPESP (grants 2016/10242-0 and 2018/06790-7). C.M. Chiessi and A.L. Albuquerque acknowledges the financial support from FAPESP (grant 2018/15123-4), CAPES (grants 564/2015 and 88881.313535/2019-01), CNPq (grants 302607/2016-1, 422255/2016-5, 302521/2017-8 and 429767/2018-8) and the Alexander von Humboldt Foundation. CAPES (grants 88887.156152/2017-00 and 88881.161151/2017-01) and CNPq (grant 406322/2018-0) currently support I.M. Venancio. S. Mulitza, M. Prange, H. Kuhnert and A. Paul were funded through the DFG Research Centre, Cluster of Excellence “The Ocean in the Earth System”. Support from the German PalMod initiative (BMBF) is also acknowledged. The CCSM3 simulations were performed on the supercomputer of the Norddeutscher Verbund für Hoch- und Höchstleistungsrechnen (HLRN). Sample material was provided by the Core Repository at the Fluminense Federal University, Brazil. This research used data acquired at the XRF Core Scanner Lab at the MARUM – Center for Marine Environmental Sciences, University of Bremen, Germany.

4.8 Supplementary material

Table 4.S1. Piston core M125-95-3 tie-points aligned to reference curve MD95-2042 (GOVIN et al., 2014).

Depth (cm)	Tie-point age	Feature	Estimated error (a)
498	47000	HS5	2141
582	59300	Final portion of MIS4	2049
738	71100	Final portion of the glacial inception	2137

The tie-points were used to link the M125-95-3 *Uvigerina* spp. stable oxygen isotopes ($\delta^{18}O$) to the reference benthic $\delta^{18}O$ curve from core MD95-2042 (SHACKLETON et al., 2002; SHACKLETON et al., 2000) with an age model improved by GOVIN et al. (2014) using the AICC2012 ice core chronology (VERES et al., 2013). The reference curve was applied to the depth interval 452-738 cm of core M125-95-3. Error estimates of $\delta^{18}O$ tie-points take into account (i) the mean resolution of the M125-95-3 *Uvigerina* spp. $\delta^{18}O$ record around the tie-point depth, (ii) the mean resolution of the reference curve around the tie-point age, (iii) a matching error visually estimated when defining tie-points, and (iv) the absolute age error of the time-scale used for the reference record.

Figure 4.S1. Benthic foraminifera oxygen isotopic composition ($\delta^{18}O$) of piston core M125-95-3 (this study) and reference curve MD95-2042 (GOVIN et al., 2014) used to extend M125-95-3 age model beyond the limit of radiocarbon ages. Black squares at the top of the panel depict calibrated radiocarbon ages. Red dashed lines depict the used $\delta^{18}O$ tie-points.

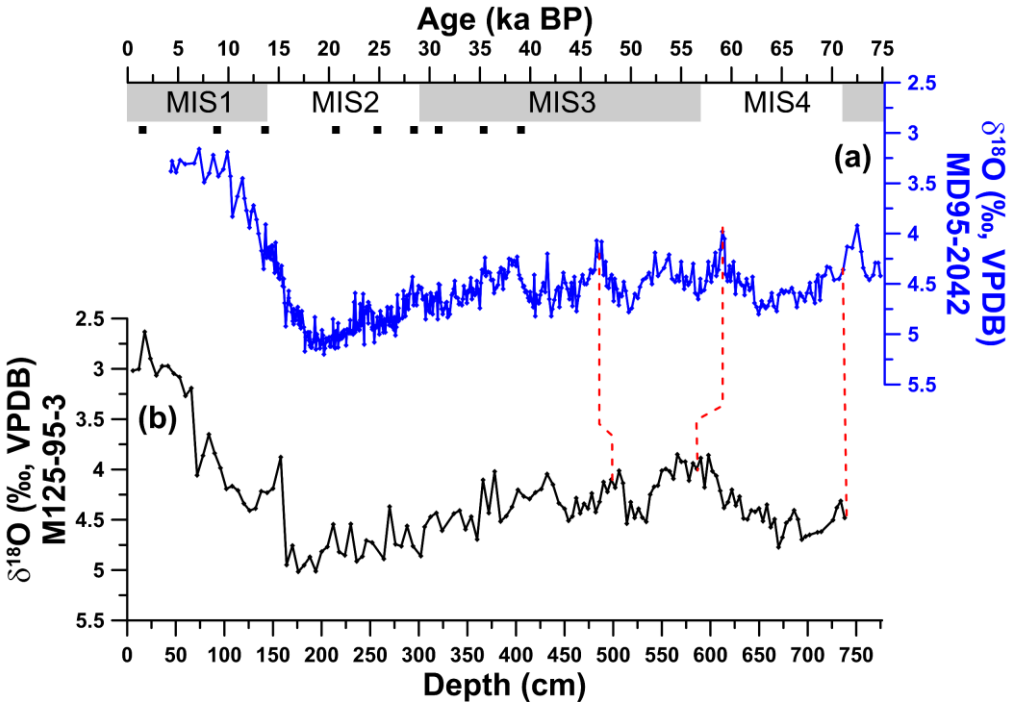

Figure 4.S2. Heinrich Stadial 1 (HS1) minus Last Glacial Maximum (LGM) seasonal mean precipitable water along with absolute vertically integrated moisture transport (kg/(m s)) during the LGM simulated with CCSM3 (COLLINS et al., 2006; PRANGE et al., 2015). (**a)** Extended austral summer (i.e., November-March (NDJFM)) precipitable water difference (HS1 minus LGM) and absolute moisture transport during the LGM, and **(b)** extended austral winter (i.e., May-September (MJJAS)) precipitable water difference (HS1 minus LGM) and absolute moisture transport during the LGM.

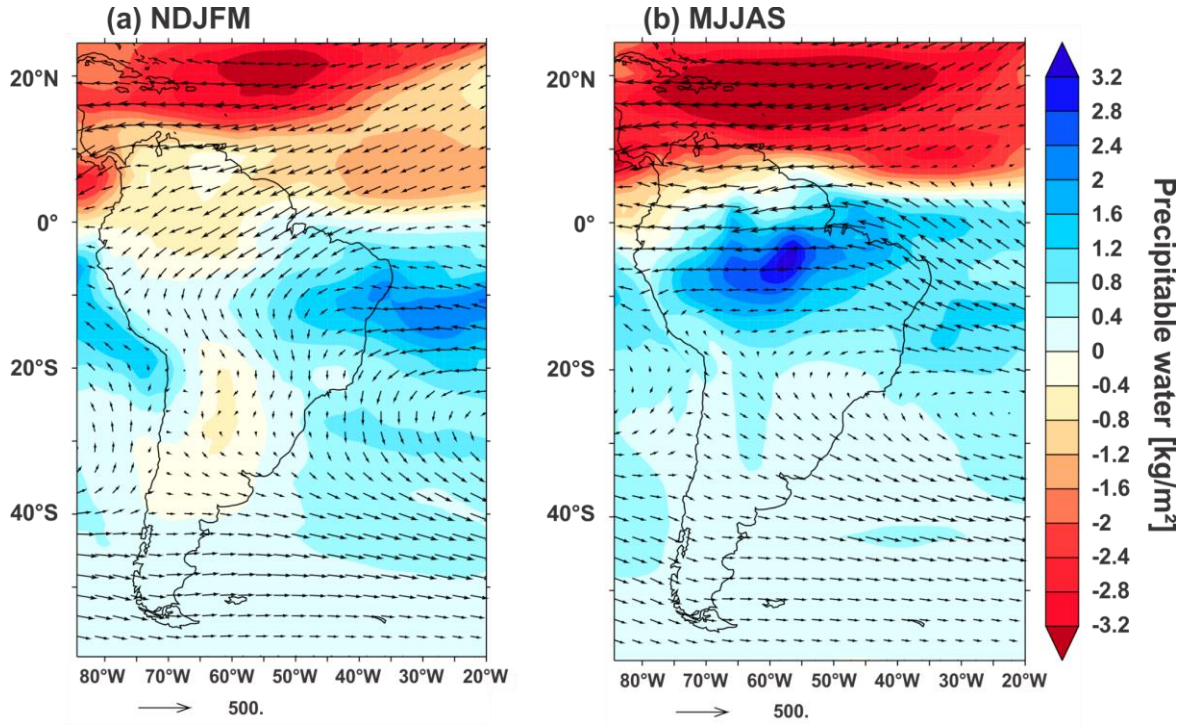

5 Constraining millennial-scale changes in Northern Component Water ventilation in the western tropical South Atlantic

Marília C. Campos[a]*, Cristiano M. Chiessi[a], Igor M. Venancio[b], Tainã M. L. Pinho[c], Stefano Crivellari[c], Henning Kuhnert[d], Gerhard Schmiedl[e], Rut A. Díaz[f], Ana Luiza S. Albuquerque[f], Rodrigo C. Portilho-Ramos[d], André Bahr[g], Stefan Mulitza[d]

[a] School of Arts, Sciences and Humanities, University of São Paulo, São Paulo, Brazil

[b] Center for Weather Forecasting and Climate Studies (CPTEC), National Institute for Space Research (INPE), Cachoeira Paulista, Brazil

[c] Institute of Geosciences, University of São Paulo, São Paulo, Brazil

[d] MARUM – Center for Marine Environmental Sciences, University of Bremen, Bremen, Germany

[e] Center for Earth System Research and Sustainability, Institute for Geology, University of Hamburg, Hamburg, Germany

[f] Graduate Program in Geochemistry, Fluminense Federal University, Niterói, Brazil

[g] Institute of Earth Sciences, Heidelberg University, Heidelberg, Germany

* Corresponding author: marilia.carvalho.campos@usp.br

Accepted for publication in *Paleoceanography and Paleoclimatology*.

5.1 Abstract

Negative excursions in the stable carbon isotopic composition ($\delta^{13}C$) at Atlantic intermediate to mid-depths are common features of millennial-scale events named Heinrich Stadials (HS). The mechanisms behind these excursions are not yet fully understood, but most hypotheses agree on the central role played by the weakening of the Atlantic meridional overturning circulation. Marine records registering millennial-scale negative $\delta^{13}C$ excursions in the Atlantic are mostly restricted to the HS of the last deglacial, while the HS of the last glacial are poorly studied. Here we constrain changes in bottom water ventilation in the western tropical South Atlantic mid-depth during HS of the last glacial and deglacial by investigating marine core M125-95-3. The concurrent decreases in benthic foraminifera $\delta^{13}C$ and increases in bulk sediment sulfur indicates an increased Northern Component Water (NCW) residence time in the western tropical South Atlantic mid-depth during HS. Furthermore, a coherent meridional

pattern emerges from the comparison of our new data to previously published mid-depth records from the western South Atlantic. While our record shows the largest negative $\delta^{13}C$ excursions during almost all HS, the western equatorial Atlantic showed medium and the subtropical South Atlantic showed the smallest negative excursions. This meridional pattern supports the notion that during HS a reduction in the NCW $\delta^{13}C$ source signal together with the accumulation of respired carbon at NCW depths drove the negative $\delta^{13}C$ excursions. We suggest that the negative $\delta^{13}C$ excursions progressively increase along the NCW southwards pathway until the signal dissipates/dilutes by mixing with Southern Component Water.

5.2 Introduction

Negative excursions in the reconstructed stable carbon isotopic composition of dissolved inorganic carbon ($\delta^{13}C_{DIC}$) at Atlantic intermediate (here, 1000-1500 m) to mid- (here, 1500-2500 m) depths have been reported to occur during millennial-scale climate change events named Heinrich Stadials (HS). These excursions are often related to a reduced Atlantic meridional overturning circulation (AMOC) (LUND et al., 2015; OPPO et al., 2015; OPPO; FAIRBANKS, 1987; TESSIN; LUND, 2013; VOIGT et al., 2017). The reduced AMOC is frequently associated with (i) changes in the proportion of Northern Component Water (NCW) relative to Southern Component Water (SCW) (KEIGWIN; LEHMAN, 1994; ZAHN et al., 1997), (ii) a shallow boundary between NCW and SCW (CURRY et al., 1999; MECKLER et al., 2013), and/or (iii) a decrease in the NCW $\delta^{13}C$ source value (LUND et al., 2015; OPPO et al., 2015; VOIGT et al., 2017). Additionally, increasing evidence suggests that the accumulation of respired carbon (^{12}C-enriched) in the ocean interior in response to increased deep water residence time also contributed to the $\delta^{13}C$ decreases in the Atlantic during these events (OPPO et al., 2015; SCHMITTNER; LUND, 2015; VOIGT et al., 2017). However, the exact mechanisms responsible for the negative $\delta^{13}C$ excursions during millennial-scale events remain elusive. Furthermore, most Atlantic paleoclimate records registering negative excursions during HS only cover the last deglacial HS (i.e., HS1 and the Younger Dryas (YD)), while records spanning the HS of the last glacial (i.e., from HS6 to HS2) with appropriate temporal resolution are scarce (e.g., BURCKEL et al., 2015; SANTOS et al., 2017).

Here we investigate marine sediment core M125-95-3 collected at the western tropical South Atlantic mid-depth (10.94°S, 1897 m) spanning the last ca. 70 thousand years (ka). The high temporal resolution of this core allows us to constrain changes in bottom water conditions during HS. To reconstruct past changes in the $\delta^{13}C_{DIC}$, we measured benthic foraminifera $\delta^{13}C$.

In addition, to independently assess past changes in bottom water ventilation and the related changes in the accumulation of respired carbon we measured bulk sediment sulfur (S) content. Our $\delta^{13}C$ data constitutes the first record in the western South Atlantic that clearly registers all HS of the last glacial and deglacial (i.e., from HS6 to the YD). The coeval decreases in $\delta^{13}C$ and increases in S during HS indicates a longer NCW residence time and accumulation of respired carbon in the western tropical South Atlantic mid-depth.

5.3 Background

The western South Atlantic is occupied by a NCW that is, in turn, enveloped by two SCW. The NCW North Atlantic Deep Water (NADW) occurs between ca. 1200 and 4000 m water depth, whereas the SCW Antarctic Intermediate Water (AAIW) and Antarctic Bottom Water (AABW) occur above and below NADW, respectively (Fig. 5.1a) (STRAMMA; ENGLAND, 1999).

The distribution of $\delta^{13}C_{DIC}$ within the oceans results from a complex combination of surface primary productivity, organic matter remineralization in greater depths, air-sea gas exchanges and their interactions with ocean circulation (Fig. 5.1a) (KROOPNICK, 1985; SARMIENTO et al., 1988). While the surface primary productivity preferentially removes nutrients and ^{12}C from upper waters, the remineralization (or respiration) of organic matter returns nutrients and ^{12}C to intermediate-deep waters (Fig. 5.1a) (SARMIENTO et al., 1988). As a result, nutrients and $\delta^{13}C_{DIC}$ have an inverse relationship (KROOPNICK, 1985). Newly formed deep water masses containing high fraction of oligotrophic surface waters (e.g., NADW) have relatively low nutrient content (i.e., low preformed nutrient) and respired carbon, resulting in high $\delta^{13}C_{DIC}$ (ca. 1‰, Fig. 5.1a – $\delta^{13}C_{DIC}$ vertical profile at 60.5°N) (KROOPNICK, 1985). These high $\delta^{13}C_{DIC}$ values spread into the deep North Atlantic. However, the aging effect and the accumulation of respired carbon along the NCW pathway southwards promote a slight and progressive decrease in its $\delta^{13}C_{DIC}$ signature (ca. 0.9‰, Fig. 5.1a, $\delta^{13}C_{DIC}$ vertical profile at 1°N). SCW, on the other hand, originate from waters with relatively high nutrients and respired carbon and, thus, lower $\delta^{13}C_{DIC}$ values spread northwards at AAIW (ca. 0.5‰) and AABW (ca. 0.4‰) levels (KROOPNICK, 1985) (Fig. 5.1a – $\delta^{13}C_{DIC}$ vertical profile at 23°S). As the water mass residence time increases, nutrients and respired carbon become more concentrated, producing lower $\delta^{13}C_{DIC}$ signatures. Since the residence time of western Atlantic deep waters is relatively short (ca. 275 years) (STUIVER et al., 1983), its $\delta^{13}C_{DIC}$ may reflect the mixing of water masses of different initial $\delta^{13}C_{DIC}$ values (i.e., NCW and SCW) and thus, be a tracer for deep water mass structure and circulation (KROOPNICK, 1985; OPPO; FAIRBANKS, 1987).

Importantly, the $\delta^{13}C_{DIC}$ may also be influenced by local processes like changes in surface primary productivity (e.g., in upwelling regions) and the related phytodetritus flux to the sea-floor, as well as by the terrigenous input of low $\delta^{13}C$ detritus (e.g., by riverine input) (MACKENSEN et al., 1993; THEODOR et al., 2016).

Figure 5.1 - Location of core M125-95-3 (yellow filled dot) and other marine records discussed herein (open dots) (see details in Table 5.1). **(a)** Modern western Atlantic WOA13 phosphate section depicts the main water masses within the western Atlantic (GARCIA et al., 2013) together with three vertical GEOSECS stable carbon isotopic composition profiles of dissolved inorganic carbon ($\delta^{13}C_{DIC}$) at 60.5°N, 1°N and 23°S (KROOPNICK, 1985). Schematic arrows show the flow direction of the main water masses. AABW: Antarctic Bottom Water; AAIW: Antarctic Intermediate Water; NADW: North Atlantic Deep Water. **(b)** Location of western South Atlantic marine sediment cores. The purple line marks the section depicted in (a). This figure was partially produced with Ocean Data View (SCHLITZER, 2018).

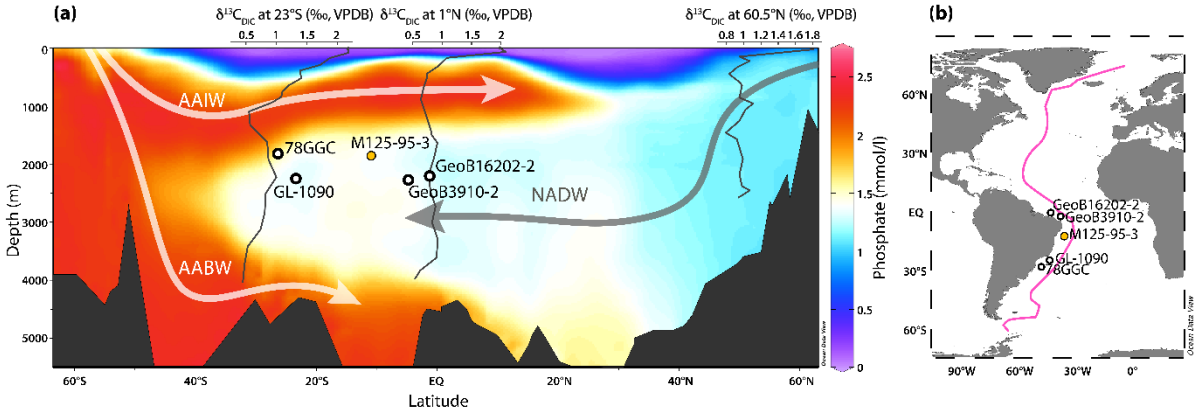

The stable oxygen isotopic composition of seawater ($\delta^{18}O_{sw}$) is also a potential tracer for water mass structure and circulation (LEGRANDE; SCHMIDT, 2006). Water masses have different $\delta^{18}O_{sw}$ signatures that are dependent on their formation conditions. Assuming negligible geothermal and pressure heating effects, bottom water $\delta^{18}O$ can only change due to mixing between water masses and thus, is a valuable water mass tracer (e.g., MEREDITH et al., 1999). It is noteworthy that absolute $\delta^{18}O_{sw}$ values are also influenced by global ice volume (e.g., SCHRAG et al., 2002). This effect is, however, nearly synchronous in specific ocean basins and water depths (WAELBROECK et al., 2011).

Since the presence of S in marine sediments is related to oxygen availability (i.e., redox conditions), changes in S concentration at sea-floor sediments can, together with other proxies, record changes in local bottom water ventilation. Organic matter in marine sediments is degraded by different terminal electron acceptors encompassing aerobic and anaerobic degradation (JØRGENSEN et al., 2019). When oxygen availability is reduced, seawater sulfate (SO_4^{2-}) becomes the dominant terminal electron acceptor. In this situation, organic matter

degradation is performed by sulfate-reducing bacteria and both pyrite and sulfurized organic matter are the results of the sulfate reduction and the main sinks of S at the sea-floor (JØRGENSEN; KASTEN, 2006; SUITS; ARTHUR, 2000). Importantly, in regions where the local flux of organic carbon exported to the sea-floor is low through time (e.g., far from upwelling systems and without river-borne nutrients input), the increase in S concentration may be related to an increase in bottom water residence time and in the accumulation of respired carbon.

Here we use species-specific benthic foraminifera $\delta^{13}C$ and $\delta^{18}O$ as well as the S content of bulk sediments to assess changes in bottom waters in the mid-depth western tropical South Atlantic.

5.4 Material and methods

5.4.1 Marine sediment core

Core M125-95-3 (10.94°S, 36.20°W, 1897 m water depth, 10.4 m core length) was collected from the continental slope in the western tropical South Atlantic during RV Meteor cruise M125 (Table 5.1) (BAHR et al., 2016). The core site is presently bathed in NADW (Fig. 5.1a). Since we focus here on the HS of the last glacial and deglacial (i.e., Marine Isotope Stages (MIS) 4, 3, and 2), we analyzed the uppermost ca. 7.4 m of the core. This section was sampled with syringes of 10 cm^3 and u-channels (2 cm width, 2 cm depth, 105 cm length). Samples for isotopic and micropaleontological analyses were wet-sieved, oven-dried at 50 °C, and the fraction larger than 125 µm was stored in glass vials. Samples for bulk sediment analyses were stored at 4 °C.

We discuss our records in the context of four other published marine sediment cores also collected at the western South Atlantic mid-depth spanning from 1.91°S to 27.48°S (Table 5.1, Fig. 5.1). Cores GeoB3910-2 (BURCKEL et al., 2015) and GL-1090 (SANTOS et al., 2017) cover most HS of the last glacial. In order to complement GeoB3910-2 upper portion and to improve the temporal resolution of GL-1090 during HS1 and the YD, we also compiled cores GeoB16202-2 (VOIGT et al., 2017) and 79GGC (TESSIN; LUND, 2013), that cover the last ca. 20 ka (Fig. 5.3d, e, g, h). We focus on mid-depth (around 2000 m) and on the western margin of the Atlantic because this region is occupied by the Deep Western Boundary Current, being ideal for tracking past changes in NCW (RHEIN et al., 1995).

Table 5.1. Marine sediment cores discussed in this study.

Core ID	Region	Latitude (˚S)	Longitude (˚W)	Water depth (m)	Reference
GeoB16202-2	Western equatorial Atlantic	1.91	41.59	2248	Voigt et al. (2017)
GeoB3910-2	Western equatorial Atlantic	4.25	36.35	2362	Burckel et al. (2015)
M125-95-3	Western tropical South Atlantic	10.94	36.20	1897	this study
GL-1090	Subtropical western South Atlantic	24.92	42.51	2225	Santos et al. (2017)
78GGC	Subtropical western South Atlantic	27.48	46.33	1820	Tessin and Lund (2013)

5.4.2 Stable isotopic composition of benthic foraminifera

$\delta^{13}C$ and $\delta^{18}O$ analyses were performed on two benthic foraminifera species with different microhabitat (MCCORKLE et al., 1990): (i) shallow infaunal species *Uvigerina* spp. (mainly *Uvigerina peregrina*; $\delta^{18}O$ results previously published in CAMPOS et al. (2019b)); and (ii) epifaunal species *Cibicidoides pachyderma*. From the sediment fraction larger than 125 μm ca. 3-10 specimens per sample were handpicked under a binocular microscope every 4-6 cm for *Uvigerina* spp. and every 2-50 cm for *C. pachyderma*. Since *C. pachyderma* (and also any other appropriate epibenthic species) is not consistently present in core M125-95-3, we only analyzed the depth interval 84-398 cm. On the other hand, *Uvigerina* spp. is present in the whole investigated section and was used to produce the main downcore $\delta^{13}C$ record of M125-95-3. *Uvigerina* spp. analyses were conducted with a gas isotope ratio mass spectrometer (Thermo Fisher Scientific MAT253plus) coupled to an automated carbonate preparation device (Kiel IV) at the MARUM – Center for Marine Environmental Sciences, University of Bremen, Germany. *Cibicidoides pachyderma* analyses were conducted with a gas isotope ratio mass spectrometer (Thermo Fisher Scientific MAT253) coupled to an automated carbonate preparation device (Kiel IV) at the Paleoceanography and Paleoclimatology Laboratory (P2L), University of São Paulo, Brazil. Output data were calibrated against in-house standard (both laboratories use Solnhofen Limestone) that is calibrated against the NBS19 standard. We report the results in per mil (parts per thousand, i.e., ‰) versus Vienna Pee Dee Belemnite (VPDB). For the

measured period, the standard deviation of in-house standard replicate measurements was 0.03‰ ($\delta^{13}C$) for both laboratories and 0.06‰ ($\delta^{18}O$) for the MARUM and 0.05‰ for the P2L. Benthic foraminifera register in their tests local bottom or pore waters conditions, depending on the species-specific microhabitat and vital effects related to isotopic fractionation during biomineralization. Thus, their $\delta^{13}C$ and $\delta^{18}O$ have been widely used to reconstruct past changes in the local bottom water $\delta^{13}C_{DIC}$ (MACKENSEN et al., 1993; MACKENSEN; SCHMIEDL, 2019; MCCORKLE et al., 1990) and $\delta^{18}O_{sw}$ (SKINNER; SHACKLETON, 2005; WAELBROECK et al., 2002; WAELBROECK et al., 2011). In order to directly compare our *Uvigerina* spp. $\delta^{13}C$ values to the $\delta^{13}C$ of epifaunal species, we applied the correction factor (0.9‰) from SHACKLETON and HALL (1984).

5.4.3 Sulfur content

S intensity was determined with a X-ray fluorescence (XRF) core scanner and an energy dispersive polarized XRF (EDP-XRF). XRF core scanner S data were collected every 5 mm down-core directly at the surface of u-channels sampled from the archive half of core M125-95-3. Analyses were performed at the MARUM – Center for Marine Environmental Sciences, University of Bremen, Germany, with the XRF Core Scanner III (AVAATECH Serial No. 12) (details regarding the method are provided in CAMPOS et al. (2019b)). EDP-XRF S analyses were performed on bulk sediment samples every 20 cm of the working half of core M125-95-3. Bulk sediment samples of around 10 cm^3 were freeze-dried and homogenized with a hand agate mortar and pestle. Analyses were performed at the Oceanography and Paleoceanography Laboratory (LOOP), Fluminense Federal University, Brazil, with an energy dispersive PANalytical Epsilon 3-X XRF spectrometer.

In marine sediments, organic matter is degraded by different terminal electron acceptors following an order of decreasing energy yield (from high to low values): oxygen, nitrate, oxides of manganese (IV) and iron (III), and sulfate (JØRGENSEN et al., 2019). Under oxygen depletion, the sulfate (SO_4^{2-}) – which is highly concentrated (ca. 28 mM) in seawater – turns the dominant terminal electron acceptor, despite the others to be energetically more favorable. Where ventilation is reduced, organic matter starts to be degraded by sulfate-reducing bacteria (degradation/anaerobic respiration of organic matter). During this process, the dissolved sulfate suffers reduction to sulfide ($H_2S + HS^- + S^{2-}$) (e.g., JØRGENSEN; KASTEN, 2006; SUITS; ARTHUR, 2000). The produced sulfide can react with ferrous iron (provided by chemical reduction of detrital minerals) forming pyrite. In another diagenetic pathway, the produced

sulfide can react with organic matter to form organic S compounds (i.e., sulfurization of organic matter) (BOTTRELL; NEWTON, 2006; JØRGENSEN et al., 2019). Both pyrite and sulfurized organic matter are the main sinks of S in marine sediments.

5.4.4 Foraminiferal assemblages

Planktonic foraminifera assemblage analyses and total benthic foraminifera counts were conducted every ca. 10 cm of core M125-95-3. Samples were dry-sieved with a 150 μm mesh and the species relative abundances were quantified from splits containing at least 300 specimens (PATTERSON; FISHBEIN, 1989). Taxonomy was based on STAINFORTH et al. (1975), BOLTOVSKOY et al. (1980) and BOLLI et al. (1989). Additionally, we counted the *Uvigerina* spp. abundance in nine samples of core M125-95-3 within the depth interval 212-282 cm, covering pre-HS2, HS2, and post-HS2. Samples were dry-sieved with a 150 μm mesh and the *Uvigerina* spp. relative abundance was quantified from splits containing at least ca. 100 benthic specimens (BOYLE, 1990; SCHMIEDL et al., 2000). Taxonomy was based on BOLTOVSKOY et al. (1980) and LUTZE (1986). Considering the water depth (i.e., 1897 m) of core M125-95-3 as well as the modern and glacial lysocline depths (VOLBERS; HENRICH, 2004), we assume that the planktonic and benthic foraminifera faunal composition of core M125-95-3 was not influenced by dissolution.

We estimate changes in surface primary productivity based on the index $R_{HP/Planktonic}$, in which HP represents the sum of the abundance of the high productivity species *Globigerina bulloides*, *Neogloboquadrina dutertrei*, *Neogloboquadrina incompta*, and *Globigerinita glutinata* divided by the sum of all planktonic species (PORTILHO-RAMOS et al., 2017). Also, we infer the local flux of organic carbon exported to the sea-floor based on (i) the benthic foraminifera accumulation rate (BFAR) (DIAS et al., 2018; HERGUERA; BERGER, 1991) and (ii) the abundance of the food indicator *Uvigerina* ssp. relative to the abundance of all benthic foraminifera, i.e., $R_{Uvigerina\ spp./Benthics}$ (BOYLE, 1990; KOHO et al., 2008; SCHMIEDL; MACKENSEN, 1997).

5.4.5 Age model

The analyzed section of core M125-95-3 covers the last ca. 70 ka with a mean sedimentation rate of 11.9 cm/ka. The chronology was obtained by combining nine planktonic foraminifera accelerator mass spectrometry (AMS) radiocarbon ages (covering the uppermost 452 cm, i.e., ca. 40 ka before present (BP)) with three M125-95-3 *Uvigerina* spp. $\delta^{18}O$ tie-points aligned to a benthic $\delta^{18}O$ reference curve from GOVIN et al. (2014). We used the calibration curve

IntCal13 (REIMER et al., 2013) with a variable simulated reservoir age from transient modeling experiments described in BUTZIN et al. (2017). The age modeling algorithm BACON v. 2.2 (BLAAUW; CHRISTEN, 2011) was used within the software PaleoDataView v. 0.8.3.4 (LANGNER; MULITZA, 2019) for age-depth modeling. Further details regarding the age model are provided in CAMPOS et al. (2019b).

5.5 Results

Uvigerina spp. $\delta^{13}C$ values range from -1.43 to 0.47‰ (Fig. 5.2g). The contrast between mean last glacial and Holocene values is ca. 0.7‰. Negative excursions (as large as 0.92‰) in the *Uvigerina* spp. $\delta^{13}C$ record occurring during MIS4-1 are associated with HS (i.e., from HS6 to the YD). Although the negative excursion associated with HS3 is also present, it is not as marked as the excursions associated with other HS. Apart from the HS excursions, another negative millennial-scale excursion occurs around 44 ka BP. *Uvigerina* spp. $\delta^{18}O$ values vary from 2.63 to 5.02‰ (Fig. 5.2i). The contrast between mean last glacial and Holocene values is ca. 1.4‰. During the last glacial (MIS4-3), relative low values are coeval with HS6 to HS4. The last deglaciation shows sharp decreases at ca. 18.4 and 11.5 ka BP, coeval (within age model uncertainties) to HS1 and the YD. *Cibicidoides pachyderma* isotopic values vary between -1.33 and -0.22‰ for $\delta^{13}C$ and 4.22 and 5.41‰ for $\delta^{18}O$ (Fig. 5.2f, h). Negative excursions are also associated with HS (i.e., from HS3 to HS1) in both records (i.e., $\delta^{13}C$ and $\delta^{18}O$).

Despite localized differences (e.g., during HS6), the $\delta^{13}C$ (Fig. 5.2f, g) and the XRF core scanner S (Fig. 5.2d) records show an inverse relationship during HS. Higher HS XRF core scanner S intensities (i.e., from HS6 to the YD) interrupt the near-constant background (i.e., ca. 100 counts/s) present throughout the investigated interval. EDP-XRF S concentrations (Fig. 5.2e) range from 0.27 to 1.17% and also show increases during most HS (i.e., from HS6 to HS1).

$R_{HP/Planktonic}$ values range from 0 to 0.14 (Fig. 5.2a), being low throughout the last ca. 70 ka. BFAR values are also low during this period, varying from ca. 12 to 820 shells cm^{-2} ka^{-1} (Fig. 5.2b). $R_{Uvigerina\ spp./Benthics}$ values vary between 10.96 to 27.55 (Fig. 5.2c), showing no clear trend during the analyzed interval, i.e., pre-HS2, HS2, and post-HS2.

Figure 5.2 - Isotopic, geochemical, and assemblage records from core M125-95-3 for the last ca. 70 ka. **(a)** Surface primary productivity index $R_{HP/Planktonic}$ (abundance of high productivity species (HP) divided by the abundance of all planktonic species). The green rectangle represents typical western Atlantic oligotrophic conditions (GARCIA et al., 2013; KUCERA et al., 2005); **(b)** Benthic foraminifera accumulation rate (BFAR); **(c)** local flux of organic carbon to the sea-floor index $R_{Uvigerina\ spp./Benthics}$ (*Uvigerina* spp. abundance relative to at least ca. 100 benthic specimens); **(d-e)** X-ray fluorescence (XRF) core scanner sulfur (S) (black line) and energy dispersive polarized (EDP) XRF S (orange circles); **(f)** *Cibicidoides pachyderma* stable carbon isotopic composition ($\delta^{13}C$); **(g)** *Uvigerina* spp. $\delta^{13}C$; **(h)** *Cibicidoides pachyderma* stable oxygen isotopic composition ($\delta^{18}O$); and **(i)** *Uvigerina* spp. $\delta^{18}O$ (previously published in CAMPOS et al. (2019b)). Black (orange) squares at the bottom of the panel depict calibrated radiocarbon ages (tie-points) with 2σ standard error. Red vertical bars represent millennial-scale events Younger Dryas (YD) and Heinrich Stadial (HS) 1 to 6. Marine Isotope Stages (MIS) are depicted below the upper axis.

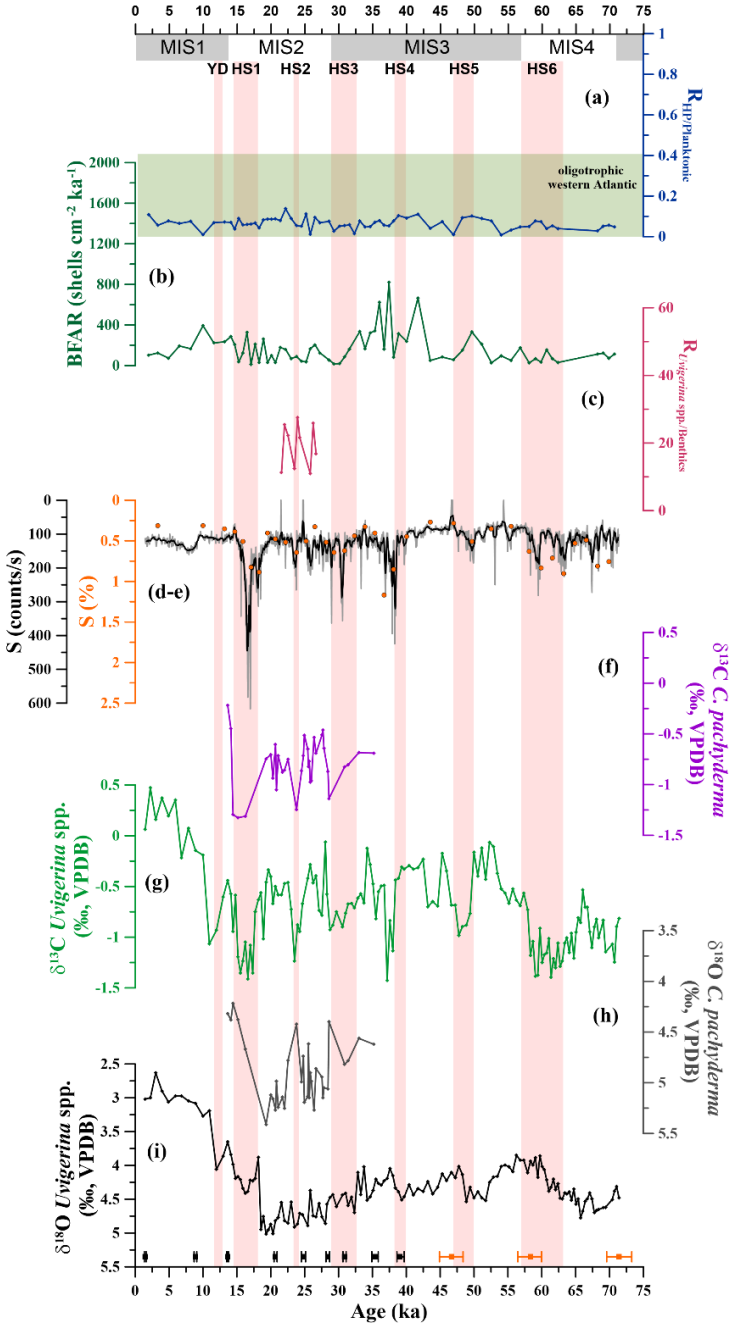

5.6 Discussion

5.6.1 Benthic foraminifera $\delta^{13}C$ signal

The $\delta^{13}C$ of epibenthic foraminifera is an optimal tracer for past changes in bottom water conditions (MACKENSEN; SCHMIEDL, 2019; MCCORKLE et al., 1990). The analyzed species *C. pachyderma* occupies an epifaunal to very shallow infaunal microhabitat (FONTANIER et al., 2002; SCHMIEDL et al., 2000). Accordingly, the $\delta^{13}C$ of *C. pachyderma* is close to bottom water $\delta^{13}C_{DIC}$ with negligible pore water effects (SCHMIEDL et al., 2004; THEODOR et al., 2016). In contrast, *Uvigerina* species commonly inhabit shallow infaunal microhabitats (e.g., KOHO et al., 2008). Shallow infaunal benthic foraminifera calcify in contact with pore water, and their $\delta^{13}C$ cannot be readily assumed to record $\delta^{13}C_{DIC}$ of the overlying bottom water. Indeed, the $\delta^{13}C_{DIC}$ of pore water is controlled by both (i) overlying bottom water $\delta^{13}C_{DIC}$ and (ii) degradation of organic matter exported to the sea-floor (e.g., from surface primary productivity and/or terrigenous input). The latter process leaves pore water ^{12}C-enriched compared to overlying bottom water, thus affecting infaunal foraminifera $\delta^{13}C$ (i.e., microhabitat effect) (MCCORKLE et al., 1985; MCCORKLE et al., 1990; ZAHN et al., 1986). Our *Uvigerina* spp. negative $\delta^{13}C$ excursions during HS of the last glacial and deglacial (i.e., from HS6 to the YD; Fig. 5.2g) could therefore be controlled by three possible processes (that could have operated together): (i) higher surface primary productivity (MCCORKLE et al., 1985); (ii) higher input and resuspension of low $\delta^{13}C$ terrigenous detritus (MILZER et al., 2016; POLYAK et al., 2003; THEODOR et al., 2016); and (iii) changes in the overlying bottom water ventilation leading to lower $\delta^{13}C_{DIC}$ (VOIGT et al., 2017).

Our study area is far from upwelling systems and it is dominated by oligotrophic western boundary currents (GARCIA et al., 2013) thus, we would not expected to have increases in surface primary productivity. Indeed, $R_{HP/Planktonic}$ show low values during the last ca. 70 ka confirming that increases in surface primary productivity did not occur during HS (Fig. 5.2a). The low $R_{HP/Planktonic}$ values also indicate that river-borne nutrients did not affect the upper water column of our core site during HS (SCHILMAN et al., 2001). Thus, changes in surface primary productivity cannot be the main driver of the negative $\delta^{13}C$ excursions in our *Uvigerina* spp. record (Fig. 5.2g).

Intervals of enhanced input of low $\delta^{13}C$ terrigenous detritus could account for the negative excursions considering that our core site is located near the mouth of the São Francisco River and that increased input of terrigenous sediments (e.g., Ti and Fe) occurred during HS (CAMPOS et al., 2019b). However, our low BFAR values during the last ca. 70 ka (Fig. 5.2b)

together with the lack of a clear trend in our $R_{Uvigerina\ spp./Benthics}$ during the analyzed interval (i.e., pre-HS2, HS2, and post HS2) (Fig. 5.2c) suggest that the negative $\delta^{13}C$ excursions were not accompanied by a marked increase in the local flux of organic carbon to the sea-floor (BOYLE, 1990; THEODOR et al., 2016). Thus, we deem the input of low $\delta^{13}C$ terrigenous detritus not to be the main driver of the negative $\delta^{13}C$ excursions in our *Uvigerina* spp. record (Fig. 5.2g). Epibenthic *C. pachyderma* $\delta^{13}C$ shows negative anomalies during HS3, HS2, and HS1 (Fig. 5.2f), i.e., all HS covered by the *C. pachyderma* record. Importantly, the magnitudes of the *C. pachyderma* negative excursions are very similar to those of *Uvigerina* spp. (Fig. 5.2g). This supports the suggestion that the local flux of organic carbon to the sea-floor was indeed low having insignificant influence in our *Uvigerina* spp. negative $\delta^{13}C$ excursions (SCHMIEDL; MACKENSEN, 2006; THEODOR et al., 2016; ZAHN et al., 1986). Taken together, we interpret the *Uvigerina* spp. negative excursions during all HS of the last glacial and deglacial (Fig. 5.2g) primarily as responses to changes in the overlying bottom water.

In the next section, we assess the possible changes that occurred in the overlying bottom water in the western South Atlantic mid-depth. We tentatively quantified the magnitude of the $\delta^{13}C$ excursions present in our record as well as in records from four other cores collected at similar depths in the western South Atlantic (Table 5.1, Fig. 5.1). Therefore, we selected, whenever possible, the three more positive $\delta^{13}C$ values of the pre-events (i.e., intervals just before the respective negative excursion) and the three more negative $\delta^{13}C$ values within the events (i.e., the negative excursions) (Fig. 5.3d, e, f, g, h) and calculated the magnitude of each excursion (i.e., pre-HS $\delta^{13}C$ minus HS $\delta^{13}C$). Because of age models uncertainties, the timing of HS can be slightly different among the considered records.

5.6.2 Western tropical South Atlantic mid-depths show the largest negative $\delta^{13}C$ excursions during HS

Atlantic depleted $\delta^{13}C$ values at intermediate and mid-depths are commonly attributed to an increased fraction of low-$\delta^{13}C$ SCW (BOYLE; KEIGWIN, 1987; DUPLESSY et al., 1988; KEIGWIN; LEHMAN, 1994; SARNTHEIN et al., 1994). A greater fraction of SCW AABW at our core site during HS could have potentially contributed to the negative $\delta^{13}C$ excursions (Figs. 5.2g, 5.3f). Additionally, during these millennial-scale events, the relatively low-$\delta^{13}C$ SCW AABW source signal could have been overprinted by increased Southern Ocean air-sea gas exchange. An increase in Southern Ocean air-sea gas exchange during HS is attributed to a reduced Southern Ocean stratification (ANDERSON et al., 2009) and a sea surface warming in

the high latitudes of the Southern Hemisphere (EPICA, 2006; LYNCH-STIEGLITZ et al., 1995). If this was the case (i.e., increased fraction of SCW AABW and/or depleted SCW AABW source signal), we would expect our $\delta^{18}O$ values to increase since SCW AABW shows a relatively higher $\delta^{18}O$ than NCW (LEGRANDE; SCHMIDT, 2006). However, they decrease during some HS and present no clear trend during others (Fig. 5.2h, i). It is noteworthy that the mentioned sea surface warming in the high latitudes of the Southern Hemisphere in response to a reduced AMOC (EPICA, 2006) would reduce the $\delta^{18}O$ values of SCW AABW (OPPO et al., 2015). But it is unlikely that this process had a predominant influence at the bottom of the water column of our core site. Also, if a decreased SCW AABW $\delta^{13}C$ source signal would have affected the bottom of the water column at our core site, we would expect the lowest mid-depth $\delta^{13}C$ HS excursions to occur to the south of our core site, what is not the case (see below). Mid-depth Atlantic water mass provenance records based on the neodymium isotopic composition of the authigenic fraction (a more robust proxy for water mass provenance than $\delta^{18}O$) show that NCW dominated the depths around 2000 m during HS (HOWE et al., 2018; ZHAO et al., 2019). Increased evidence suggest that the deglacial Atlantic negative $\delta^{13}C$ excursions may be related to changes in NCW (LUND et al., 2015; OPPO et al., 2015; SCHMITTNER; LUND, 2015; VOIGT et al., 2017; ZHAO et al., 2019). During events of weak AMOC (i.e., HS), the reduced input of high $\delta^{13}C$ surface waters into the deep North Atlantic due to decreased convection would promote a decrease in the source signal of the NCW (LUND et al., 2015; OPPO et al., 2015). Additionally, the reduced ventilation and consequent increased NCW residence time would have led to an increase in the accumulation of respired carbon at NCW depths throughout the Atlantic (SCHMITTNER; LUND, 2015). Thus, the decreased NCW $\delta^{13}C$ source signal during HS was accentuated along the NCW pathway southwards by the accumulation of respired carbon. Proxies of water mass residence time and flow rates should confirm this scenario. In fact, ^{14}C-depleted values (CHEN et al., 2015; LUND et al., 2015; ROBINSON et al., 2005; THORNALLEY et al., 2011) and high sedimentary $^{231}Pa/^{230}Th$ (HENRY et al., 2016; MCMANUS et al., 2004; MULITZA et al., 2017; SÜFKE et al., 2019) (Fig. 5.3b, c) from the western Atlantic suggest a reduced ventilation at NCW depths coeval with fresh water input into the high latitudes of the North Atlantic (marked by pulses of ice-rafted debris – IRD; Fig. 5.3a).

Considering the progressive character of the $\delta^{13}C$ decrease, we would expect the negative excursions to be smaller near the NCW source region, i.e., reflecting almost exclusively the reduction in the NCW $\delta^{13}C$ source signal, and the highest further south in the Atlantic, i.e.,

reflecting a combination of reduced NCW $\delta^{13}C$ source signal and accumulation of respired carbon at NCW depths. Then, the signal would dissipate/dilute by mixing with SCW (LUND et al., 2015; SCHMITTNER; LUND, 2015; TESSIN; LUND, 2013). Indeed, northern North Atlantic did not show markedly negative excursions during HS (e.g., ELLIOT et al., 2002) and the largest $\delta^{13}C$ negative excursion was reported to occur as far south as the western equatorial Atlantic intermediate depths (1.58°S, 1400 m) during HS1 (VOIGT et al., 2017). However, most western South Atlantic marine records reporting negative excursions during HS with appropriate temporal resolution only cover the last deglacial (i.e., HS1 and the YD) leaving aside the glacial HS (i.e., HS6-HS2). Exceptions have been reported, so far, for two records from the western South Atlantic mid-depth, i.e., GeoB3910-2 (4.25°S; Fig. 5.3e) from the western equatorial Atlantic covering the interval ca. 50-11 ka (BURCKEL et al., 2015) and GL-1090 (24.92°S; Fig. 5.3g) from the western subtropical South Atlantic covering the last ca. 185 ka (SANTOS et al., 2017) (Table 5.1; Fig. 5.1). Our new $\delta^{13}C$ record (Fig. 5.3f) covers the last ca. 70 ka with a high temporal resolution, being ideal not only to constrain NCW ventilation in the western tropical South Atlantic mid-depth during HS but also to fill the gap of marine records between 4.24°S and 24.92°S. Furthermore, core M125-95-3 provides the first western South Atlantic $\delta^{13}C$ record that clearly registers all HS of the last glacial and deglacial (i.e., from HS6 to the YD) (Fig. 5.3) (LYNCH-STIEGLITZ et al., 2014).

The compilation of western South Atlantic mid-depth records together with our new record reveal the existence of a coherent meridional pattern of negative $\delta^{13}C$ excursions during most HS (Figs. 5.3, 5.4, 5.5, 5.S1). Core M125-95-3 shows systematically larger $\delta^{13}C$ negative excursions, exception made for HS3 in which core GL-1090 shows the same magnitude of M125-95-3, and the YD in which core GeoB16202-2 shows a slightly higher magnitude (Figs. 5.4). The negative $\delta^{13}C$ excursion around 44 ka BP that can be seen in our record and in GeoB3910-2 record (BURCKEL et al., 2015) (Fig. 5.3e, f) is coeval with Greenland Stadial 12 (RASMUSSEN et al., 2014), a stadial that is also related to an AMOC slowdown that was, however, weaker than HS. Since our focus here relies on HS, we do not further discuss this event. It is important to mention that MIS4 is characterized as a period of intense oceanic carbon sequestration (BEREITER et al., 2012) that could have overprinted the negative $\delta^{13}C$ excursions during HS6 (Fig. 5.3f, g).

The meridional pattern of negative $\delta^{13}C$ excursions during most HS supports the notion that the combined effect of (i) changes in the $\delta^{13}C$ NCW source signal and (ii) the accumulation of respired carbon at mid-depth produced the largest negative $\delta^{13}C$ excursions in the western

tropical South Atlantic (i.e., M125-95-3 core site) from where it gradually lost magnitude by mixing with SCW until reaching the subtropical western South Atlantic (i.e., GL-1090 and 78GGC core sites) (Fig. 5.5) (LUND et al., 2015; SCHMITTNER; LUND, 2015; TESSIN; LUND, 2013). Importantly, our independent proxy for bottom water ventilation, i.e., bulk sediment S content, shows increases during all HS of the last glacial and deglacial (exception made for the YD) indicating an increased residence time of NCW in the western tropical South Atlantic (Figs. 5.2d, e, 5.3i, j).

To our knowledge, the use of S to track millennial-scale changes in bottom water ventilation is unprecedented (HARFF et al., 2011; PASQUIER et al., 2017; SLUIJS et al., 2008). Its use is grounded on the fact that an increase in the concentration of S at the sea-floor is tightly related to local depletion in oxygen availability (JØRGENSEN et al., 2019; JØRGENSEN; KASTEN, 2006). Since the flux of organic matter to the sea-floor was low at our core site throughout the investigated period (Fig. 5.2b, c), the S increases during HS mainly reflect changes in oxygen availability of the bottom water (i.e., NCW). A reduced ventilation and accumulation of respired carbon at NCW depths would decrease oxygen availability via aerobic organic matter degradation favoring the S accumulation at the sea-floor (i.e., via sulfate-reducing bacteria anaerobic organic matter degradation). Despite the overall good similarity, our benthic $\delta^{13}C$ and S records also show localized differences (e.g., during HS6). These localized differences most probably arise because of the partially different phenomena controlling both proxies.

The persistent negative $\delta^{13}C$ excursions and positive S excursions during HS of the last glacial and deglacial in our core (Fig. 5.3f, i, j) suggest that, even under different boundary conditions, similar mechanisms resulted in an increased NCW residence time and accumulation of respired carbon in the western tropical South Atlantic mid-depth. Moreover, the synchronism between past increases in atmospheric CO_2 (CO_{2atm}) (AHN; BROOK, 2008; 2014) and decreases in $\delta^{13}CO_{2atm}$ (BAUSKA et al., 2018; EGGLESTON et al., 2016) during millennial-scale climate change events in the one hand, and in the AMOC-related marine carbon cycle records on the other hand (BURCKEL et al., 2015; SANTOS et al., 2017; TESSIN; LUND, 2013; VOIGT et al., 2017) suggests that the AMOC played a relevant role in modulating the global carbon cycle during HS.

Figure 5.3 - Paleoceanographic records from the Atlantic. **(a)** Heinrich layers indicated by the presence of ice-rafted debris (IRD) from the stack curve of LISIECKI and STERN (2016); **(b)** western equatorial Atlantic $^{231}Pa/^{230}Th$ (MULITZA et al., 2017); **(c)** Bermuda Rise $^{231}Pa/^{230}Th$ (HENRY et al., 2016; MCMANUS et al., 2004); **(d)** benthic (i.e., *Cibicides wuellerstorfi*, *Cibicidoides kullenbergi*, and *Cibicides lobatulus*) stable carbon isotopic composition ($\delta^{13}C$) from core GeoB16202-2, western equatorial Atlantic (VOIGT et al., 2017); **(e)** benthic (*Cibicides wuellerstorfi*) $\delta^{13}C$ from core GeoB3910-2, western equatorial Atlantic (BURCKEL et al., 2015); **(f)** benthic (i.e., *Uvigerina* spp. corrected for comparison to epibenthic species; correction factor based on SHACKLETON and HALL (1984)) $\delta^{13}C$ from core M125-95-3, western tropical South Atlantic (this study); **(g)** benthic (i.e., *Cibicides wuellerstorfi*) $\delta^{13}C$ from core GL-1090, western subtropical South Atlantic (SANTOS et al., 2017); **(h)** benthic (i.e., *Cibicidoides* spp.) $\delta^{13}C$ from core 78GGC, western subtropical South Atlantic (TESSIN; LUND, 2013); **(i-j)** X-ray fluorescence (XRF) core scanner sulfur (S) (black line) and energy dispersive polarized (EDP) XRF S (orange circles) (this study). All benthic $\delta^{13}C$ records (d)-(h) derive from mid-depth western South Atlantic cores ranging from 1820 to 2362 m water depth. Black filled circles in records (d)-(h) indicate the data-points used to calculate the magnitude of the negative $\delta^{13}C$ excursions (more details are found in Fig. 5.4). Black (orange) squares at the bottom of the panel depict calibrated radiocarbon ages (tie-points) with 2σ standard error. Red vertical bars represent millennial-scale events Younger Dryas (YD) and Heinrich Stadial (HS) 1 to 6. Marine Isotope Stages (MIS) are depicted below the upper axis.

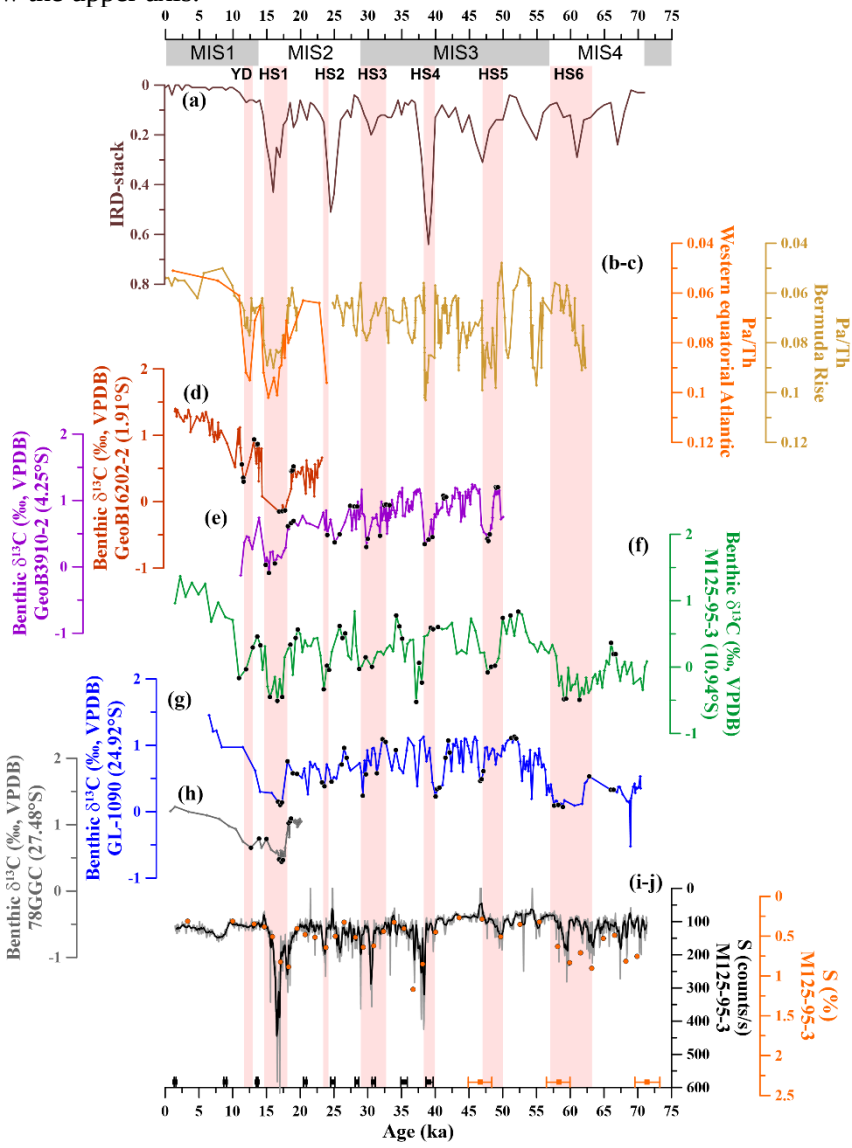

Figure 5.4 - Heinrich Stadial (HS) magnitude of the negative $\delta^{13}C$ excursions of western Atlantic cores (color coded according to Fig. 5.3) GeoB16202-2 (equatorial Atlantic) (VOIGT et al., 2017), GeoB3910-2 (equatorial Atlantic) (BURCKEL et al., 2015), M125-95-3 (tropical South Atlantic) (this study), GL-1090 (subtropical South Atlantic) (SANTOS et al., 2017), and 78GGC (subtropical South Atlantic) (TESSIN; LUND, 2013). Excursions were calculated considering the three more positive values of the pre-HS and the three more negative values of the HS. The Younger Dryas (YD) and HS1 to 6 are depicted.

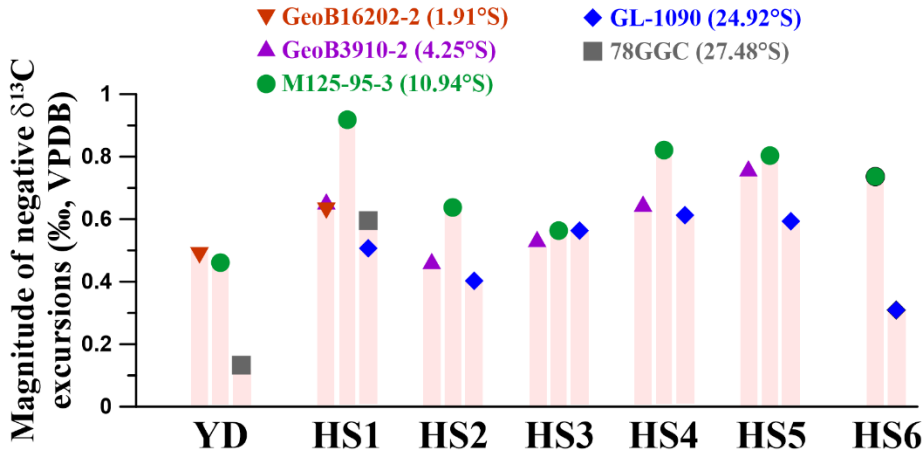

Figure 5.5 - Schematic representation of the western Atlantic during Heinrich Stadials (i.e., under a weak Atlantic meridional overturning circulation). Arrows depict source region and the main pathway of the Southern Component Water (SCW) and Northern Component Water (NCW). NCW dashed arrow indicates decreased convection and aging of this water mass. Open and filled dots indicate core sites of GeoB16202-2 (equatorial western Atlantic) (VOIGT et al., 2017), GeoB3910-2 (equatorial western Atlantic) (BURCKEL et al., 2015), M125-95-3 (tropical western South Atlantic) (this study), GL-1090 (subtropical western South Atlantic) (SANTOS et al., 2017), and 78GGC (subtropical western South Atlantic) (TESSIN; LUND, 2013). The blue shading represents the magnitude of the NCW negative $\delta^{13}C$ excursion (accumulation of respired carbon) which gradually increases southwards at mid-depth, peaking in the western tropical South Atlantic (i.e., M125-95-3 core site) from where it starts to dissipate/dilute by mixing with SCW towards the subtropical western South Atlantic (i.e., GL-1090 and 78GGC core sites).

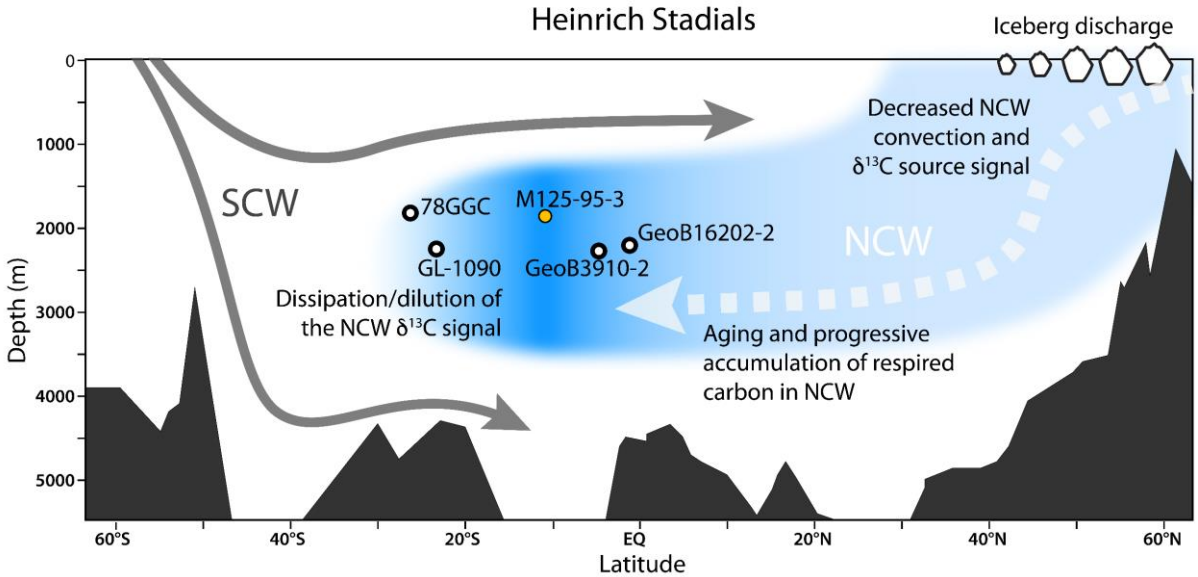

5.7 Conclusions

We present new high-resolution $\delta^{13}C$ and S records from the western tropical South Atlantic mid-depth for the last ca. 70 ka. This is the first western South Atlantic $\delta^{13}C$ record that clearly registers all HS of the last glacial and deglacial, filling the gap of shorter and lower temporal resolution marine records between 4.24°S and 24.92°S. The concurrent $\delta^{13}C$ decreases and S increases during HS in our records suggest reduced ventilation and consequent accumulation of respired carbon at NCW depths. Based on the comparison of our new data to existing western South Atlantic marine records collected around the same water depth, we conclude that (i) even under different boundary conditions negative $\delta^{13}C$ excursions occurred during all HS of the last glacial and deglacial, and (ii) the magnitude of the negative excursions suggests a coherent meridional pattern. This meridional pattern supports the notion that the HS reduction in the NCW $\delta^{13}C$ source signal together with the accumulation of respired carbon at Atlantic NCW depths promoted a progressive depletion in the NCW $\delta^{13}C$ signature along its southwards advection. The highest negative $\delta^{13}C$ excursions occurred in the western tropical South Atlantic, from where the signal started to dissipate/dilute by mixing with SCW.

Acknowledgments

Logistic and technical assistance was provided by the captain and crew of the R/V Meteor. New data shown herein are archived in Pangaea (doi:10.1594/PANGAEA.915451). M.C. Campos acknowledges the financial support from FAPESP (grants 2016/10242-0 and 2018/06790-7). C.M. Chiessi acknowledges the financial support from FAPESP (grant 2018/15123-4), CAPES (grants 564/2015 and 88881.313535/2019-01), CNPq (grants 302607/2016-1 and 422255/2016-5) and the Alexander von Humboldt Foundation. CAPES (grants 88887.156152/2017-00 and 88881.161151/2017-01) and CNPq (grant 406322/2018-0) currently support I.M. Venancio. T.M.L. Pinho acknowledges the financial support from FAPESP (grant 2019/10642-6). S. Crivellari acknowledges the financial support from CAPES (grant 88887.196044/2018-00). A.L.S. Albuquerque is a senior CNPq researcher (grants 302521-2017-8 and 429767/2018-8), and acknowledges the financial support from CAPES (Finance Code 001). S. Mulitza and H. Kuhnert were funded through the DFG Research Centre, Cluster of Excellence “The Ocean in the Earth System”. A. Bahr received funding from the Deutsche Forschungsgemeinschaft (DFG) via Grant BA 3809/9-1.

5.8 Supplementary material

Figure 5.S1. Benthic $\delta^{13}C$ records from the mid-depth western South Atlantic. **(a)** *Uvigerina* spp. $\delta^{13}C$ (corrected for comparison to epibenthic species; the correction factor of 0.9‰ was applied (SHACKLETON; HALL, 1984)) from core M125-95-3, western tropical South Atlantic (this study); **(b)** *Cibicides wuellerstorfi* $\delta^{13}C$ from core GeoB3910-2, western equatorial Atlantic (BURCKEL et al., 2015); and **(c)** *Cibicides wuellerstorfi* $\delta^{13}C$ from core GL-1090, western subtropical South Atlantic (SANTOS et al., 2017). Black (orange) squares at the bottom of the panel depict calibrated radiocarbon ages (tie-points) with 2σ standard error. Red vertical bars represent millennial-scale events Younger Dryas (YD) and Heinrich Stadial (HS) 1 to 6. Marine Isotope Stages (MIS) are depicted below the upper axis.

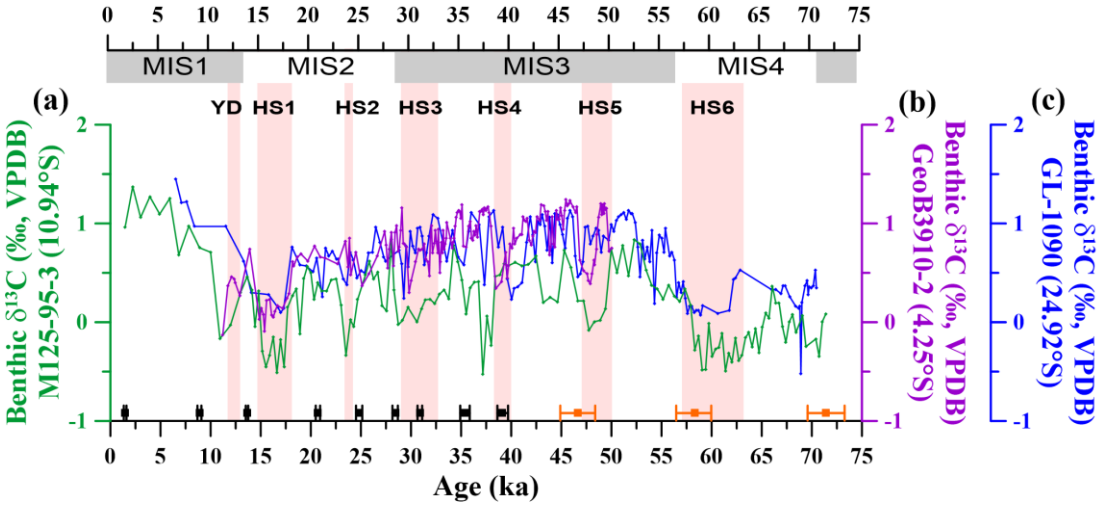

6 The transfer of millennial-scale Agulhas Leakage signals to the western tropical South Atlantic

Marília C. Campos[a*], Cristiano M. Chiessi[a] et al.

[a] School of Arts, Sciences and Humanities, University of São Paulo, São Paulo, Brazil

* Corresponding author: marilia.carvalho.campos@usp.br

Manuscript in preparation

6.1 Abstract

A small fraction of warm and saline upper waters from the Indian Ocean Agulhas Current invades the South Atlantic through the so-called Agulhas Leakage (AL). Paleorecords and model simulations suggest that this leakage is an important driver of changes in the Atlantic meridional overturning circulation during Heinrich Stadials (HS). However, accumulation and transport of heat and salt from the AL region to high latitudes of the North Atlantic remains unclear. Here we reconstruct western tropical South Atlantic sea surface temperature and salinity from a core located mid-way the AL region and the equator, and compare our results to published data from the AL region. Both cores show mixed-layer accumulation of heat and salt during HS. However, the systematically smaller positive excursions in our core suggest that surface heat and salt was lost/diluted along the route from the AL region to the western tropical South Atlantic. Thus, Indian Ocean salt that eventually reached the high latitudes of the North Atlantic helping on the recovering of the AMOC was most probably transported mainly within the thermocline.

6.2 Introduction

Millennial-scale changes in northern North Atlantic formation and southward transport of cold, relatively fresh and deep waters is a well-studied topic. Paradoxically, its southern South Atlantic counterpart, i.e., millennial-scale changes in the northward transport of warm, relatively saline and shallow waters that partially come from the Indian Ocean, remains poorly understood. The Indian Ocean surface and thermocline waters that enter the South Atlantic derive from the Agulhas Current through the so-called Agulhas Leakage (AL). The AL is thought to be an important driver of changes in the strength of the Atlantic meridional overturning circulation (AMOC) on different time-scales (BEAL et al., 2011). Model simulations and marine records suggest that the enhanced inflow and northward transport of

warm and saline AL waters ended up strengthening the AMOC during glacial-interglacial transitions (CALEY et al., 2012; KNORR; LOHMANN, 2003; PEETERS et al., 2004) as well as during stadial-interstadial millennial-scale transitions (BEAL et al., 2011; CHIESSI et al., 2008). During millennial-scale stadials called Heinrich Stadials (HS), the weak AMOC reduced the cross-equatorial transport of heat and salt that, in turn, accumulated in the Southern Hemisphere (MIX et al., 1986). After some time, the northward advection of the salt excess to the regions of deep water formation in the northern North Atlantic contributed to reestablish the AMOC strength (GONG et al., 2013; KNORR; LOHMANN, 2007).

Here we investigate the sea surface accumulation and transport of heat and salt from the AL region, i.e., southeastern subtropical South Atlantic, to the western tropical South Atlantic during HS. Therefore, we performed stable oxygen isotopes and Mg/Ca analyses on shallow-dwelling planktonic foraminifera from marine sediment core M125-95-3, collected in the western tropical South Atlantic (10.94°S), and compared our results to previously published records from a marine core collected from the AL region. The comparison shows that data from both cores support the HS thermal and haline bipolar seesaw theory (BROECKER, 1998; LOHMANN, 2003), i.e., accumulation of heat and salt in the Southern Hemisphere during events of weak AMOC (i.e., HS). However, the systematically smaller positive excursions in our core suggest that surface heat and salt was lost and diluted, respectively, along the route from the southeastern subtropical to the western tropical South Atlantic.

6.3 Regional setting

Our marine sediment core was collected from the bifurcation of the southern branch of the South Equatorial Current (SSEC) (Fig. 6.1). There, the mixed layer is occupied by warm (>22°C) and saline (>36.5 psu) oligotrophic Tropical Water (TW) (GARCIA et al., 2013; LOCARNINI et al., 2013; ZWENG et al., 2013). The SSEC bifurcation occurs between 8° and 13°S originating the northwestward-flowing North Brazil Current (NBC) and the southward-flowing Brazil Current (BC) (SILVA et al., 2009). These currents play an important role in the distribution of heat and salt between the hemispheres. While the NBC transports a large amount of heat and salt across the equator to the North Atlantic during periods of strong AMOC, the BC can store and redirect towards subtropical latitudes of the South Atlantic a significant portion of the heat and salt not delivered northwards during periods of weak AMOC (MAIER-REIMER et al., 1990). The SSEC bifurcation shifts seasonally in response to the regional wind fields (Fig. 6.1). During austral summer (winter), the Intertropical Convergence Zone (ITCZ)

is in its southernmost (northernmost) position and the SSEC bifurcation shifts northward (southward) (RODRIGUES et al., 2007).

Figure 6.1 - Location of marine cores M125-95-3 (green dot; this study) and MD02-2594 (purple diamond; DYEZ et al. (2014)) together with a schematic representation of the large-scale upper circulation in the South Atlantic (STRAMMA; ENGLAND, 1999). Antarctic Circumpolar Current: ACC; Agulhas Current: AC; AL: Agulhas Leakage; Brazil Current: BC; North Brazil Current: NBC; South Atlantic Current: SAC; Southern branch of the South Equatorial Current: SSEC. The Intertropical Convergence Zone (ITCZ) and the Southern Hemisphere Westerlies (SW) are depicted as yellow dashed band and grey arrows, respectively.

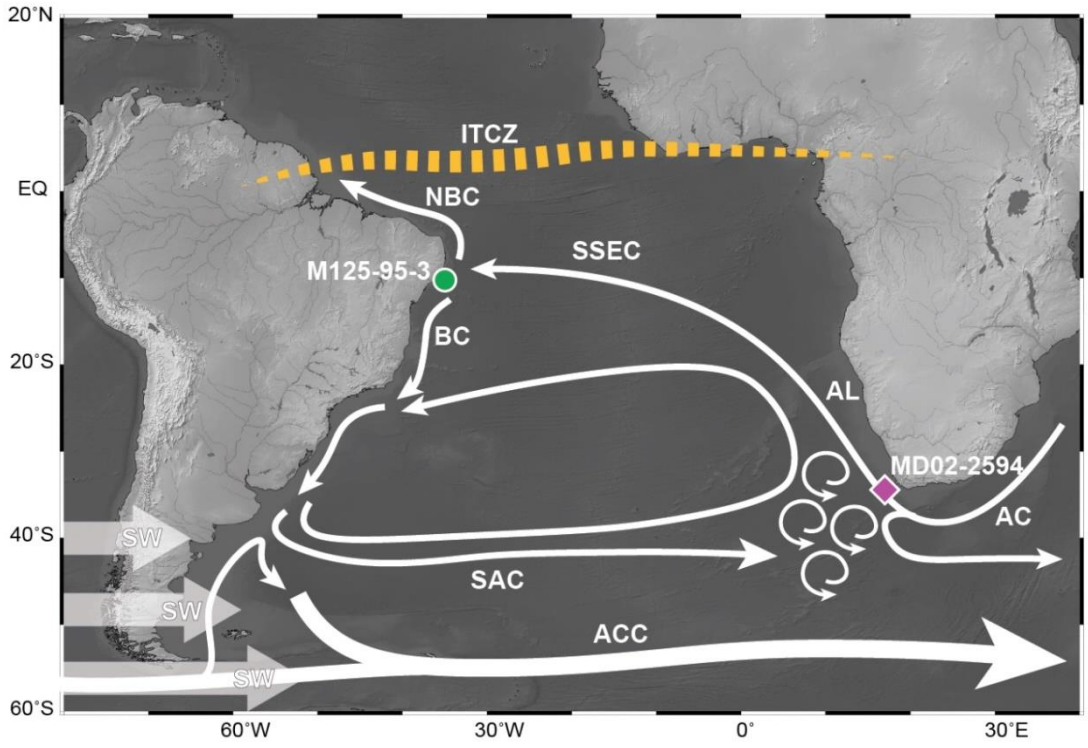

The SSEC is the closest route between the southeastern subtropical South Atlantic and the western tropical South Atlantic (Fig. 6.1). At the southeastern subtropical South Atlantic, a small fraction of the Agulhas Current enters the South Atlantic throughout an Indian-Atlantic Ocean gateway situated around the southern tip of Africa (Fig. 6.1). These waters are called AL and they enter the South Atlantic as rings, i.e., Agulhas rings (ARHAN et al., 2011), while the majority of the Agulhas Current retroflects back into the Indian Ocean (Fig. 6.1). The Agulhas Current is the strongest western boundary current in the Southern Hemisphere carrying 70-78 Sv of warm and saline surface and thermocline waters from the tropical South Indian Ocean towards the southern tip of Africa (LUTJEHARMS, 2006). The AL transports into the South Atlantic 2-15 Sv by shedding ca. five rings per year (RICHARDSON, 2007). The magnitude of the leakage is thought to be controlled by the latitudinal position of the Southern Hemisphere Westerlies and the associated oceanic Subtropical Front (Fig. 6.1) (BIASTOCH et al., 2009).

A persistent leakage of warm and saline AL waters could impact the Atlantic thermohaline properties by affecting its stratification and deep convection being, thus, a potential driver of AMOC changes on different time-scales (BEAL et al., 2011).

6.4 Material and methods

Marine sediment core M125-95-3 (10.94°S, 36.20°W, 1897 m water depth, 10.4 m core length) was collected from the continental slope in the western tropical South Atlantic during RV Meteor cruise M125 (Fig. 6.1) (BAHR et al., 2016). We focus on the upmost ca. 7.4 m of the core which covers the last ca. 70 thousand years before present (ka BP; present is 1950) (CAMPOS et al., 2019b), i.e., Marine Isotope Stages (MIS) 4-1, containing thus the HS of the last glacial and deglacial. In addition, we also discuss data from marine core MD02-2594 collected from the Agulhas Bank slope (34.71°S, 17.34°E, 2440 m water depth, 7.5 m core length) (Fig. 6.1) (DYEZ et al., 2014). We restrict our comparison to the Agulhas Bank and the SSEC bifurcation regions since they represent the extremes of the shortest route between the AL region and the western tropical South Atlantic (Fig. 6.1).

The chronology of core M125-95-3 is based on nine planktonic foraminifera accelerator mass spectrometry radiocarbon ages (covering the last ca. 40 ka) and three M125-95-3 *Uvigerina* spp. $\delta^{18}O$ tie-points aligned to a benthic $\delta^{18}O$ reference curve from GOVIN et al. (2014). The calibration curve IntCal13 (REIMER et al., 2013) and variable simulated reservoir ages (BUTZIN et al., 2017) were used to calibrate the raw radiocarbon ages. The age model and sedimentation rates were calculated using the modelling tool BACON v. 2.2 (BLAAUW; CHRISTEN, 2011) within the software PaleoDataView v. 0.8.3.4 (LANGNER; MULITZA, 2019). Details regarding the age model are provided in CAMPOS et al. (2019b).

In order to reconstruct past mixed layer conditions, we used $\delta^{18}O$ and Mg/Ca-based sea surface temperature (SST) (Mg/Ca-SST hereafter) records derived from *Globigerinoides ruber* pink analyses. From the sediment fraction 250-350 μm ca. 10 (20) specimens per sample were handpicked under a binocular microscope every 2 (6) cm for $\delta^{18}O$ (Mg/Ca-SST) analyses. While the *G. ruber* pink $\delta^{18}O$ analyses for the uppermost 230 cm were conducted with a Finnigan MAT 252 mass spectrometer coupled to a Kiel III carbonate preparation device at the State Key Laboratory of Marine Geology (Tongji University, China), the rest of the $\delta^{18}O$ analyses were conducted with a Thermo Fisher Scientific MAT253plus mass spectrometer coupled to a Kiel IV carbonate preparation device at the MARUM – Center for Marine Environmental Sciences (University of Bremen, Germany). Output data were calibrated against

in-house standards that are themselves calibrated against the NBS19 standard. We report the isotopic results in per mil (parts per thousand, i.e., ‰) versus Vienna Peedee Belemnite (VPDB). For the measured period, the standard deviation of in-house standard replicate measurements was 0.07‰ for the State Key Laboratory of Marine Geology and 0.06‰ for the MARUM. Mg/Ca-SST analyses were conducted according to the standard cleaning protocol for foraminiferal Mg/Ca analyses suggested by BARKER et al. (2003). The samples were analyzed with a Thermo Finnigan Element 2 sector field inductively coupled plasma (ICP) mass spectrometer (ICP-MS) at the Petrology of the Ocean Crust ICP-MS Laboratory (Faculty of Geosciences, University of Bremen, Germany). Exception is made for the interval between 92-194 cm which was analyzed with an Agilent Technologies 700 series ICP optical emission spectrometer (ICP-OES) with autosampler ASX-520 Cetac and micro-nebulizer at the MARUM. Instrumental precision of ICP-MS and ICP-OES were monitored through analyses of an in-house standard solution (which was the same for both ICP) of theoretical value 3.40 mmol mol^{-1}. Mean long-term standard deviation were 0.012 mmol mol^{-1}. We used the *G. ruber* pink calibration equation from REGENBERG et al. (2009) (i.e., Mg/Ca = 0.23 exp (0.111 * SST)) to convert Mg/Ca into SST. The uncertainty estimated for *G. ruber* p Mg/Ca calibration is within +/- 1.0 °C (REGENBERG et al., 2009). The SST reconstruction uncertainty is estimated by propagating uncertainties from the analytical measurements (i.e., 0.012 mmol mol^{-1}, which is equivalent to 0.04 °C) and from the used Mg/Ca-SST calibration equation (i.e., 1.0 °C).

Based on our *G. ruber* pink $\delta^{18}O$ and Mg/Ca-SST as well as the paleotemperature equation described in MULITZA et al. (2003) (i.e., SST = - 4.44 (($\delta^{18}O_{calcite}$ - $\delta^{18}O_{sea\ water}$) + 14.20) we estimated the $\delta^{18}O$ of surface sea water ($\delta^{18}O_{ssw}$). To convert the $\delta^{18}O_{ssw}$ values from VPDB to Vienna Standard Mean Ocean Water (VSMOW), we applied the conversion constant of HUT (1987) (i.e., 0.27‰). In order to extract the effects of changes in global ice volume from $\delta^{18}O_{ssw}$ and obtain ice volume corrected $\delta^{18}O_{ssw}$ ($\delta^{18}O_{ivc\text{-}ssw}$), we applied the sea level correction from WAELBROECK et al. (2002) (i.e., $\delta^{18}O_{ivc\text{-}ssw}$ = $\delta^{18}O_{ssw}$ - (ESL*1/130), where ESL is the estimated sea level difference to preindustrial sea level in meters). The $\delta^{18}O_{ivc\text{-}ssw}$ estimated error is a combination of the SST reconstruction uncertainty (i.e., which is equivalent of 0.22‰; MULITZA et al. (2003)) plus the analytical error of the *G. ruber* pink $\delta^{18}O$ (i.e., 0.065‰, which represents the mean between the standard deviation of both laboratories). Thus, the propagation of uncertainties for $\delta^{18}O_{ivc\text{-}ssw}$ is around 0.23‰. Since the $\delta^{18}O_{ivc\text{-}ssw}$ and sea surface salinity

(SSS) are governed by the same factors (i.e., precipitation, evaporation, continental discharge and advection), the $\delta^{18}O_{ivc\text{-}ssw}$ is used here as a proxy for SSS.

6.5 Results and discussion

Last glacial and deglacial paleoclimate records indicate that the HS were marked by cold temperatures over Greenland (Fig. 6.3a) (RASMUSSEN et al., 2014) and the surface North Atlantic (BARD et al., 2000), and also by pulses of ice-rafted debris at the northern North Atlantic (Fig. 6.3b) (LISIECKI; STERN, 2016). On the other hand, the Southern Hemisphere presented warmer temperatures (Fig. 6.3i) (BARBANTE et al., 2006), increased surface oceanic salinity (SIMON et al., 2015) as well as increased continental precipitation over tropical regions, e.g., most tropical South America (e.g., Fig. 6.3c) (CAMPOS et al., 2019b). These abrupt events are related to periods of AMOC slowdown and consequent reduction in the cross-equatorial heat and salt transport. This interhemispheric asymmetric response to HS is usually termed thermal and haline bipolar seesaw (BROECKER, 1998; LOHMANN, 2003). Furthermore, since higher SST enhances evaporation, the Southern Hemisphere warming would further increase SSS (LOHMANN, 2003).

Our Mg/Ca-SST record shows positive excursions (up to 27.4 °C at ca. 15.6 ka BP) during HS (Fig. 6.2c). Exceptions are made for HS5 and the YD. During these events, the sedimentation rate is around 6 cm ka^{-1}, being considerably lower than during the other HS (Fig. 6.2a).

The relatively low sedimentation rate together with the 6 cm resolution of our Mg/Ca-SST record may have hidden the signal of HS5 and the YD. $\delta^{18}O_{ivc\text{-}ssw}$ shows positive (negative) excursions during HS6, HS3 and HS2 (HS4 and HS1) (Fig. 6.2b). For the same reasons described for Mg/Ca-SST record, HS5 (despite it seems to present negative excursion) and the YD $\delta^{18}O_{ivc\text{-}ssw}$ will not be interpreted.

Figure 6.2 - Marine sediment core M125-95-3 records for the last 70 ka. **(a)** Sedimentation rate; **(b)** ice volume corrected surface sea water stable oxygen isotopic composition ($\delta^{18}O_{ivc\text{-}ssw}$), a proxy for sea surface salinity; **(c)** Mg/Ca-based sea surface temperature (Mg/Ca-SST) based on *Globigerinoides ruber* pink (*G. ruber* p); and **(d)** *G. ruber* p $\delta^{18}O$. Dark green, red and light green lines in records (b), (c) and (d), respectively, represent three-point running averages. Black (orange) squares at the bottom of the panel depict calibrated radiocarbon ages (tie-points) with 2σ standard error. Red vertical bars represent abrupt millennial scale events Heinrich Stadial (HS) 6-1 and the Younger Dryas (YD). Marine Isotope Stages (MIS) are depicted below the upper axis.

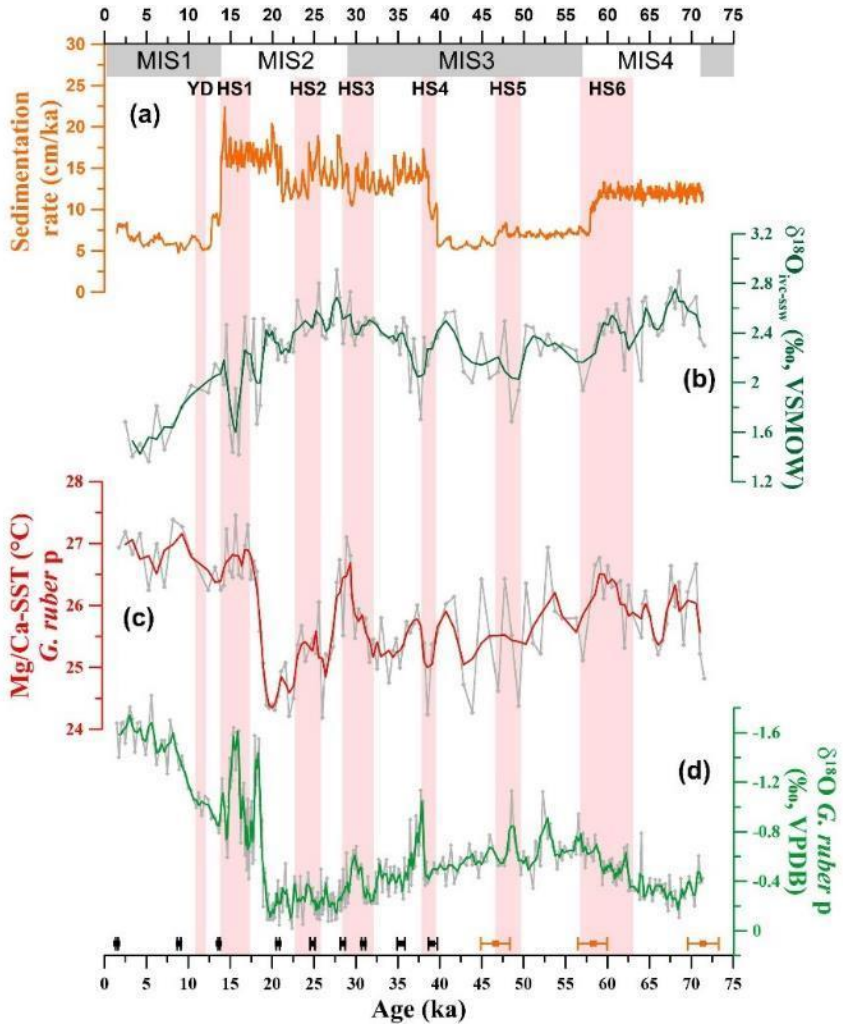

Our HS positive Mg/Ca-SST excursions (Fig. 6.3e) are in accordance with the thermal bipolar seesaw theory (BROECKER, 1998). AL core MD02-2594 (Fig. 6.3g) (DYEZ et al., 2014) also recorded a similar feature. However, the magnitude of the positive excursions differs between both records (Fig. 6.4b). We identified systematically smaller Mg/Ca-SST changes in M125-95-3 than in MD02-2594 during all HS, except for HS1 in which both records show similar positive excursions (Fig. 6.4b).

Figure 6.3 - Marine and continental paleoclimate records from Greenland, Antarctica and the Atlantic Ocean. **(a)** North Greenland Ice Core Project (NGRIP) $\delta^{18}O$ (RASMUSSEN et al., 2014); **(b)** northern North Atlantic stack of ice-rafted debris (IRD) (LISIECKI; STERN, 2016); **(c)** ln(Ti/Ca) from marine sediment core M125-95-3 (CAMPOS et al., 2019b); **(d)** ice volume corrected surface sea water stable oxygen isotopic composition ($\delta^{18}O_{ivc\text{-}ssw}$), a proxy for sea surface salinity from marine sediment core M125-95-3 (this study); **(e)** Mg/Ca-based sea surface temperature (Mg/Ca-SST) from marine sediment core M125-95-3 (this study); **(f)** $\delta^{18}O_{ivc\text{-}ssw}$ from marine sediment core MD02-2594 (DYEZ et al., 2014); **(g)** Mg/Ca-SST from marine sediment core MD02-2594 (DYEZ et al., 2014); **(h)** abundance of *Neogloboquadrina pachyderma* sinistral (*N. pachyderma* s) from marine sediment core GeoB1711-4 (COLLINS et al., 2014; LITTLE et al., 1997); and **(i)** EPICA Community Members - Dronning Maud Land (EDML) $\delta^{18}O$ (BARBANTE et al., 2006). Dark green and red lines in records (d), (e), (f), and (g) represent three-point running averages. Black (orange) squares at the bottom of the panel depict calibrated radiocarbon ages (tie-points) with 2σ standard error. Blue-to-red vertical bars represent abrupt millennial scale events Heinrich Stadial (HS) 6-1 and the Younger Dryas (YD). Marine Isotope Stages (MIS) are depicted below the upper axis.

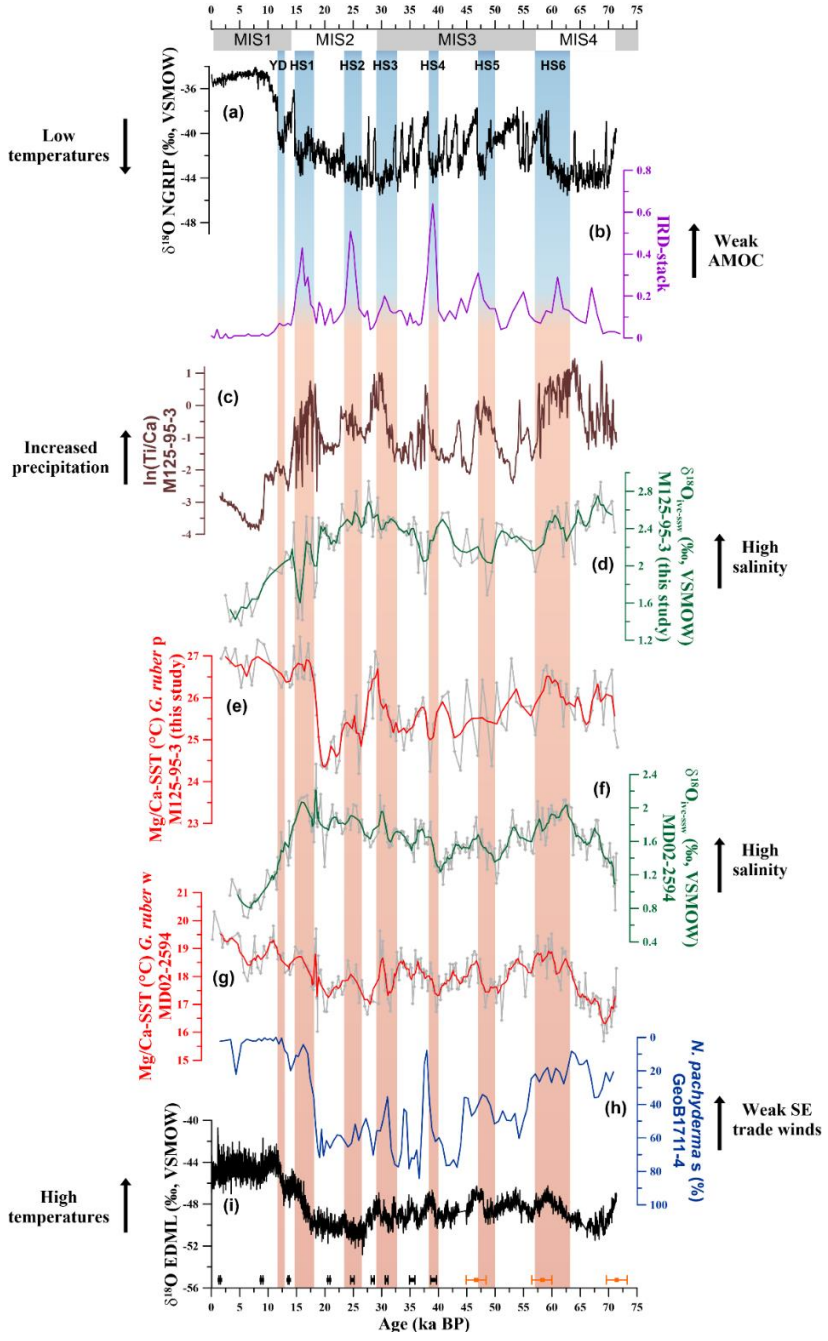

Considering that (i) the M125-95-3 core site is located at the SSEC bifurcation and, thus, should reflect SSEC properties (Fig. 6.1) and (ii) the SSEC is the most direct route between the AL region and western tropical South Atlantic (Fig. 6.1), the identified pattern may be related to a loss of heat to the atmosphere along the route southeastern subtropical-western tropical South Atlantic. Indeed, modern observations suggest that Agulhas rings decay rapidly in the Cape Basin (SCHMID et al., 2003), losing to the atmosphere part of their anomalously high surface heat content (VAN AKEN et al., 2003). Also, model simulations show that along their northward transport within the Atlantic Ocean, warm AL waters progressively lose heat to the atmosphere (BEAL et al., 2011; HAARSMA et al., 2011; WEIJER et al., 2002).

Our positive $\delta^{18}O_{ivc\text{-}ssw}$ excursions during HS6, HS3 and HS2 (Fig. 6.3d) are in accordance with the haline bipolar seesaw theory (LOHMANN, 2003). Similarly to the loose of heat, a salt loss trend seems to occur along the route southeastern subtropical-western tropical South Atlantic, i.e., M125-95-3 positive $\delta^{18}O_{ivc\text{-}ssw}$ excursions are smaller than AL core MD02-2594 excursions (Fig. 6.4a). The strength of the AL could contribute to explain the smaller M125-95-3 excursions during these events. The model analyzed by SIMON et al. (2015) showed a weakening of the Agulhas Current during a weak AMOC experiment. The authors suggested that, despite Agulhas Current SSS increases during HS, a weakening of this current would result in reduced salt transport by the AL into the South Atlantic. Another factor that could account for the smaller M125-95-3 excursions is the dilution of SSS via direct precipitation (e.g., PORTILHO-RAMOS et al., 2017; VENANCIO et al., 2020). Indeed, CAMPOS et al. (2019b) showed higher atmospheric precipitable water over our core site during HS.

Our negative $\delta^{18}O_{ivc\text{-}ssw}$ excursions during HS4 and HS1 contradict the haline bipolar seesaw theory. CAMPOS et al. (2019b) showed increased precipitation over the adjacent continent, i.e., eastern South America, during all HS (Fig. 6.3c). The increased precipitation over the continent most probably increased the discharge of fresh river waters impacting the upper water column of our core site. On the other hand, CAMPOS et al. (2020, under review, Chapter 5) showed that, despite higher continental precipitation, the upper water column of our core site was not affected by river-born nutrients, indicating that the low-salinity river plume did not substantially affected the upper water column of our core site. Furthermore, considering BAHR et al. (2013) and VENANCIO et al. (2020), the $\delta^{18}O_{ivc\text{-}ssw}$ may not faithfully record changes in riverine input. Thus, we cannot affirm that our negative $\delta^{18}O_{ivc\text{-}ssw}$ excursions during HS4 and HS1 are related to increased input of low-salinity river water. Instead, they most probably reflect primary local precipitation-evaporation oceanic balance. Assuming a linear relationship

between the magnitude of the AMOC slowdown during HS and the magnitude of precipitation increase over core site M125-95-3 (similarly to the one described by MULITZA et al. (2017)), the negative $\delta^{18}O_{ivc\text{-}ssw}$ excursions should be related to stronger HS. Indeed, according to the North Atlantic ice-rafted debris pulses (Fig. 6.3b) (LISIECKI; STERN, 2016) as well as the abundance of a cold-water foraminifera species in the southeastern South Atlantic, a proxy for SE trade winds strength (i.e., weak SE trade winds are associated with a weak AMOC) (Fig. 6.3h) (LITTLE et al., 1997), HS4 and HS1 were two of the strongest HS of the last ca. 70 ka. For the other HS, direct oceanic precipitation may not have been strong enough to produce negative excursions in $\delta^{18}O_{ivc\text{-}ssw}$, but it could have still contributed to the smaller M125-95-3 excursions compared to those of MD02-2594 (Fig. 6.4a).

We suggest that the heat and salt imported from the Indian Ocean surface waters during HS were only partially transferred to the western tropical South Atlantic. Thus, the northward advection of the salt excess to the regions of deep water formation in the northern North Atlantic that contributed to recover the AMOC strength was most probably transported mainly within the thermocline waters.

Figure 6.4 – Amplitude of Heinrich Stadials (HS) excursions in **(a)** ice volume corrected surface sea water stable oxygen isotopic composition ($\delta^{18}O_{ivc\text{-}ssw}$) (a proxy for sea surface salinity) and **(b)** Mg/Ca-based sea surface temperature (Mg/Ca-SST) for marine sediment cores M125-95-3 (green dot; this study) and MD02-2594 (purple diamond; DYEZ et al. (2014)). The excursions were calculated by selecting, whenever possible, the three more positive values of the pre-HS and the three more negative values within HS (i.e., pre-HS minus HS). Black dashed line in panel (a) depicts zero anomaly.

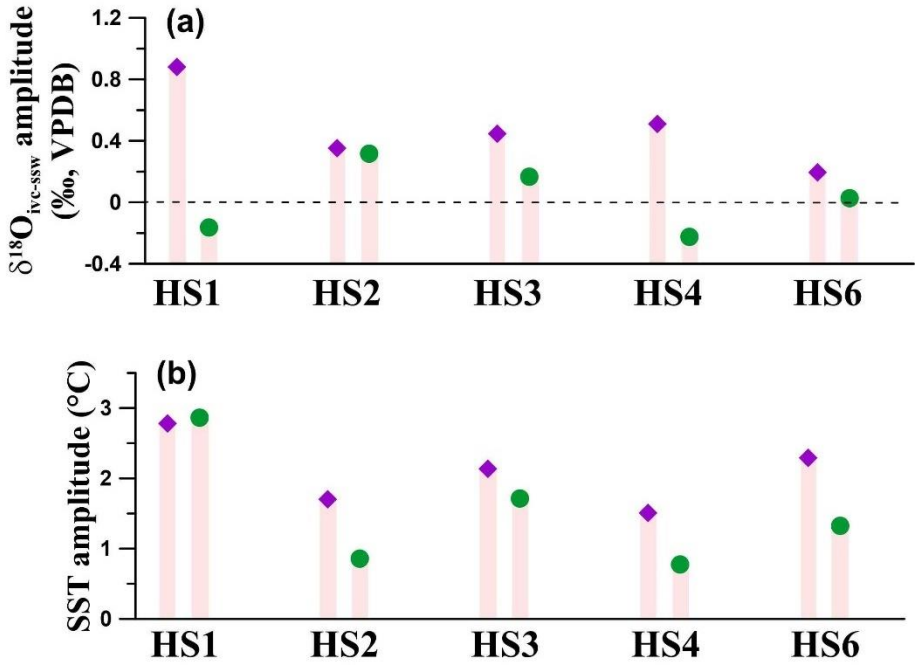

6.6 Conclusions

We show 70 ka data from marine sediment core M125-95-3 collected from the western tropical South Atlantic (10.94°S), at the SSEC bifurcation. This key location allowed us to reconstruct mixed layer conditions in the portion of the western South Atlantic that is closest to the AL region, and on the route of AL waters to the North Atlantic. We compared our Mg/Ca-SST and $\delta^{18}O_{ivc\text{-}ssw}$ data to previously published data from core MD02-2594 collected from the Agulhas Bank. Both cores show positive Mg/Ca-SST and $\delta^{18}O_{ivc\text{-}ssw}$ excursions during HS. Additionally, M125-95-3 shows systematically smaller positive excursions when compared to MD02-2594. This suggests that part of the surface heat and salt imported from the Indian Ocean was lost and diluted, respectively, along the route from the AL region to the western tropical South Atlantic. Finally, Indian Ocean salt that eventually reached the high latitudes of the North Atlantic helping on the recovering of the AMOC was most probably transported mainly within the thermocline.

Acknowledgements

Logistic and technical assistance was provided by the captain and crew of R/V Meteor. New data shown herein will be archived in Pangaea (www.pangaea.de). M.C. Campos acknowledges the financial support from FAPESP (grants 2016/10242-0 and 2018/06790-7). C.M. Chiessi acknowledges the financial support from FAPESP (grant 2018/15123-4), CAPES (grants 564/2015 and 88881.313535/2019-01), CNPq (grants 302607/2016-1 and 422255/2016-5) and the Alexander von Humboldt Foundation.

7 Final remarks

7.1 Summary and conclusions

In this thesis, marine sediment core M125-95-3 collected from the E South American continental margin, in the western tropical South Atlantic (10.94°S), was investigated for the last 70 ka. The main focus was understanding how South American hydroclimate (Chapter 4), the western tropical South Atlantic bottom ventilation (Chapter 5), and upper water column conditions (Chapter 6) were affected by changes related to the HS of the last glacial and deglacial periods. The conclusions presented herein are based on inorganic geochemistry (i.e., planktonic foraminifera, Mg/Ca, bulk sediment major elements), isotopic geochemistry (i.e., planktonic and benthic foraminifera stable oxygen isotopes, benthic foraminifera stable carbon isotope), micropaleontological (i.e., planktonic foraminifera assemblages, benthic foraminifera counts) and outputs from a high-resolution version of an atmosphere-ocean general circulation model. The main conclusions are highlighted below and Figure 7.1 summarizes them in an integrated way.

Regarding South American hydroclimate during the last glacial and deglacial HS, the main conclusions are:

- Data and model results shown herein suggest that the meridional impact of HS-induced precipitation anomalies over South America decreases from north to south, and that the São Francisco River drainage basin is the southernmost basin in the South American Atlantic seaboard that experienced substantial increases in precipitation.
- A complex combination of dynamic and thermodynamic processes was responsible for precipitation anomalies over tropical South America.
- E South America experienced positive precipitation anomalies which are attributed to an austral summer anomalous cyclonic circulation and moisture transport from the anomalously warm South Atlantic into the continent.
- Due to the cooling of the North Atlantic, the atmospheric moisture content over the Northern Hemisphere was reduced. Thus, in the austral summer, cooler and drier air was transported from the tropical North Atlantic into the continent, resulting in reduced transport of moisture to feed rainfall over tropical South America.
- Due to the warming of the South Atlantic, the atmospheric moisture content over the Southern Hemisphere was increased. Thus, in the austral winter, warmer and wetter air was transported from the equatorial Atlantic into the continent, resulting in wetter conditions over vast portions of tropical South America.

Regarding western tropical South Atlantic bottom ventilation during last glacial and deglacial HS, the main conclusions are:

- The weak AMOC reduced the input of high $\delta^{13}C$ surface waters into the deep North Atlantic promoting a decrease in the source signal of NCW. Additionally, the reduced ventilation and consequent increased NCW residence time led to the accumulation of respired carbon at NCW depths throughout the Atlantic. Thus, NCW $\delta^{13}C$ source signal reduction together with accumulation of respired carbon drove $\delta^{13}C$ negative excursions.
- The $\delta^{13}C$ and S records unambiguously indicate a reduced NCW ventilation in the western tropical South Atlantic mid-depths.
- The negative $\delta^{13}C$ excursions progressively increased along the NCW southwards pathway, reaching maxima values at the western tropical South Atlantic, from where the signal started to dissipate/dilute by mixing with SCW.
- Even under different boundary conditions, negative $\delta^{13}C$ excursions occurred in the mid-depth western tropical South Atlantic during all HS of the last glacial and deglacial suggesting that similar mechanisms may have operated.
- The synchronism of changes in CO_{2atm}, $\delta^{13}CO_{2atm}$, and AMOC-related marine carbon cycle records suggests that the AMOC played a relevant role in modulating the global carbon cycle on millennial time-scale.

Regarding upper western tropical South Atlantic changes during last glacial and deglacial HS, the main conclusions are:

- The comparison between records from the AL region and the western tropical South Atlantic shows accumulation of heat and salt in the South Atlantic during HS.
- The systematically smaller western tropical South Atlantic positive SST and SSS excursions suggests that surface heat and salt was lost/diluted along the route from the AL region to the western tropical South Atlantic.
- The heat and salt imported from the Indian Ocean during HS were only partially transferred to the western tropical South Atlantic.
- Indian Ocean salt that eventually reached the high latitudes of the North Atlantic helping on the recovering of the AMOC was most probably transported mainly within the thermocline.

Figure 7.1 – Schematic representation of the main changes that occurred to the western Atlantic and the adjacent Americas during Heinrich Stadials, as described in this thesis. Filled yellow dot indicate the site of marine sediment core M125-95-3 (western tropical South Atlantic) investigated herein. Black arrows indicate austral summer (winter) moisture flux from the tropical South Atlantic (equatorial North Atlantic) to eastern South America (tropical South America). Grey arrows (continuous and dashed) depict source region and the main pathway of the Southern Component Water (SCW) and Northern Component Water (NCW). NCW dashed line indicates decreased convection and ventilation of this water mass. The blue shading represents the magnitude of the negative NCW $\delta^{13}C$ excursions (light blue suggests small excursion, deep blue suggests large excursion) which gradually increases southwards at mid-depths, reaching its maximum in the western tropical South Atlantic (i.e., the site of core M125-95-3) from where it starts to dissipate/dilute by mixing with SCW. The red shadow depicts the accumulation of sea surface temperature (SST) and salinity (SSS) in the upper South Atlantic. Figure partially produced with Ocean Data View (SCHLITZER, 2018).

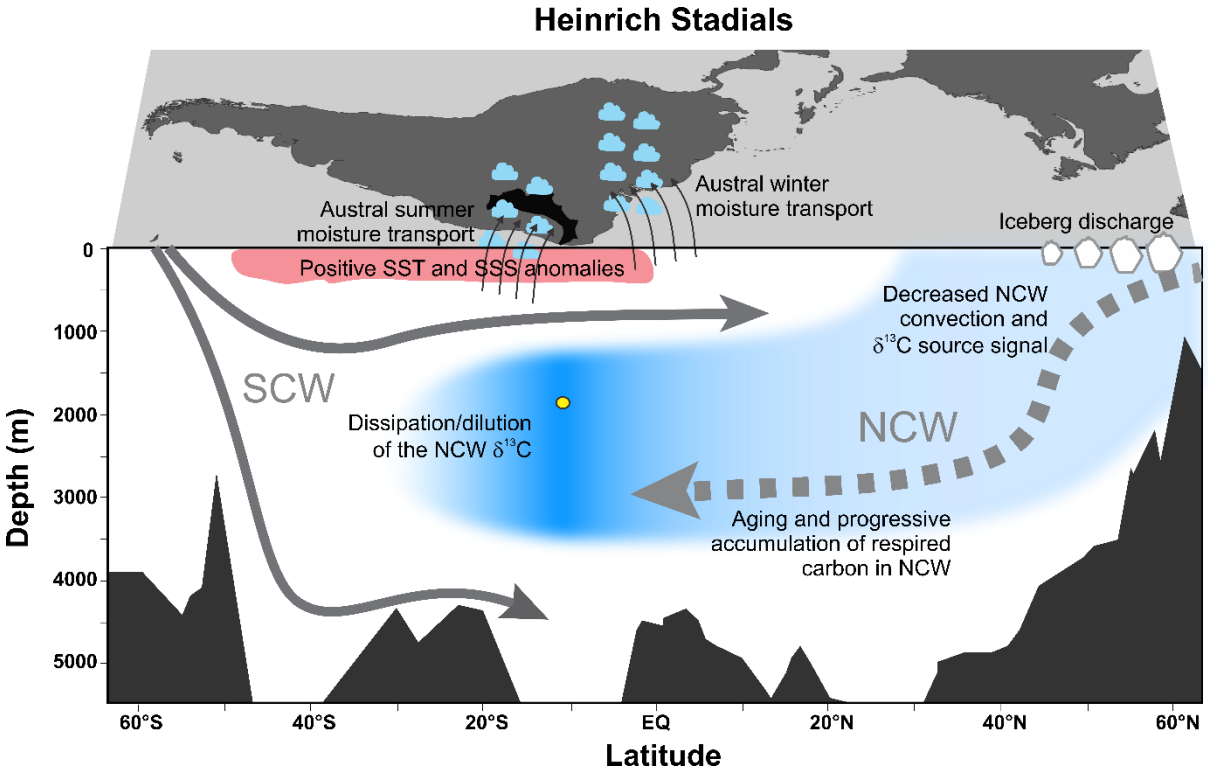

Taken together, we have shown that past events of decreases in AMOC strength had a profound impact over South American hydroclimate as well as in the western tropical South Atlantic bottom ventilation and upper water column. Direct and indirect instrumental measurements of the AMOC strength show its weakening over the last decades. Recent modelling studies suggest that this weakening will persist, and probably intensify, throughout this century. A marked weakening of the AMOC together with other changes in the climate system (e.g., greenhouse gases increase, relative sea level rise, ocean acidification etc.) pose major threats to global flora, fauna and society. Therefore, the conclusions of this thesis may subsidize the debate of possible impacts that future climate change may have over tropical South America and in the western tropical South Atlantic.

7.2 Future studies

Our knowledge about South American paleoclimate and western South Atlantic paleoceanography is fragmented and sparse (PBMC, 2014). The scientific questions approached herein contribute to reduce these deficiencies, however, they target a small number of the long list of unanswered questions. Here we suggest future studies that, in light of the results presented in this thesis, could tackle at least part of the unanswered questions.

Chapter 4 shows that E South America experienced positive precipitation anomalies during HS. This finding was mainly based on the delivery of terrigenous sediments from the adjacent drainage basin (i.e., São Francisco River drainage basin) to the continental margin where marine sediment core M125-95-3 was collected (i.e., western tropical South Atlantic). Precipitation changes over tropical regions may cause not only changes in the riverine transport of sediments but also changes in vegetation. HS vegetation changes in E South America is a topic of great relevance since this region is thought to be a past corridor that linked the Amazonian and Atlantic rainforests through the expansion of both biomes over nowadays semi-arid regions (BOUIMETARHAN et al., 2018; DUPONT et al., 2010; WANG et al., 2004). Marine sediments are also valuable archives of vegetation types and composition. While the $\delta^{13}C$ composition of long chain *n*-alkanes (epicuticular leaf-waxes from higher plants) allow to differentiate between vegetation types using the C3 (forest) and C4 (savanna) photosynthetic pathways (e.g., HÄGGI et al., 2017; HÄGGI et al., 2016), the pollen assemblage allows to reconstruct the vegetational species composition (e.g., GU et al., 2018; GU et al., 2017). Thus, long chain *n*-alkanes $\delta^{13}C$ and palynological analyses to marine sediment core M125-95-3 could yield important results.

Another issue that arose from Chapter 4 is the need for a broad approach that goes beyond the SAMS while scrutinizing tropical South American hydroclimate changes during the last glacial and deglacial. This need has also been identified for the Holocene (WARD et al., 2019) and the last millennium (WORTHAM et al., 2017), in which inconsistencies related to SAMS records may indicate that other mechanisms could have played a role. Thus, an inclusive approach to explain South American HS hydroclimate conditions that goes beyond the classically invoked changes in SAMS is required. Such an approach should consider not only mean annual conditions but also seasonal conditions.

Chapter 5 shows that a weak AMOC decreased the ventilation of the mid-depth western South Atlantic during the last glacial and deglacial HS. The decreased ventilation allowed the accumulation of respired carbon at NCW depths. The latter has implications on seawater chemistry (e.g., reduced oxygen, increased pH, reduced formation of carbonate structures). The

weakening of the AMOC observed in the last decades and projected weakening for the future may drastically change seawater chemistry. Thus, investigating in more detail the effects that the HS-related decreases in ventilation had over the mid-depth western South Atlantic may provide valuable information.

Still regarding Chapter 5, when investigating past AMOC weakening events, it is also important to reconstruct the $\delta^{13}C$ of the upper water column. The western tropical South Atlantic thermocline is of particular interest since it is occupied by SACW, which is mainly formed by waters originated from the Southern Ocean (STRAMMA; SCHOTT, 1999) (STRAMMA; ENGLAND, 1999). Thus, changes in the SACW $\delta^{13}C$ in the western tropical South Atlantic may reflect changes in the Southern Ocean $\delta^{13}C$, which is mainly related to changes in ventilation. Assessing past changes in Southern Ocean ventilation is relevant because this ocean is believed to be the main source of CO_2 to the atmosphere during HS (e.g., ANDERSON et al., 2009; CAMPOS et al., 2017; NINNEMANN; CHARLES, 1997).

In Chapter 6 we show the accumulation and transport of heat and salt from the AL region to the western tropical South Atlantic (i.e., M125-95-3 core site) during HS. Since the western equatorial Atlantic is the bottleneck for the northward return flow of the AMOC, a better understanding of changes in heat and salt at this region during AMOC reorganization events is needed, particularly for periods older than the last glacial (e.g., Termination II). Termination II led to the Last Interglacial period that was warmer than the preindustrial. Termination II and the Last Interglacial are appropriate case studies to assess possible consequences of current climate change. So far, no records from the western equatorial Atlantic (i.e., the very pathway from the South to the North Atlantic) covering Termination II are available to deal with this issue.

Finally, the above-mentioned scientific questions make clear the utmost importance of an integrated effort that involves an interdisciplinary/multidisciplinary group in order to deal the complex environmental issues facing society.

References[1]

AHN, J.; BROOK, E. J. Atmospheric CO2 and climate on millennial time scales during the last glacial period. **Science**, 322, n. 5898, p. 83-85, Oct 3 2008.

AHN, J.; BROOK, E. J. Siple Dome ice reveals two modes of millennial CO2 change during the last ice age. **Nat Commun**, 5, p. 3723, Apr 29 2014.

ANA. Conjuntura dos recursos hídricos no Brasil: regiões hidrográficas brasileiras. : Agência Nacional das Águas 2015.

ANA. **Saiba mais**. 2017. Disponível em: http://www3.ana.gov.br/portal/ANA/sala-de-situacao/sao-francisco/saiba-mais.

ANAND, P.; ELDERFIELD, H.; CONTE, M. H. Calibration of Mg/Ca thermometry in planktonic foraminifera from a sediment trap time series. **Paleoceanography**, 18, n. 2, 2003.

ANDERSEN, K. K.; AZUMA, N.; BARNOLA, J.-M.; BIGLER, M. et al. High-resolution record of Northern Hemisphere climate extending into the last interglacial period. **Nature**, 431, n. 7005, p. 147, 2004.

ANDERSON, R. F.; ALI, S.; BRADTMILLER, L. I.; NIELSEN, S. H. et al. Wind-driven upwelling in the Southern Ocean and the deglacial rise in atmospheric CO2. **Science**, 323, n. 5920, p. 1443-1448, 2009.

ARHAN, M.; SPEICH, S.; MESSAGER, C.; DENCAUSSE, G. et al. Anticyclonic and cyclonic eddies of subtropical origin in the subantarctic zone south of Africa. **Journal of Geophysical Research: Oceans**, 116, n. C11, 2011.

ARZ, H. W.; PÄTZOLD, J.; WEFER, G. Correlated millennial-scale changes in surface hydrography and terrigenous sediment yield inferred from last-glacial marine deposits off northeastern Brazil. **Quaternary Research**, 50, n. 2, p. 157-166, 1998.

ARZ, H. W.; PÄTZOLD, J.; WEFER, G. The deglacial history of the western tropical Atlantic as inferred from high resolution stable isotope records off northeastern Brazil. **Earth and Planetary Science Letters**, 167, n. 1-2, p. 105-117, 1999.

BAHR, A.; ALBUQUERQUE, A. L. S.; ARDENGHI, N.; BATENBURG, S. J. et al. **South American Hydrological Balance and Paleoceanography during the Late Pleistocene and Holocene (SAMBA)**. 2016. (4947148311550).

BAHR, A.; HOFFMANN, J.; SCHÖNFELD, J.; SCHMIDT, M. W. et al. Low-latitude expressions of high-latitude forcing during Heinrich Stadial 1 and the Younger Dryas in northern South America. **Global and Planetary Change**, 160, p. 1-9, 2018.

BAHR, A.; SCHÖNFELD, J.; HOFFMANN, J.; VOIGT, S. et al. Comparison of Ba/Ca and δOWATER18 as freshwater proxies: A multi-species core-top study on planktonic foraminifera from the vicinity of the Orinoco River mouth. **Earth and Planetary Science Letters**, 383, p. 45-57, 2013.

[1] Following the Associação Brasileira de Normas Técnicas (ABNT NBR 6023).

BAKER, P. A.; RIGSBY, C. A.; SELTZER, G. O.; FRITZ, S. C. et al. Tropical climate changes at millennial and orbital timescales on the Bolivian Altiplano. **nature**, 409, n. 6821, p. 698-701, 2001.

BAKKER, P.; SCHMITTNER, A.; LENAERTS, J.; ABE-OUCHI, A. et al. Fate of the Atlantic Meridional Overturning Circulation: Strong decline under continued warming and Greenland melting. **Geophysical Research Letters**, 43, n. 23, p. 12,252-212,260, 2016.

BARBANTE, C.; BARNOLA, J. M.; BECAGLI, S.; BEER, J. et al. One-to-one coupling of glacial climate variability in Greenland and Antarctica. **Nature**, 444, n. 7116, p. 195-198, 2006/11/01 2006.

BARD, E. Correction of accelerator mass spectrometry 14C ages measured in planktonic foraminifera: paleoceanographic implications. **Paleoceanography**, 3, n. 6, p. 635-645, 1988.

BARD, E.; ROSTEK, F.; TURON, J.-L.; GENDREAU, S. Hydrological impact of Heinrich events in the subtropical northeast Atlantic. **Science**, 289, n. 5483, p. 1321-1324, 2000.

BARKER, S.; GREAVES, M.; ELDERFIELD, H. A study of cleaning procedures used for foraminiferal Mg/Ca paleothermometry. **Geochemistry, Geophysics, Geosystems**, 4, n. 9, 2003.

BAUSKA, T. K.; BROOK, E. J.; MARCOTT, S.; BAGGENSTOS, D. et al. Controls on millennial-scale atmospheric CO2 variability during the last glacial period. **Geophysical Research Letters**, 45, n. 15, p. 7731-7740, 2018.

BEAL, L. M.; DE RUIJTER, W. P.; BIASTOCH, A.; ZAHN, R. On the role of the Agulhas system in ocean circulation and climate. **Nature**, 472, n. 7344, p. 429-436, 2011.

BEHLING, H.; ARZ, H. W.; PÄTZOLD, J.; WEFER, G. Late Quaternary vegetational and climate dynamics in southeastern Brazil, inferences from marine cores GeoB 3229-2 and GeoB 3202-1. **Palaeogeography, Palaeoclimatology, Palaeoecology**, 179, n. 3-4, p. 227-243, 2002.

BERBERY, E. H.; BARROS, V. R. The hydrologic cycle of the La Plata basin in South America. **Journal of Hydrometeorology**, 3, n. 6, p. 630-645, 2002.

BEREITER, B.; LÜTHI, D.; SIEGRIST, M.; SCHÜPBACH, S. et al. Mode change of millennial CO2 variability during the last glacial cycle associated with a bipolar marine carbon seesaw. **Proceedings of the National Academy of Sciences**, 109, n. 25, p. 9755-9760, 2012.

BIASTOCH, A.; BÖNING, C. W.; SCHWARZKOPF, F. U.; LUTJEHARMS, J. Increase in Agulhas leakage due to poleward shift of Southern Hemisphere westerlies. **Nature**, 462, n. 7272, p. 495-498, 2009.

BLAAUW, M.; CHRISTEN, J. A. Flexible paleoclimate age-depth models using an autoregressive gamma process. **Bayesian analysis**, 6, n. 3, p. 457-474, 2011.

BOLLI, H. M.; SAUNDERS, J. B.; PERCH-NIELSEN, K. **Plankton Stratigraphy: Volume 1, Planktic Foraminifera, Calcareous Nannofossils and Calpionellids**. CUP Archive, 1989. 0521367190.

BOLTOVSKOY, E.; GIUSSANI, G.; WATANABE, S.; WRIGHT, R. Atlas of benthic shelf foraminifera of the southwest atlantic Junk. bv. **Pub. The Hague-Boston-London**, 1980.

BOND, G.; HEINRICH, H.; BROECKER, W.; LABEYRIE, L. et al. Evidence for massive discharges of icebergs into the North Atlantic ocean during the last glacial period. **Nature**, 360, n. 6401, p. 245-249, 1992.

BOTTRELL, S. H.; NEWTON, R. J. Reconstruction of changes in global sulfur cycling from marine sulfate isotopes. **Earth-Science Reviews**, 75, n. 1-4, p. 59-83, 2006.

BOUIMETARHAN, I.; CHIESSI, C. M.; GONZÁLEZ-ARANGO, C.; DUPONT, L. et al. Intermittent development of forest corridors in northeastern Brazil during the last deglaciation: Climatic and ecologic evidence. **Quaternary Science Reviews**, 192, p. 86-96, 2018.

BOYLE, E. A. Quaternary deepwater paleoceanography. **Science**, 249, n. 4971, p. 863-870, Aug 24 1990.

BOYLE, E. A.; KEIGWIN, L. North Atlantic thermohaline circulation during the past 20,000 years linked to high-latitude surface temperature. **Nature**, 330, n. 6143, p. 35, 1987.

BROCCOLI, A. J.; DAHL, K. A.; STOUFFER, R. J. Response of the ITCZ to Northern Hemisphere cooling. **Geophysical Research Letters**, 33, n. 1, 2006.

BROECKER, W. S. Paleocean circulation during the last deglaciation: a bipolar seesaw? **Paleoceanography**, 13, n. 2, p. 119-121, 1998.

BRYDEN, H. L.; LONGWORTH, H. R.; CUNNINGHAM, S. A. Slowing of the Atlantic meridional overturning circulation at 25 N. **Nature**, 438, n. 7068, p. 655-657, 2005.

BURCKEL, P.; WAELBROECK, C.; GHERARDI, J. M.; PICHAT, S. et al. Atlantic Ocean circulation changes preceded millennial tropical South America rainfall events during the last glacial. **Geophysical Research Letters**, 42, n. 2, p. 411-418, 2015.

BUTZIN, M.; KÖHLER, P.; LOHMANN, G. Marine radiocarbon reservoir age simulations for the past 50,000 years. **Geophysical Research Letters**, 44, n. 16, p. 8473-8480, 2017.

CALEY, T.; GIRAUDEAU, J.; MALAIZÉ, B.; ROSSIGNOL, L. et al. Agulhas leakage as a key process in the modes of Quaternary climate changes. **Proceedings of the National Academy of Sciences**, 109, n. 18, p. 6835-6839, 2012.

CAMPOS, M. C.; CHIESSI, C. M.; MULITZA, S. **Campos, MC et al. (2019): XRF Ti/Ca ratios of sediment core GeoB6212-1**. 2019a. Disponível em: https://doi.pangaea.de/10.1594/PANGAEA.897977.

CAMPOS, M. C.; CHIESSI, C. M.; PRANGE, M.; MULITZA, S. et al. A new mechanism for millennial scale positive precipitation anomalies over tropical South America. **Quaternary Science Reviews**, 225, p. 105990, 2019b.

CAMPOS, M. C.; CHIESSI, C. M.; VOIGT, I.; PIOLA, A. R. et al. δ13C decreases in the upper western South Atlantic during Heinrich Stadials 3 and 2. **Clim. Past**, 13, n. 4, p. 345-358, 2017.

CARVALHO, L. M.; JONES, C.; LIEBMANN, B. Extreme precipitation events in southeastern South America and large-scale convective patterns in the South Atlantic convergence zone. **Journal of Climate**, 15, n. 17, p. 2377-2394, 2002.

CARVALHO, L. M.; JONES, C.; LIEBMANN, B. The South Atlantic convergence zone: Intensity, form, persistence, and relationships with intraseasonal to interannual activity and extreme rainfall. **Journal of Climate**, 17, n. 1, p. 88-108, 2004.

CHAVES, R. R.; NOBRE, P. Interactions between sea surface temperature over the South Atlantic Ocean and the South Atlantic Convergence Zone. **Geophysical Research Letters**, 31, n. 3, 2004.

CHEN, T.; ROBINSON, L. F.; BURKE, A.; SOUTHON, J. et al. Synchronous centennial abrupt events in the ocean and atmosphere during the last deglaciation. **Science**, 349, n. 6255, p. 1537-1541, 2015.

CHIESSI, C. M.; MULITZA, S.; PÄTZOLD, J.; WEFER, G., 2010, **How different proxies record precipitation variability over southeastern South America**. IOP Publishing, 2010. 012007.

CHIESSI, C. M.; MULITZA, S.; PÄTZOLD, J.; WEFER, G. et al. Possible impact of the Atlantic Multidecadal Oscillation on the South American summer monsoon. **Geophysical Research Letters**, 36, n. 21, 2009.

CHIESSI, C. M.; MULITZA, S.; PAUL, A.; PÄTZOLD, J. et al. South Atlantic interocean exchange as the trigger for the Bølling warm event. **Geology**, 36, n. 12, p. 919-922, 2008.

CHIESSI, C. M.; ULRICH, S.; MULITZA, S.; PÄTZOLD, J. et al. Signature of the Brazil-Malvinas Confluence (Argentine Basin) in the isotopic composition of planktonic foraminifera from surface sediments. **Marine Micropaleontology**, 64, n. 1-2, p. 52-66, 2007.

CLÉROUX, C.; DEMENOCAL, P.; ARBUSZEWSKI, J.; LINSLEY, B. Reconstructing the upper water column thermal structure in the Atlantic Ocean. **Paleoceanography**, 28, n. 3, p. 503-516, 2013.

COLLINS, J. A.; SCHEFUß, E.; GOVIN, A.; MULITZA, S. et al. Insolation and glacial–interglacial control on southwestern African hydroclimate over the past 140 000 years. **Earth and Planetary Science Letters**, 398, p. 1-10, 2014.

COLLINS, W. D.; BITZ, C. M.; BLACKMON, M. L.; BONAN, G. B. et al. The community climate system model version 3 (CCSM3). **Journal of Climate**, 19, n. 11, p. 2122-2143, 2006.

COOK, K. H.; VIZY, E. K. South American climate during the Last Glacial Maximum: delayed onset of the South American monsoon. **Journal of Geophysical Research: Atmospheres**, 111, n. D2, 2006.

CRIVELLARI, S.; CHIESSI, C. M.; KUHNERT, H.; HÄGGI, C. et al. Increased Amazon freshwater discharge during late Heinrich Stadial 1. **Quaternary Science Reviews**, 181, p. 144-155, 2018.

CRIVELLARI, S.; CHIESSI, C. M.; KUHNERT, H.; HÄGGI, C. et al. Thermal response of the western tropical Atlantic to slowdown of the Atlantic Meridional Overturning Circulation. **Earth and Planetary Science Letters**, 519, p. 120-129, 2019.

CROWLEY, T. J. North Atlantic deep water cools the Southern Hemisphere. **Paleoceanography**, 7, n. 4, p. 489-497, 1992.

CRUZ, F. W.; BURNS, S. J.; JERCINOVIC, M.; KARMANN, I. et al. Evidence of rainfall variations in Southern Brazil from trace element ratios (Mg/Ca and Sr/Ca) in a Late Pleistocene stalagmite. **Geochimica et Cosmochimica Acta**, 71, n. 9, p. 2250-2263, 2007.

CRUZ, F. W.; BURNS, S. J.; KARMANN, I.; SHARP, W. D. et al. Insolation-driven changes in atmospheric circulation over the past 116,000 years in subtropical Brazil. **Nature**, 434, n. 7029, p. 63-66, 2005.

CRUZ, F. W.; VUILLE, M.; BURNS, S. J.; WANG, X. et al. Orbitally driven east–west antiphasing of South American precipitation. **Nature Geoscience**, 2, n. 3, p. 210-214, 2009.

CURRY, W.; MARCHITTO, T.; MCMANUS, J.; OPPO, D. et al. Millennial-scale changes in ventilation of the thermocline, intermediate, and deep waters of the glacial North Atlantic. **Geophysical Monograph-American Geophysical Union**, 112, p. 59-76, 1999.

DEPLAZES, G.; LÜCKGE, A.; PETERSON, L. C.; TIMMERMANN, A. et al. Links between tropical rainfall and North Atlantic climate during the last glacial period. **Nature Geoscience**, 6, n. 3, p. 213-217, 2013.

DIAS, B. B.; BARBOSA, C. F.; FARIA, G. R.; SEOANE, J. C. S. et al. The effects of multidecadal-scale phytodetritus disturbances on the benthic foraminiferal community of a Western Boundary Upwelling System, Brazil. **Marine Micropaleontology**, 139, p. 102-112, 2018.

DIMA, M.; LOHMANN, G. Evidence for two distinct modes of large-scale ocean circulation changes over the last century. **Journal of Climate**, 23, n. 1, p. 5-16, 2010.

DOMINGUEZ, J. The Sao Francisco strandplain: a paradigm for wave-dominated deltas? **Geological Society, London, Special Publications**, 117, n. 1, p. 217-231, 1996.

DUARTE, C. S.; VIANA, A. R. Santos Drift System: stratigraphic organization and implications for late Cenozoic palaeocirculation in the Santos Basin, SW Atlantic Ocean. **Geological Society, London, Special Publications**, 276, n. 1, p. 171-198, 2007.

DUPLESSY, J.-C.; LABEYRIE, L.; JUILLET-LECLERC, A.; MAITRE, F. et al. Surface salinity reconstruction of the North Atlantic Ocean during the last glacial maximum. **Oceanol. Acta**, 14, n. 4, p. 311-324, 1991.

DUPLESSY, J.; SHACKLETON, N.; FAIRBANKS, R.; LABEYRIE, L. et al. Deepwater source variations during the last climatic cycle and their impact on the global deepwater circulation. **Paleoceanography**, 3, n. 3, p. 343-360, 1988.

DUPONT, L. M.; SCHLÜTZ, F.; EWAH, C. T.; JENNERJAHN, T. C. et al. Two-step vegetation response to enhanced precipitation in Northeast Brazil during Heinrich event 1. **Global Change Biology**, 16, n. 6, p. 1647-1660, 2010.

DYEZ, K. A.; ZAHN, R.; HALL, I. R. Multicentennial Agulhas leakage variability and links to North Atlantic climate during the past 80,000 years. **Paleoceanography**, 29, n. 12, p. 1238-1248, 2014.

EGGLESTON, S.; SCHMITT, J.; BEREITER, B.; SCHNEIDER, R. et al. Evolution of the stable carbon isotope composition of atmospheric CO2 over the last glacial cycle. **Paleoceanography**, 31, n. 3, p. 434-452, 2016.

ELLIOT, M.; LABEYRIE, L.; DUPLESSY, J.-C. Changes in North Atlantic deep-water formation associated with the Dansgaard–Oeschger temperature oscillations (60–10 ka). **Quaternary Science Reviews**, 21, n. 10, p. 1153-1165, 2002.

EMILIANI, C. Pleistocene temperatures. **The Journal of Geology**, 63, n. 6, p. 538-578, 1955.

EPICA, C. M. One-to-one coupling of glacial climate variability in Greenland and Antarctica. **Nature**, 444, n. 7116, p. 195, 2006.

EROKHINA, O.; ROGOZHINA, I.; PRANGE, M.; BAKKER, P. et al. Dependence of slope lapse rate over the Greenland ice sheet on background climate. **Journal of Glaciology**, 63, n. 239, p. 568-572, 2017.

FAUGÈRES, J.-C.; STOW, D. A. Bottom-current-controlled sedimentation: a synthesis of the contourite problem. **Sedimentary Geology**, 82, n. 1-4, p. 287-297, 1993.

FELIS, T.; MERKEL, U.; ASAMI, R.; DESCHAMPS, P. et al. Pronounced interannual variability in tropical South Pacific temperatures during Heinrich Stadial 1. **Nature Communications**, 3, n. 1, p. 1-7, 2012.

FIGUEROA, S. N.; SATYAMURTY, P.; DA SILVA DIAS, P. L. Simulations of the summer circulation over the South American region with an eta coordinate model. **Journal of the atmospheric sciences**, 52, n. 10, p. 1573-1584, 1995.

FONTANIER, C.; JORISSEN, F.; LICARI, L.; ALEXANDRE, A. et al. Live benthic foraminiferal faunas from the Bay of Biscay: faunal density, composition, and microhabitats. **Deep Sea Research Part I: Oceanographic Research Papers**, 49, n. 4, p. 751-785, 2002.

GARCIA, H. E.; LOCARNINI, R. A.; BOYER, T. P.; ANTONOV, J. I. et al. World ocean atlas 2013. Volume 4, Dissolved inorganic nutrients (phosphate, nitrate, silicate). 2013.

GARREAUD, R. D.; VUILLE, M.; COMPAGNUCCI, R.; MARENGO, J. Present-day south american climate. **Palaeogeography, Palaeoclimatology, Palaeoecology**, 281, n. 3-4, p. 180-195, 2009.

GONG, X.; KNORR, G.; LOHMANN, G.; ZHANG, X. Dependence of abrupt Atlantic meridional ocean circulation changes on climate background states. **Geophysical Research Letters**, 40, n. 14, p. 3698-3704, 2013.

GOVIN, A.; CHIESSI, C. M.; ZABEL, M.; SAWAKUCHI, A. O. et al. Terrigenous input off northern South America driven by changes in Amazonian climate and the North Brazil Current retroflection during the last 250 ka. **Clim. Past**, 10, n. 2, p. 843-862, 2014.

GOVIN, A.; HOLZWARTH, U.; HESLOP, D.; FORD KEELING, L. et al. Distribution of major elements in Atlantic surface sediments (36 N–49 S): Imprint of terrigenous input and continental weathering. **Geochemistry, Geophysics, Geosystems**, 13, n. 1, 2012.

GROENEVELD, J.; CHIESSI, C. M. Mg/Ca of Globorotalia inflata as a recorder of permanent thermocline temperatures in the South Atlantic. **Paleoceanography**, 26, n. 2, 2011.

GU, F.; CHIESSI, C. M.; ZONNEVELD, K. A.; BEHLING, H. Late Quaternary environmental dynamics inferred from marine sediment core GeoB6211-2 off southern Brazil. **Palaeogeography, Palaeoclimatology, Palaeoecology**, 496, p. 48-61, 2018.

GU, F.; ZONNEVELD, K. A.; CHIESSI, C. M.; ARZ, H. W. et al. Long-term vegetation, climate and ocean dynamics inferred from a 73,500 years old marine sediment core (GeoB2107-3) off southern Brazil. **Quaternary Science Reviews**, 172, p. 55-71, 2017.

HAARSMA, R. J.; CAMPOS, E. J.; DRIJFHOUT, S.; HAZELEGER, W. et al. Impacts of interruption of the Agulhas leakage on the tropical Atlantic in coupled ocean–atmosphere simulations. **Climate dynamics**, 36, n. 5-6, p. 989-1003, 2011.

HÄGGI, C.; CHIESSI, C. M.; MERKEL, U.; MULITZA, S. et al. Response of the Amazon rainforest to late Pleistocene climate variability. **Earth and Planetary Science Letters**, 479, p. 50-59, 2017.

HÄGGI, C.; SAWAKUCHI, A. O.; CHIESSI, C. M.; MULITZA, S. et al. Origin, transport and deposition of leaf-wax biomarkers in the Amazon Basin and the adjacent Atlantic. **Geochimica et Cosmochimica Acta**, 192, p. 149-165, 2016.

HARFF, J.; ENDLER, R.; EMELYANOV, E.; KOTOV, S. et al. Late Quaternary climate variations reflected in Baltic Sea sediments. *In*: **The Baltic Sea Basin**: Springer, 2011. p. 99-132.

HEINRICH, H. Origin and consequences of cyclic ice rafting in the northeast Atlantic Ocean during the past 130,000 years. **Quaternary research**, 29, n. 2, p. 142-152, 1988.

HEMMING, S. R. Heinrich events: Massive late Pleistocene detritus layers of the North Atlantic and their global climate imprint. **Reviews of Geophysics**, 42, n. 1, 2004.

HENRY, L.; MCMANUS, J. F.; CURRY, W. B.; ROBERTS, N. L. et al. North Atlantic ocean circulation and abrupt climate change during the last glaciation. **Science**, 353, n. 6298, p. 470-474, 2016.

HERGUERA, J. C.; BERGER, W. Paleoproductivity from benthic foraminifera abundance: Glacial to postglacial change in the west-equatorial Pacific. **Geology**, 19, n. 12, p. 1173-1176, 1991.

HESSLER, I.; DUPONT, L.; BONNEFILLE, R.; BEHLING, H. et al. Millennial-scale changes in vegetation records from tropical Africa and South America during the last glacial. **Quaternary Science Reviews**, 29, n. 21-22, p. 2882-2899, 2010.

HÖNISCH, B.; ALLEN, K. A.; LEA, D. W.; SPERO, H. J. et al. The influence of salinity on Mg/Ca in planktic foraminifers–Evidence from cultures, core-top sediments and complementary δ18O. **Geochimica et Cosmochimica Acta**, 121, p. 196-213, 2013.

HOWE, J. N.; HUANG, K.-F.; OPPO, D. W.; CHIESSI, C. M. et al. Similar mid-depth Atlantic water mass provenance during the Last Glacial Maximum and Heinrich Stadial 1. **Earth and Planetary Science Letters**, 490, p. 51-61, 2018.

HOWE, J. N. W.; PIOTROWSKI, A. M.; NOBLE, T. L.; MULITZA, S. et al. North Atlantic Deep Water Production during the Last Glacial Maximum. **Nature Communications**, 7, n. 1, p. 11765, 2016/06/03 2016.

HUT, G. Stable isotope reference samples for geochemical and hydrological investigations. Consultant Group Meeting IAEA, Vienna, 16–18 September 1985, Report to the Director General. **International Atomic Energy Agency, Vienna**, 42, 1987.

JAESCHKE, A.; RÜHLEMANN, C.; ARZ, H.; HEIL, G. et al. Coupling of millennial-scale changes in sea surface temperature and precipitation off northeastern Brazil with high-latitude climate shifts during the last glacial period. **Paleoceanography**, 22, n. 4, 2007.

JOHNS, W. E.; LEE, T.; BEARDSLEY, R.; CANDELA, J. et al. Annual cycle and variability of the North Brazil Current. **Journal of Physical Oceanography**, 28, n. 1, p. 103-128, 1998.

JØRGENSEN, B. B.; FINDLAY, A. J.; PELLERIN, A. The Biogeochemical Sulfur Cycle of Marine Sediments. **Frontiers in microbiology**, 10, p. 849-849, 2019.

JØRGENSEN, B. B.; KASTEN, S. Sulfur cycling and methane oxidation. *In*: **Marine geochemistry**: Springer, 2006. p. 271-309.

JUNQUAS, C.; VERA, C.; LI, L.; LE TREUT, H. Summer precipitation variability over Southeastern South America in a global warming scenario. **Climate dynamics**, 38, n. 9-10, p. 1867-1883, 2012.

KAGEYAMA, M.; MERKEL, U.; OTTO-BLIESNER, B.; PRANGE, M. et al. Climatic impacts of fresh water hosing under Last Glacial Maximum conditions: a multi-model study. **Climate of the Past**, 9, n. 2, p. 935-953, 2013.

KANNER, L. C.; BURNS, S. J.; CHENG, H.; EDWARDS, R. L. High-latitude forcing of the South American summer monsoon during the last glacial. **Science**, 335, n. 6068, p. 570-573, 2012.

KEIGWIN, L. D.; LEHMAN, S. J. Deep circulation change linked to Heinrich event 1 and Younger Dryas in a middepth North Atlantic core. **Paleoceanography**, 9, n. 2, p. 185-194, 1994.

KNIGHT, J. R.; ALLAN, R. J.; FOLLAND, C. K.; VELLINGA, M. et al. A signature of persistent natural thermohaline circulation cycles in observed climate. **Geophysical Research Letters**, 32, n. 20, 2005.

KNOPPERS, B.; EKAU, W.; FIGUEIREDO, A. G. The coast and shelf of east and northeast Brazil and material transport. **Geo-Marine Letters**, 19, n. 3, p. 171-178, 1999.

KNORR, G.; LOHMANN, G. Southern Ocean origin for the resumption of Atlantic thermohaline circulation during deglaciation. **Nature**, 424, n. 6948, p. 532-536, 2003/07/01 2003.

KNORR, G.; LOHMANN, G. Rapid transitions in the Atlantic thermohaline circulation triggered by global warming and meltwater during the last deglaciation. **Geochemistry, Geophysics, Geosystems**, 8, n. 12, 2007.

KOHO, K.; GARCÍA, R. d.; DE STIGTER, H.; EPPING, E. et al. Sedimentary labile organic carbon and pore water redox control on species distribution of benthic foraminifera: A case study from Lisbon–Setúbal Canyon (southern Portugal). **Progress in Oceanography**, 79, n. 1, p. 55-82, 2008.

KOUTAVAS, A.; LYNCH-STIEGLITZ, J.; MARCHITTO, T. M.; SACHS, J. P. El Nino-like pattern in ice age tropical Pacific sea surface temperature. **Science**, 297, n. 5579, p. 226-230, 2002.

KROOPNICK, P. The distribution of 13C of ΣCO2 in the world oceans. **Deep Sea Research Part A. Oceanographic Research Papers**, 32, n. 1, p. 57-84, 1985.

KUCERA, M.; WEINELT, M.; KIEFER, T.; PFLAUMANN, U. et al. Reconstruction of sea-surface temperatures from assemblages of planktonic foraminifera: multi-technique approach based on geographically constrained calibration data sets and its application to glacial Atlantic and Pacific Oceans. **Quaternary Science Reviews**, 24, n. 7-9, p. 951-998, 2005.

KUHLBRODT, T.; GRIESEL, A.; MONTOYA, M.; LEVERMANN, A. et al. On the driving processes of the Atlantic meridional overturning circulation. **Reviews of Geophysics**, 45, n. 2, 2007.

LANGNER, M.; MULITZA, S. PaleoDataView–a software toolbox for the collection, homogenization and visualization of marine proxy data. **Climate of the Past**, 15, n. 6, p. 2067-2072, 2019.

LEA, D. W.; MASHIOTTA, T. A.; SPERO, H. J. Controls on magnesium and strontium uptake in planktonic foraminifera determined by live culturing. **Geochimica et Cosmochimica Acta**, 63, n. 16, p. 2369-2379, 1999.

LEDRU, M.-P.; CECCANTINI, G.; GOUVEIA, S. E.; LÓPEZ-SÁEZ, J. A. et al. Millenial-scale climatic and vegetation changes in a northern Cerrado (Northeast, Brazil) since the Last Glacial Maximum. **Quaternary Science Reviews**, 25, n. 9-10, p. 1110-1126, 2006.

LEDUC, G.; VIDAL, L.; CARTAPANIS, O.; BARD, E. Modes of eastern equatorial Pacific thermocline variability: Implications for ENSO dynamics over the last glacial period. **Paleoceanography**, 24, n. 3, 2009.

LEGRANDE, A. N.; SCHMIDT, G. A. Global gridded data set of the oxygen isotopic composition in seawater. **Geophysical research letters**, 33, n. 12, 2006.

LENTON, T. M.; HELD, H.; KRIEGLER, E.; HALL, J. W. et al. Tipping elements in the Earth's climate system. **Proceedings of the national Academy of Sciences**, 105, n. 6, p. 1786-1793, 2008.

LENTZ, S. J. Seasonal variations in the horizontal structure of the Amazon Plume inferred from historical hydrographic data. **Journal of Geophysical Research: Oceans**, 100, n. C2, p. 2391-2400, 1995.

LEWIS, S.; LEGRANDE, A.; KELLEY, M.; SCHMIDT, G. Water vapour source impacts on oxygen isotope variability in tropical precipitation during Heinrich events. **Clim. Past**, 6, n. 3, p. 325-343, 2010.

LINDZEN, R. S.; NIGAM, S. On the role of sea surface temperature gradients in forcing low-level winds and convergence in the tropics. **Journal of the Atmospheric Sciences**, 44, n. 17, p. 2418-2436, 1987.

LISIECKI, L. E.; RAYMO, M. E. A Pliocene-Pleistocene stack of 57 globally distributed benthic δ18O records. **Paleoceanography**, 20, n. 1, 2005.

LISIECKI, L. E.; STERN, J. V. Regional and global benthic δ18O stacks for the last glacial cycle. **Paleoceanography**, 31, n. 10, p. 1368-1394, 2016.

LITTLE, M.; SCHNEIDER, R.; KROON, D.; PRICE, B. et al. Rapid palaeoceanographic changes in the Benguela Upwelling System for the last 160,000 years as indicated by abundances of planktonic foraminifera. **Palaeogeography, Palaeoclimatology, Palaeoecology**, 130, n. 1-4, p. 135-161, 1997.

LIU, W.; XIE, S.-P.; LIU, Z.; ZHU, J. Overlooked possibility of a collapsed Atlantic Meridional Overturning Circulation in warming climate. **Science Advances**, 3, n. 1, p. e1601666, 2017.

LIU, Z.; LU, Z.; WEN, X.; OTTO-BLIESNER, B. L. et al. Evolution and forcing mechanisms of El Niño over the past 21,000 years. **Nature**, 515, n. 7528, p. 550-553, 2014.

LOCARNINI, R. A.; MISHONOV, A. V.; ANTONOV, J. I.; BOYER, T. P. et al. **World Ocean Atlas 2013. Vol. 1: Temperature**. p. 40-40. 2013. (2011063574).

LOHMANN, G. Atmospheric and oceanic freshwater transport during weak Atlantic overturning circulation. **Tellus A: Dynamic Meteorology and Oceanography**, 55, n. 5, p. 438-449, 2003.

LUND, D.; TESSIN, A.; HOFFMAN, J.; SCHMITTNER, A. Southwest Atlantic water mass evolution during the last deglaciation. **Paleoceanography**, 30, n. 5, p. 477-494, 2015.

LUTJEHARMS, J. R. **The agulhas current**. Springer, 2006.

LUTZE, G. F. Uvigerina species of the eastern North Atlantic. *In*: VAN DER ZWAAN, G. J.;JORISSEN, F. J.*, et al* (Ed.). Bull, 35: Utrecht Micropaleontol., 1986. p. 21-46.

LYNCH-STIEGLITZ, J.; SCHMIDT, M. W.; HENRY, L. G.; CURRY, W. B. et al. Muted change in Atlantic overturning circulation over some glacial-aged Heinrich events. **Nature Geoscience**, 7, n. 2, p. 144, 2014.

LYNCH-STIEGLITZ, J.; STOCKER, T. F.; BROECKER, W. S.; FAIRBANKS, R. G. The influence of air-sea exchange on the isotopic composition of oceanic carbon: Observations and modeling. **Global Biogeochemical Cycles**, 9, n. 4, p. 653-665, 1995.

MACKENSEN, A.; HUBBERTEN, H. W.; BICKERT, T.; FISCHER, G. et al. The δ13C in benthic foraminiferal tests of Fontbotia wuellerstorfi (Schwager) relative to the δ13C of dissolved inorganic carbon in southern ocean deep water: implications for glacial ocean circulation models. **Paleoceanography**, 8, n. 5, p. 587-610, 1993.

MACKENSEN, A.; SCHMIEDL, G. Stable carbon isotopes in paleoceanography: Atmosphere, oceans, and sediments. **Earth-Science Reviews**, p. 102893, 2019.

MAIER-REIMER, E.; MIKOLAJEWICZ, U.; CROWLEY, T. Ocean general circulation model sensitivity experiment with an open Central American Isthmus. **Paleoceanography**, 5, n. 3, p. 349-366, 1990.

MARENGO, J. A.; LIEBMANN, B.; KOUSKY, V. E.; FILIZOLA, N. P. et al. Onset and end of the rainy season in the Brazilian Amazon Basin. **Journal of Climate**, 14, n. 5, p. 833-852, 2001.

MARSHALL, J.; DONOHOE, A.; FERREIRA, D.; MCGEE, D. The ocean's role in setting the mean position of the Inter-Tropical Convergence Zone. **Climate Dynamics**, 42, n. 7-8, p. 1967-1979, 2014.

MCCORKLE, D. C.; EMERSON, S. R.; QUAY, P. D. Stable carbon isotopes in marine porewaters. **Earth and Planetary Science Letters**, 74, n. 1, p. 13-26, 1985.

MCCORKLE, D. C.; KEIGWIN, L. D.; CORLISS, B. H.; EMERSON, S. R. The influence of microhabitats on the carbon isotopic composition of deep-sea benthic foraminifera. **Paleoceanography**, 5, n. 2, p. 161-185, 1990.

MCMANUS, J. F.; FRANCOIS, R.; GHERARDI, J.-M.; KEIGWIN, L. D. et al. Collapse and rapid resumption of Atlantic meridional circulation linked to deglacial climate changes. **Nature**, 428, n. 6985, p. 834, 2004.

MECKLER, A.; SIGMAN, D. M.; GIBSON, K.; FRANÇOIS, R. et al. Deglacial pulses of deep-ocean silicate into the subtropical North Atlantic Ocean. **Nature**, 495, n. 7442, p. 495, 2013.

MEREDITH, M. P.; HEYWOOD, K. J.; FREW, R. D.; DENNIS, P. F. Formation and circulation of the water masses between the southern Indian Ocean and Antarctica: Results from $\delta^{18}O$. **Journal of marine research**, 57, n. 3, p. 449-470, 1999.

MERKEL, U.; PRANGE, M.; SCHULZ, M. ENSO variability and teleconnections during glacial climates. **Quaternary Science Reviews**, 29, n. 1-2, p. 86-100, 2010.

MILLO, C.; STRIKIS, N. M.; VONHOF, H. B.; DEININGER, M. et al. Last glacial and Holocene stable isotope record of fossil dripwater from subtropical Brazil based on analysis of fluid inclusions in stalagmites. **Chemical Geology**, 468, p. 84-96, 2017.

MILZER, G.; GIRAUDEAU, J.; RÜHLEMANN, C.; FAUST, J. et al. Benthic stable isotope variability in the Trondheimsfjord during the last 50 years: Proxy records of mixing dynamics related to NAO. **Estuarine, Coastal and Shelf Science**, 172, p. 34-46, 2016.

MIX, A. C.; RUDDIMAN, W. F.; MCINTYRE, A. Late Quaternary paleoceanography of the Tropical Atlantic, 1: Spatial variability of annual mean sea-surface temperatures, 0-20,000 years BP. **Paleoceanography**, 1, n. 1, p. 43-66, 1986.

MOHTADI, M.; PRANGE, M.; STEINKE, S. Palaeoclimatic insights into forcing and response of monsoon rainfall. **Nature**, 533, n. 7602, p. 191-199, 2016.

MULITZA, S.; BOLTOVSKOY, D.; DONNER, B.; MEGGERS, H. et al. Temperature: δ18O relationships of planktonic foraminifera collected from surface waters. **Palaeogeography, Palaeoclimatology, Palaeoecology**, 202, n. 1-2, p. 143-152, 2003.

MULITZA, S.; CHIESSI, C. M.; SCHEFUß, E.; LIPPOLD, J. et al. Synchronous and proportional deglacial changes in Atlantic meridional overturning and northeast Brazilian precipitation. **Paleoceanography**, 32, n. 6, p. 622-633, 2017.

MULITZA, S.; PRANGE, M.; STUUT, J. B.; ZABEL, M. et al. Sahel megadroughts triggered by glacial slowdowns of Atlantic meridional overturning. **Paleoceanography**, 23, n. 4, 2008.

NACE, T. E.; BAKER, P. A.; DWYER, G. S.; SILVA, C. G. et al. The role of North Brazil Current transport in the paleoclimate of the Brazilian Nordeste margin and paleoceanography of the western tropical Atlantic during the late Quaternary. **Palaeogeography, palaeoclimatology, palaeoecology**, 415, p. 3-13, 2014.

NEELIN, J. D.; HELD, I. M. Modeling tropical convergence based on the moist static energy budget. **Monthly Weather Review**, 115, n. 1, p. 3-12, 1987.

NINNEMANN, U. S.; CHARLES, C. D. Regional differences in Quaternary Subantarctic nutrient cycling: Link to intermediate and deep water ventilation. **Paleoceanography**, 12, n. 4, p. 560-567, 1997.

NÜRNBERG, D.; BIJMA, J.; HEMLEBEN, C. Assessing the reliability of magnesium in foraminiferal calcite as a proxy for water mass temperatures. **Geochimica et Cosmochimica Acta**, 60, n. 5, p. 803-814, 1996.

OLIVEIRA, K. S. S.; DA SILVA QUARESMA, V. Temporal variability in the suspended sediment load and streamflow of the Doce River. **Journal of South American Earth Sciences**, 78, p. 101-115, 2017.

OLSON, D. B.; PODESTÁ, G. P.; EVANS, R. H.; BROWN, O. B. Temporal variations in the separation of Brazil and Malvinas Currents. **Deep Sea Research Part A. Oceanographic Research Papers**, 35, n. 12, p. 1971-1990, 1988.

OPPO, D. W.; CURRY, W. B.; MCMANUS, J. F. What do benthic δ13C and δ18O data tell us about Atlantic circulation during Heinrich Stadial 1? **Paleoceanography**, 30, n. 4, p. 353-368, 2015.

OPPO, D. W.; FAIRBANKS, R. G. Variability in the deep and intermediate water circulation of the Atlantic Ocean during the past 25,000 years: Northern Hemisphere modulation of the Southern Ocean. **Earth and Planetary Science Letters**, 86, n. 1, p. 1-15, 1987.

PASQUIER, V.; SANSJOFRE, P.; RABINEAU, M.; REVILLON, S. et al. Pyrite sulfur isotopes reveal glacial− interglacial environmental changes. **Proceedings of the National Academy of Sciences**, 114, n. 23, p. 5941-5945, 2017.

PATTERSON, R. T.; FISHBEIN, E. Re-examination of the statistical methods used to determine the number of point counts needed for micropaleontological quantitative research. **Journal of Paleontology**, 63, n. 2, p. 245-248, 1989.

PATZ, J. A.; CAMPBELL-LENDRUM, D.; HOLLOWAY, T.; FOLEY, J. A. Impact of regional climate change on human health. **Nature**, 438, n. 7066, p. 310-317, 2005.

PEETERS, F. J. C.; ACHESON, R.; BRUMMER, G.-J. A.; DE RUIJTER, W. P. M. et al. Vigorous exchange between the Indian and Atlantic oceans at the end of the past five glacial periods. **Nature**, 430, n. 7000, p. 661-665, 2004/08/01 2004.

PETERSON, L. C.; HAUG, G. H.; HUGHEN, K. A.; RÖHL, U. Rapid changes in the hydrologic cycle of the tropical Atlantic during the last glacial. **Science**, 290, n. 5498, p. 1947-1951, 2000.

PETERSON, R. G.; STRAMMA, L. Upper-level circulation in the South Atlantic Ocean. **Progress in oceanography**, 26, n. 1, p. 1-73, 1991.

PIOLA, A. R.; MATANO, R. P.; PALMA, E. D.; MÖLLER JR, O. O. et al. The influence of the Plata River discharge on the western South Atlantic shelf. **Geophysical Research Letters**, 32, n. 1, 2005.

POGGEMANN, D. W.; NÜRNBERG, D.; HATHORNE, E.; FRANK, M. et al. Deglacial heat uptake by the Southern Ocean and rapid northward redistribution via Antarctic Intermediate Water. **Paleoceanography and Paleoclimatology**, 33, n. 11, p. 1292-1305, 2018.

POLYAK, L.; STANOVOY, V.; LUBINSKI, D. J. Stable isotopes in benthic foraminiferal calcite from a river-influenced Arctic marine environment, Kara and Pechora Seas. **Paleoceanography**, 18, n. 1, 2003.

PORTILHO-RAMOS, R.; CHIESSI, C.; ZHANG, Y.; MULITZA, S. et al. Coupling of equatorial Atlantic surface stratification to glacial shifts in the tropical rainbelt. **Scientific reports**, 7, n. 1, p. 1561, 2017.

PRANGE, M.; STEPH, S.; LIU, H.; KEIGWIN, L. D. et al. Hydroclimatic variability in the Panama Bight Region during Termination 1 and the Holocene. *In*: **Integrated analysis of interglacial climate dynamics (INTERDYNAMIC)**: Springer, 2015. p. 63-68.

RAHMSTORF, S. Ocean circulation and climate during the past 120,000 years. **Nature**, 419, n. 6903, p. 207-214, 2002.

RAHMSTORF, S.; BOX, J.; FEULNER, G.; MANN, M. E. et al. Erratum: Corrigendum: Evidence for an exceptional twentieth-century slowdown in Atlantic Ocean overturning. **Nature Climate Change**, 5, n. 10, p. 956-956, 2015.

RASMUSSEN, S. O.; BIGLER, M.; BLOCKLEY, S. P.; BLUNIER, T. et al. A stratigraphic framework for abrupt climatic changes during the Last Glacial period based on three synchronized Greenland ice-core records: refining and extending the INTIMATE event stratigraphy. **Quaternary Science Reviews**, 106, p. 14-28, 2014.

REGENBERG, M.; STEPH, S.; NÜRNBERG, D.; TIEDEMANN, R. et al. Calibrating Mg/Ca ratios of multiple planktonic foraminiferal species with δ18O-calcification temperatures: Paleothermometry for the upper water column. **Earth and Planetary Science Letters**, 278, n. 3-4, p. 324-336, 2009.

REIMER, P. J.; BARD, E.; BAYLISS, A.; BECK, J. W. et al. IntCal13 and Marine13 radiocarbon age calibration curves 0–50,000 years cal BP. **Radiocarbon**, 55, n. 4, p. 1869-1887, 2013.

RHEIN, M.; STRAMMA, L.; SEND, U. The Atlantic deep western boundary current: Water masses and transports near the equator. **Journal of Geophysical Research: Oceans**, 100, n. C2, p. 2441-2457, 1995.

RICHARDSON, P. L. Agulhas leakage into the Atlantic estimated with subsurface floats and surface drifters. **Deep Sea Research Part I: Oceanographic Research Papers**, 54, n. 8, p. 1361-1389, 2007.

ROBERTSON, A. W.; MECHOSO, C. R. Interannual and interdecadal variability of the South Atlantic convergence zone. **Monthly weather review**, 128, n. 8, p. 2947-2957, 2000.

ROBINSON, L. F.; ADKINS, J. F.; KEIGWIN, L. D.; SOUTHON, J. et al. Radiocarbon variability in the western North Atlantic during the last deglaciation. **Science**, 310, n. 5753, p. 1469-1473, 2005.

RODRIGUES, R. R.; ROTHSTEIN, L. M.; WIMBUSH, M. Seasonal variability of the South Equatorial Current bifurcation in the Atlantic Ocean: A numerical study. **Journal of Physical Oceanography**, 37, n. 1, p. 16-30, 2007.

ROHLING, E. J.; COOKE, S. Stable oxygen and carbon isotopes in foraminiferal carbonate shells. *In*: **Modern foraminifera**: Springer, 1999. p. 239-258.

RUDDIMAN, W. F. **Earth's climate: past and future**. Macmillan, 2001. 0716737418.

SANTOS, T. P.; LESSA, D. O.; VENANCIO, I. M.; CHIESSI, C. M. et al. Prolonged warming of the Brazil Current precedes deglaciations. **Earth and Planetary Science Letters**, 463, p. 1-12, 2017.

SARMIENTO, J.; TOGGWEILER, J.; NAJJAR, R. Ocean carbon-cycle dynamics and atmospheric pCO2. **Philosophical Transactions of the Royal Society of London. Series A, Mathematical and Physical Sciences**, 325, n. 1583, p. 3-21, 1988.

SARNTHEIN, M.; WINN, K.; JUNG, S. J.; DUPLESSY, J. C. et al. Changes in east Atlantic deepwater circulation over the last 30,000 years: Eight time slice reconstructions. **Paleoceanography**, 9, n. 2, p. 209-267, 1994.

SCHETTINI, C. Near bed sediment transport in the Itajaí-Açu River estuary, southern Brazil. *In*: **Proceedings in Marine Science**: Elsevier, 2002. v. 5, p. 499-512.

SCHILMAN, B.; ALMOGI-LABIN, A.; BAR-MATTHEWS, M.; LABEYRIE, L. et al. Long-and short-term carbon fluctuations in the Eastern Mediterranean during the late Holocene. **Geology**, 29, n. 12, p. 1099-1102, 2001.

SCHLITZER, R. **Ocean Data View, https://odv.awi.de**. 2018.

SCHMID, C.; BOEBEL, O.; ZENK, W.; LUTJEHARMS, J. et al. Early evolution of an Agulhas Ring. **Deep Sea Research Part II: Topical Studies in Oceanography**, 50, n. 1, p. 141-166, 2003.

SCHMIEDL, G.; DE BOVÉE, F.; BUSCAIL, R.; CHARRIERE, B. et al. Trophic control of benthic foraminiferal abundance and microhabitat in the bathyal Gulf of Lions, western Mediterranean Sea. **Marine Micropaleontology**, 40, n. 3, p. 167-188, 2000.

SCHMIEDL, G.; MACKENSEN, A. Late Quaternary paleoproductivity and deep water circulation in the eastern South Atlantic Ocean: Evidence from benthic foraminifera. **Palaeogeography, Palaeoclimatology, Palaeoecology**, 130, n. 1-4, p. 43-80, 1997.

SCHMIEDL, G.; MACKENSEN, A. Multispecies stable isotopes of benthic foraminifers reveal past changes of organic matter decomposition and deepwater oxygenation in the Arabian Sea. **Paleoceanography**, 21, n. 4, 2006.

SCHMIEDL, G.; PFEILSTICKER, M.; HEMLEBEN, C.; MACKENSEN, A. Environmental and biological effects on the stable isotope composition of recent deep-sea benthic foraminifera from the western Mediterranean Sea. **Marine Micropaleontology**, 51, n. 1-2, p. 129-152, 2004.

SCHMITTNER, A.; LUND, D. Early deglacial Atlantic overturning decline and its role in atmospheric CO 2 rise inferred from carbon isotopes (δ 13 C). **Climate of the Past**, 11, n. 2, p. 135-152, 2015.

SCHNEIDER, T.; BISCHOFF, T.; HAUG, G. H. Migrations and dynamics of the intertropical convergence zone. **Nature**, 513, n. 7516, p. 45-53, 2014.

SCHRAG, D. P.; ADKINS, J. F.; MCINTYRE, K.; ALEXANDER, J. L. et al. The oxygen isotopic composition of seawater during the Last Glacial Maximum. **Quaternary Science Reviews**, 21, n. 1-3, p. 331-342, 2002.

SHACKLETON, N. J.; CHAPMAN, M.; SÁNCHEZ-GOÑI, M. F.; PAILLER, D. et al. The classic marine isotope substage 5e. **Quaternary Research**, 58, n. 1, p. 14-16, 2002.

SHACKLETON, N. J.; HALL, M. A. Oxygen and carbon isotope stratigraphy of DSDP Hole 552A: Plio-Pleistocene glacial history. **Initial Rep. Deep Sea Drill. Project**, 81, p. 599-609, 1984.

SHACKLETON, N. J.; HALL, M. A.; VINCENT, E. Phase relationships between millennial-scale events 64,000–24,000 years ago. **Paleoceanography**, 15, n. 6, p. 565-569, 2000.

SILVA, M.; ARAUJO, M.; SERVAIN, J.; PENVEN, P. et al. High-resolution regional ocean dynamics simulation in the southwestern tropical Atlantic. **Ocean Modelling**, 30, n. 4, p. 256-269, 2009.

SIMON, M. H.; GONG, X.; HALL, I. R.; ZIEGLER, M. et al. Salt exchange in the Indian-Atlantic Ocean Gateway since the Last Glacial Maximum: A compensating effect between Agulhas Current changes and salinity variations? **Paleoceanography**, 30, n. 10, p. 1318-1327, 2015.

SKINNER, L.; SHACKLETON, N. An Atlantic lead over Pacific deep-water change across Termination I: implications for the application of the marine isotope stage stratigraphy. **Quaternary Science Reviews**, 24, n. 5-6, p. 571-580, 2005.

SLUIJS, A.; RÖHL, U.; SCHOUTEN, S.; BRUMSACK, H. J. et al. Arctic late Paleocene–early Eocene paleoenvironments with special emphasis on the Paleocene-Eocene thermal maximum (Lomonosov Ridge, Integrated Ocean Drilling Program Expedition 302). **Paleoceanography**, 23, n. 1, 2008.

SROKOSZ, M.; BRYDEN, H. Observing the Atlantic Meridional Overturning Circulation yields a decade of inevitable surprises. **Science**, 348, n. 6241, p. 1255575, 2015.

STAINFORTH, R.; LAMB, J. L.; LUTERBACHER, H.; BEARD, J. H. et al. Cenozoic planktonic foraminiferal zonation and characteristics of index forms. 1975.

STEPH, S.; REGENBERG, M.; TIEDEMANN, R.; MULITZA, S. et al. Stable isotopes of planktonic foraminifera from tropical Atlantic/Caribbean core-tops: Implications for reconstructing upper ocean stratification. **Marine Micropaleontology**, 71, n. 1-2, p. 1-19, 2009.

STOUFFER, R. J.; YIN, J.; GREGORY, J.; DIXON, K. et al. Investigating the causes of the response of the thermohaline circulation to past and future climate changes. **Journal of Climate**, 19, n. 8, p. 1365-1387, 2006.

STRAMMA, L.; ENGLAND, M. On the water masses and mean circulation of the South Atlantic Ocean. **Journal of Geophysical Research: Oceans**, 104, n. C9, p. 20863-20883, 1999.

STRAMMA, L.; IKEDA, Y.; PETERSON, R. G. Geostrophic transport in the Brazil Current region north of 20 S. **Deep Sea Research Part A. Oceanographic Research Papers**, 37, n. 12, p. 1875-1886, 1990.

STRAMMA, L.; SCHOTT, F. The mean flow field of the tropical Atlantic Ocean. **Deep Sea Research Part II: Topical Studies in Oceanography**, 46, n. 1-2, p. 279-303, 1999.

STRÍKIS, N. M.; CHIESSI, C. M.; CRUZ, F. W.; VUILLE, M. et al. Timing and structure of Mega-SACZ events during Heinrich Stadial 1. **Geophysical Research Letters**, 42, n. 13, p. 5477-5484A, 2015.

STRÍKIS, N. M.; CRUZ, F. W.; BARRETO, E. A.; NAUGHTON, F. et al. South American monsoon response to iceberg discharge in the North Atlantic. **Proceedings of the National Academy of Sciences**, 115, n. 15, p. 3788-3793, 2018.

STUIVER, M.; QUAY, P. D.; OSTLUND, H. Abyssal water carbon-14 distribution and the age of the world oceans. **Science**, 219, n. 4586, p. 849-851, 1983.

SÜFKE, F.; PÖPPELMEIER, F.; GOEPFERT, T. J.; REGELOUS, M. et al. Constraints on the northwestern Atlantic deep water circulation from 231Pa/230Th during the last 30,000 years. **Paleoceanography and Paleoclimatology**, 2019.

SUITS, N. S.; ARTHUR, M. A. Sulfur diagenesis and partitioning in Holocene Peru shelf and upper slope sediments. **Chemical Geology**, 163, n. 1-4, p. 219-234, 2000.

TALENTO, S.; BARREIRO, M. Control of the South Atlantic Convergence Zone by extratropical thermal forcing. **Climate dynamics**, 50, n. 3-4, p. 885-900, 2018.

TESSIN, A.; LUND, D. Isotopically depleted carbon in the mid-depth South Atlantic during the last deglaciation. **Paleoceanography**, 28, n. 2, p. 296-306, 2013.

THEODOR, M.; SCHMIEDL, G.; JORISSEN, F.; MACKENSEN, A. Stable carbon isotope gradients in benthic foraminifera as proxy for organic carbon fluxes in the Mediterranean Sea. **Biogeosciences**, 13, n. 23, p. 6385-6404, 2016.

THOMAS, C. D.; CAMERON, A.; GREEN, R. E.; BAKKENES, M. et al. Extinction risk from climate change. **Nature**, 427, n. 6970, p. 145-148, 2004.

THORNALLEY, D. J.; BARKER, S.; BROECKER, W. S.; ELDERFIELD, H. et al. The deglacial evolution of North Atlantic deep convection. **science**, 331, n. 6014, p. 202-205, 2011.

TIMMERMANN, A.; OKUMURA, Y.; AN, S.-I.; CLEMENT, A. et al. The influence of a weakening of the Atlantic meridional overturning circulation on ENSO. **Journal of climate**, 20, n. 19, p. 4899-4919, 2007.

TJALLINGII, R.; RÖHL, U.; KÖLLING, M.; BICKERT, T. Influence of the water content on X-ray fluorescence core-scanning measurements in soft marine sediments. **Geochemistry, Geophysics, Geosystems**, 8, n. 2, 2007.

VAN AKEN, H.; VAN VELDHOVEN, A.; VETH, C.; DE RUIJTER, W. et al. Observations of a young Agulhas ring, Astrid, during MARE in March 2000. **Deep Sea Research Part II: Topical Studies in Oceanography**, 50, n. 1, p. 167-195, 2003.

VAN DER WIEL, K.; MATTHEWS, A. J.; STEVENS, D. P.; JOSHI, M. M. A dynamical framework for the origin of the diagonal South Pacific and South Atlantic convergence zones. **Quarterly Journal of the Royal Meteorological Society**, 141, n. 691, p. 1997-2010, 2015.

VENANCIO, I.; MULITZA, S.; GOVIN, A.; SANTOS, T. et al. Millennial-to Orbital-Scale Responses of Western Equatorial Atlantic Thermocline Depth to Changes in the Trade Wind System Since the Last Interglacial. **Paleoceanography and Paleoclimatology**, 33, n. 12, p. 1490-1507, 2018.

VENANCIO, I.; SHIMIZU, M.; SANTOS, T.; LESSA, D. et al. Changes in surface hydrography at the western tropical Atlantic during the Younger Dryas. **Global and Planetary Change**, 184, p. 103047, 2020.

VERES, D.; BAZIN, L.; LANDAIS, A.; TOYÉ MAHAMADOU KELE, H. et al. The Antarctic ice core chronology (AICC2012): an optimized multi-parameter and multi-site dating approach for the last 120 thousand years. **Climate of the Past**, 9, n. 4, p. 1733-1748, 2013.

VOIGT, I.; CRUZ, A.; MULITZA, S.; CHIESSI, C. et al. Variability in mid-depth ventilation of the western Atlantic Ocean during the last deglaciation. **Paleoceanography**, 32, n. 9, p. 948-965, 2017.

VOIGT, I.; HENRICH, R.; PREU, B. M.; PIOLA, A. R. et al. A submarine canyon as a climate archive—interaction of the Antarctic Intermediate Water with the Mar del Plata Canyon (Southwest Atlantic). **Marine Geology**, 341, p. 46-57, 2013.

VOLBERS, A.; HENRICH, R. Calcium carbonate corrosiveness in the South Atlantic during the Last Glacial Maximum as inferred from changes in the preservation of Globigerina bulloides: A proxy to determine deep-water circulation patterns? **Marine Geology**, 204, n. 1-2, p. 43-57, 2004.

VUILLE, M.; BURNS, S. J.; TAYLOR, B. L.; CRUZ JÚNIOR, F. W. d. et al. A review of the South American monsoon history as recorded in stable isotopic proxies over the past two millennia. **Climate of the Past**, 8, n. 4, p. 1309-1321, 2012.

WAELBROECK, C.; LABEYRIE, L.; MICHEL, E.; DUPLESSY, J. C. et al. Sea-level and deep water temperature changes derived from benthic foraminifera isotopic records. **Quaternary Science Reviews**, 21, n. 1-3, p. 295-305, Jan 2002.

WAELBROECK, C.; SKINNER, L. C.; LABEYRIE, L.; DUPLESSY, J. C. et al. The timing of deglacial circulation changes in the Atlantic. **Paleoceanography**, 26, n. 3, Aug 19 2011.

WALISER, D. E.; GAUTIER, C. A satellite-derived climatology of the ITCZ. **Journal of climate**, 6, n. 11, p. 2162-2174, 1993.

WANG, X.; AULER, A. S.; EDWARDS, R. L.; CHENG, H. et al. Wet periods in northeastern Brazil over the past 210 kyr linked to distant climate anomalies. **Nature**, 432, n. 7018, p. 740-743, 2004.

WANG, X.; AULER, A. S.; EDWARDS, R. L.; CHENG, H. et al. Interhemispheric anti-phasing of rainfall during the last glacial period. **Quaternary Science Reviews**, 25, n. 23-24, p. 3391-3403, 2006.

WARD, B. M.; WONG, C. I.; NOVELLO, V. F.; MCGEE, D. et al. Reconstruction of Holocene coupling between the South America Monsoon System and local moisture variability from speleothem δ18O and 87Sr/86Sr records. **Quaternary Science Reviews**, 210, p. 51-63, 2019.

WEAVER, A. J.; SEDLÁČEK, J.; EBY, M.; ALEXANDER, K. et al. Stability of the Atlantic meridional overturning circulation: A model intercomparison. **Geophysical Research Letters**, 39, n. 20, 2012.

WEIJER, W.; DE RUIJTER, W. P.; STERL, A.; DRIJFHOUT, S. S. Response of the Atlantic overturning circulation to South Atlantic sources of buoyancy. **Global and Planetary Change**, 34, n. 3-4, p. 293-311, 2002.

WORTHAM, B. E.; WONG, C. I.; SILVA, L. C.; MCGEE, D. et al. Assessing response of local moisture conditions in central Brazil to variability in regional monsoon intensity using speleothem 87Sr/86Sr values. **Earth and Planetary Science Letters**, 463, p. 310-322, 2017.

XIE, P.; ARKIN, P. A. Global precipitation: A 17-year monthly analysis based on gauge observations, satellite estimates, and numerical model outputs. **Bulletin of the American Meteorological Society**, 78, n. 11, p. 2539-2558, 1997.

ZAHN, R.; SCHÖNFELD, J.; KUDRASS, H.; PARK, M. et al. Thermohaline instability in the North Atlantic during meltwater events: Stable isotope and ice-rafted detritus records from Core SO75-26KL, Portuguese Margin. **Paleoceanography**, 12, n. 5, p. 696-710, 1997.

ZAHN, R.; WINN, K.; SAMTHEIN, M. Benthic foraminiferal delta 13C and accumulation rates of organic carbon: Uvigerina peregrina group and Cibicidoides wuellerstorfi. **Paleoceanography**, 1, n. 1, p. 27-42, Mar 1986.

ZHANG, R.; DELWORTH, T. L. Simulated tropical response to a substantial weakening of the Atlantic thermohaline circulation. **Journal of climate**, 18, n. 12, p. 1853-1860, 2005.

ZHANG, Y.; CHIESSI, C. M.; MULITZA, S.; SAWAKUCHI, A. O. et al. Different precipitation patterns across tropical South America during Heinrich and Dansgaard-Oeschger stadials. **Quaternary Science Reviews**, 177, p. 1-9, 2017.

ZHANG, Y.; CHIESSI, C. M.; MULITZA, S.; ZABEL, M. et al. Origin of increased terrigenous supply to the NE South American continental margin during Heinrich Stadial 1 and the Younger Dryas. **Earth and Planetary Science Letters**, 432, p. 493-500, 2015.

ZHANG, Y.; ZHANG, X.; CHIESSI, C. M.; MULITZA, S. et al. Equatorial Pacific forcing of western Amazonian precipitation during Heinrich Stadial 1. **Scientific reports**, 6, n. 1, p. 1-7, 2016.

ZHAO, N.; OPPO, D. W.; HUANG, K.-F.; HOWE, J. N. et al. Glacial–interglacial Nd isotope variability of North Atlantic Deep Water modulated by North American ice sheet. **Nature Communications**, 10, n. 1, p. 1-10, 2019.

ZHOU, J.; LAU, K. Does a monsoon climate exist over South America? **Journal of climate**, 11, n. 5, p. 1020-1040, 1998.

ZULAR, A.; SAWAKUCHI, A. O.; CHIESSI, C. M.; D'HORTA, F. M. et al. The role of abrupt climate change in the formation of an open vegetation enclave in northern Amazonia during the late Quaternary. **Global and planetary change**, 172, p. 140-149, 2019.

ZWENG, M. M.; REAGAN, J. R.; ANTONOV, J. I.; LOCARNINI, R. A. et al. World ocean atlas 2013. volume 2, salinity. 2013.